UNIVERSIDADE FEDERAL DE PERNAMBUCO

CENTRO DE CIÊNCIAS BIOLÓGICAS

PROGRAMA DE PÓS-GRADUAÇÃO EM BIOLOGIA VEGETAL

ESTRUTURA CENTROMÉRICA E ADAPTAÇÕES MEIÓTICAS EM ESPÉCIES HOLOCÊNTRICAS DO GÊNERO *Rhynchospora* (CYPERACEAE)

ANDRÉ SECO MARQUES DA SILVA

RECIFE

2016

UNIVERSIDADE FEDERAL DE PERNAMBUCO

CENTRO DE CIÊNCIAS BIOLÓGICAS

PROGRAMA DE PÓS-GRADUAÇÃO EM BIOLOGIA VEGETAL

ESTRUTURA CENTROMÉRICA E ADAPTAÇÕES MEIÓTICAS EM ESPÉCIES HOLOCÊNTRICAS DO GÊNERO *Rhynchospora* (CYPERACEAE)

Tese de doutorado apresentado por ANDRÉ SECO MARQUES DA SILVA ao curso de Pós-Graduação em Biologia Vegetal da Universidade Federal de Pernambuco, como um dos requisitos para a obtenção do grau de doutor em Biologia Vegetal, na área de concentração Sistemática e Evolução.

Orientadora: Andrea Pedrosa-Harand

Co-Orientador: Andreas Houben

RECIFE

2016

ANDRÉ SECO MARQUES DA SILVA

ESTRUTURA CENTROMÉRICA E ADAPTAÇÕES MEIÓTICAS EM ESPÉCIES HOLOCÊNTRICAS DO GÊNERO *RHYNCHOSPORA* (CYPERACEAE)

APROVADA EM: 15/02/2016

BANCA EXAMINADORA:

_____

Prof. Dra. Andrea Pedrosa-Harand (Orientadora) – UFPE

_____

Prof. Dr. Diogo Cavalcanti Cabral-de-Mello – Unesp/Rio Claro

_____

Prof. Dr. Rita de Cássia Moura – UPE

_____

Prof. Dr. Ana Maria Benko Iseppon – UFPE

_____

Prof. Dr. Luiz Gustavo Rodrigues Souza – UFPE

Recife – PE

2016

Resumo

Cromossomos holocêntricos são caracterizados pela ausência de constrição primária e apresentam normalmente a proteína centromérica CENH3 distribuída ao longo de um eixo em cada cromátide. Embora muitos organismos com cromossomos monocêntricos apresentem sequências de DNA centroméricas específicas e associadas com a CENH3, nenhuma sequência centromérica havia sido identificada em organismos com cromossomos holocêntricos até o momento. Além disso, vários estudos reportam adaptações meióticas em espécies com cromossomos holocêntricos. Sendo observada em alguns casos uma inversão da ordem dos eventos meióticos (meiose invertida ou pós-reducional). Assim, o presente trabalho objetivou estudar a organização centromérica e a meiose de espécies com cromossomos holocêntricos do gênero *Rhynchospora* (Cyperaceae). Foi realizada uma análise citogenômica da organização e composição dos holocentrômeros de *Rhynchospora pubera* (2*n* = 10), sendo reportada a primeira descoberta de sequências centroméricas em espécies com cromossomos holocêntricos. Foi observado que os holocentrômeros de *R. pubera* são compostos principalmente por arranjos de DNA satélite (Tyba) e retroelementos centroméricos (CRRh) distribuídos pelo genoma. A análise detalhada da sucessão dos eventos meióticos de *R. pubera* e *R. tenuis* (2*n* = 4) reportou uma prófase inicial semelhante a de monocêntricos. No entanto, foi verificado que as cromátides-irmãs separam para polos opostos durante a anáfase I e os homólogos segregam somente durante a meiose II, comprovando uma meiose invertida para ambas as espécies. Curiosamente, durante a meiose de *R. pubera* foi observado uma organização diferencial dos centrômeros. Ao contrário do observado em mitose, durante meiose não foi observado a formação de holocentrômeros em forma de linha, sendo, na verdade, observado estruturas centroméricas aglomeradas. O restabelecimento de holocentrômeros em forma de linha se deu durante a primeira mitose do pólen.

Palavras-chave: cromossomos holocêntricos, CENH3, CENP-C, holocentrômero, meiose invertida, *Rhynchospora*

Abstract

Holocentric chromosomes are characterized by the absence primary constriction and normally show the centromeric protein CENH3 distributed along the axis of each chromatid. Although many monocentric organisms show centromere-specific DNA sequences associated to CENH3, no centromeric sequences had been identified in any holocentric organism so far. Furthermore, many studies report meiotic adaptations in holocentric species. In some cases is observed an inversion of the order of meiotic events. This type of meiosis has been named of inverted or post-reductional meiosis and would be exclusive of holocentric organisms. Thus, the present work aimed to study the centromere organization and meiosis of holocentric species of the genus *Rhynchospora* (Cyperaceae). A cytogenomic analysis of the composition and organization of the holocentromeres of *Rhynchospora pubera* (2*n* = 10) has been performed, being reported the first centromeric sequences from a holocentric species. It was observed that the holocentromeres of *R. pubera* are composed mainly by arrays of satellite DNA (Tyba) and centromeric retrotransposons (CRRh) distributed genome-wide. The detailed analysis of the succession of meiotic events of *R. pubera* and *R. tenuis* (2*n* = 4) demonstrated an early meiotic prophase similar to that of monocentric. However, it was verified that sister chromatids separate to opposite poles during anaphase I, while homologs only segregate at meiosis II. These results prove the inverted meiosis for both species. Curiously, it was observed during meiosis of *R. pubera* a differential organization of centromere units. In contrast to the observed in mitosis, during meiosis we did not observed the formation of line-like holocentromeres, being in fact observed the formation of cluster-like holocentromeres. The reestablishment of a line-like holocentromere occurred during the first pollen mitosis.

Key words: holocentric chromosomes, CENH3, CENP-C, holocentromere, inverted meiosis, *Rhynchospora*

Índice

1. Apresentação

O centrômero é a região cromossômica responsável pela segregação das cromátides-irmãs durante a mitose e a meiose. Os centrômeros são compostos em geral por sequências específicas centroméricas (cenDNA) e proteínas específicas que servem como sítios de interação com outras proteínas cinetocóricas e ligação dos microtúbulos nos cromossomos eucariontes durante a divisão celular (CHEERAMBATHUR; DESAI, 2014). Os cromossomos são normalmente classificados em monocêntricos e holocêntricos, no que diz respeito à localização e distribuição da placa cinetocórica. Os holocêntricos diferem dos cromossomos monocêntricos pela ausência de um centrômero localizado ou constrição primária, apresentando atividade cinetocórica e associação com os microtúbulos ao longo de quase toda a extensão de ambas as cromátides. A origem desses cromossomos parece ter se dado de forma independente várias vezes durante a evolução, sendo reportados em diversos grupos não relacionados de animais e plantas (MELTERS et al., 2012; BURES et al., 2013). Em plantas, eles estão presentes em grupos diferentes, mas principalmente nas famílias Cyperacae e Juncaceae, nas quais estão normalmente associados com uma grande variedade de números cromossômicos (MELTERS et al., 2012; HIPP et al., 2013).

A composição proteica do cinetócoro é conservada entre organismos monocêntricos e holocêntricos (OEGEMA; HYMAN, 2006), porém não se sabe o processo causador da formação dos centrômeros holocinéticos (holocentrômeros) enfatizando o fato de que os estudos em organismos com cromossomos holocêntricos podem ser esclarecedores para se compreender as características conservadas e divergentes de estrutura e função cromossômica. A variante centromérica da histona H3 (CENH3) é a principal marca epigenética para o centrômero e tem sido detectada na grande maioria dos eucariotos estudados, de protistas a animais e plantas (STEINER; HENIKOFF, 2015). O cinetócoro é ainda composto por várias outras proteínas conservadas que definem os domínios cinetocóricos internos e externos. A proteína CENP-C é uma componente chave do cinetócoro interno e provê uma ligação entre as porções internas e externas do cinetócoro (EARNSHAW, 2015).

A identificação e caracterização de proteínas centroméricas em vários organismos permitiu um melhor entendimento da organização dos centrômeros em várias espécies com cromossomos monocêntricos e holocêntricos (MADDOX et al., 2004; NAGAKI et al., 2005; HECKMANN et al., 2011; WANG et al., 2011). A imunodetecção com CENH3 em cromossomos metafásicos mitóticos holocêntricos de *Caenorhabditis elegans* (BUCHWITZ et al., 1999; MOORE et al., 1999) e espécies de *Luzula* (Juncaceae) (NAGAKI et al., 2005; HECKMANN et al., 2011) mostraram estrutura semelhante: uma placa longa cinetocórica bem diferenciada ao longo de cada cromátide irmã, exceto nas regiões distais. Curiosamente, durante a intérfase, numerosos sinais dispersos e pequenos foram observados distribuídos ao longo do núcleo, sugerindo que múltiplas regiões dos cromossomos se unem durante a condensação para formar os “holocentrômeros”. Foi demonstrado recentemente que os holocentrômeros de *C. elegans* são organizados como várias unidades centroméricas dispersas, mas discretamente localizadas (STEINER; HENIKOFF, 2014). Essas observações recentes suportam o modelo "policêntrico", uma vez que o cinetócoro contínuo metafásico seria o resultado da união de pequenas unidades cinetocóricas.

A cromatina centromérica em organismos eucarióticos geralmente apresenta uma associação precisa da CENH3 e cenDNA (LAMB; BIRCHLER, 2003). O DNA centromérico é frequentemente composto por repetições em série (chamadas de *tandem repeats* ou DNA satélite) e/ou outras sequências de DNA repetitivas, como alguns retrotransposons *Ty3/gypsy* (NEUMANN et al., 2011; PLOHL et al., 2014). Apesar de alguns trabalhos recentes terem tentado encontrar cenDNA em organismos com cromossomos holocêntricos, nenhum cenDNA foi encontrado em co-localização com CENH3 e/ou validado por CENH3-ChIP nesses organismos (HAIZEL et al., 2005; GASSMANN et al., 2012; HECKMANN et al., 2013; MESTROVIC et al., 2013; SUBIRANA; MESSEGUER, 2013; STEINER; HENIKOFF, 2014).

Pelo fato desses cromossomos apresentarem atividade cinetocórica ao longo de toda a extensão da cromátide, são esperadas adaptações meióticas para permitir a correta segregação cromossômica. Na meiose típica apresentada por cromossomos monocêntricos, o meiócito passa por duas divisões consecutivas, uma meiose I

reducional, seguida por uma meiose II equacional, nas quais ocorrem, respectivamente, a segregação dos cromossomos homólogos e a separação das cromátides-irmãs (DURO; MARSTON, 2015; OHKURA, 2015). No entanto, em alguns organismos com cromossomos holocêntricos, ocorre uma alteração na ordem dos eventos meióticos e, por isso se diz que a meiose seria invertida ou pós-reducional. Este tipo de meiose tem sido reportado em algumas espécies de plantas e animais holocêntricos, como é o caso de membros das famílias Juncaceae e Cyperaceae e em alguns insetos (MELTERS et al., 2012). Embora alguns trabalhos tenham relatado a ocorrência de meiose invertida em plantas com cromossomos holocêntricos, ainda restam dúvidas se a meiose invertida seria o modelo geral para plantas que apresentam este tipo cromossômico.

O gênero *Rhynchospora* Vahl (Cyperaceae) foi caracterizado pela presença de cromossomos holocêntricos há duas décadas (VANZELA et al., 1996; LUCEÑO et al., 1998; VANZELA et al., 1998). A descrição e caracterização dos cromossomos holocêntricos deste grupo foi baseada na ausência de uma constrição primária, migração paralela das cromátides-irmãs em anáfase e distribuição dos microtúbulos do fuso mitótico ao longo de cada cromátide-irmã (VANZELA et al., 1996; LUCEÑO et al., 1998; GUERRA et al., 2006). Dentre as espécies do gênero, *Rhynchospora pubera* e *R. tenuis* se destacam pela presença de cromossomos relativamente grandes e um baixo número cromossômico, 2*n* = 10 e 2*n* = 4, respectivamente.

No presente trabalho, as espécies *R. pubera* (2*n* = 10) e *R. tenuis* (2*n* = 4) foram utilizadas como modelos para se estudar três objetivos centrais: 1) Caracterizar a organização e composição dos holocentrômeros em mitose; 2) Caracterizar a ordem os eventos meióticos testando a hipótese de meiose invertida no grupo; 3) Caracterizar a organização dos holocentrômeros na meiose. O primeiro capítulo da tese aborda então os resultados referentes ao primeiro objetivo e relata a inédita identificação e caracterização de sequências associadas aos holocentrômeros de uma espécie holocêntrica. O segundo capítulo demonstra, através da utilização de técnicas citomoleculares em *R. pubera* e *R. tenuis,* a ocorrência de meiose invertida nessas espécies. Por fim, o terceiro capítulo reporta a caracterização de uma organização diferencial dos centrômeros durante mitose e meiose em *R. pubera*.

2. Revisão de literatura

2.1. Centrômero

O centrômero é tradicionalmente definido como a constrição primária de um cromossomo metafásico condensado. O centrômero é formado por um complexo multiprotéico associado normalmente a sequências específicas de DNA que interage com os microtúbulos do fuso que medeiam a transmissão fiel do material genético durante a mitose e a meiose (Figura 1a). As proteínas cinetocóricas são responsáveis pela coesão das cromátides-irmãs, o movimento dos cromossomos e a regulação do ciclo celular (DORN; MADDOX, 2012). A criação e manutenção de centrômeros ativos são baseadas principalmente na presença da variante centromérica da histona H3 (CENH3), também denominada CENP-A (EARNSHAW et al., 2013). A CENH3 substitui parcialmente a histona H3 canônica em nucleossomos centroméricos e, assim, é a principal marca que define os centrômeros epigeneticamente, iniciando a formação do cinetócoro (SULLIVAN et al., 2001; KALITSIS; CHOO, 2012; HENIKOFF; SMITH, 2015). Essa proteína possui a cauda C-terminal conservada, conhecida como o *histone-fold-domain*, que inclui a região *loop1*, responsável pelo seu direcionamento aos nucleossomos centroméricos (BLACK et al., 2004; LERMONTOVA et al., 2006). Já a cauda N-terminal apresenta uma grande variação no tamanho e composição dos aminoácidos entre espécies (Figura 1b) (HENIKOFF; DALAL, 2005; HENIKOFF; SMITH, 2015), sendo necessária para a interação com componentes cinetocóricos (CHEN et al., 2000).

Embora a CENH3 seja a marca epigenética para o centrômero, o cinetócoro é composto também por várias outras proteínas conservadas que definem os domínios cinetocóricos internos e externos (Figura 1a). Dentre essas proteínas, a proteína do cinetócoro interno CENP-C é uma componente chave do cinetócoro eucarioto e fornece uma ligação crítica entre as porções internas e externas do cinetócoro (EARNSHAW, 2015). Foi demonstrado que a CENP-C tem a habilidade de reconhecer especificamente a CENH3 definindo a cromatina centromérica ativa (CARROLL et al., 2010; KATO et al., 2013; FALK et al., 2015). A organização do cinetócoro é conservada na maioria dos eucariotos, no entanto achados recentes desafiaram essa suposição

(AKIYOSHI; GULL, 2014; DRINNENBERG et al., 2014). Foi mostrado que cinetoplastídeos constroem seus cinetócoros usando um conjunto diferente de proteínas, que não apresentam homologia com proteínas cinetocóricas convencionais de outros eucariotos (AKIYOSHI; GULL, 2014). Foi demonstrado também, que a transição à holocentricidade em algumas linhagens de insetos está associada com a perda dos genes da CENH3 e CENP-C, enquanto outras proteínas cinetocóricas encontravam-se conservadas (DRINNENBERG et al., 2014).

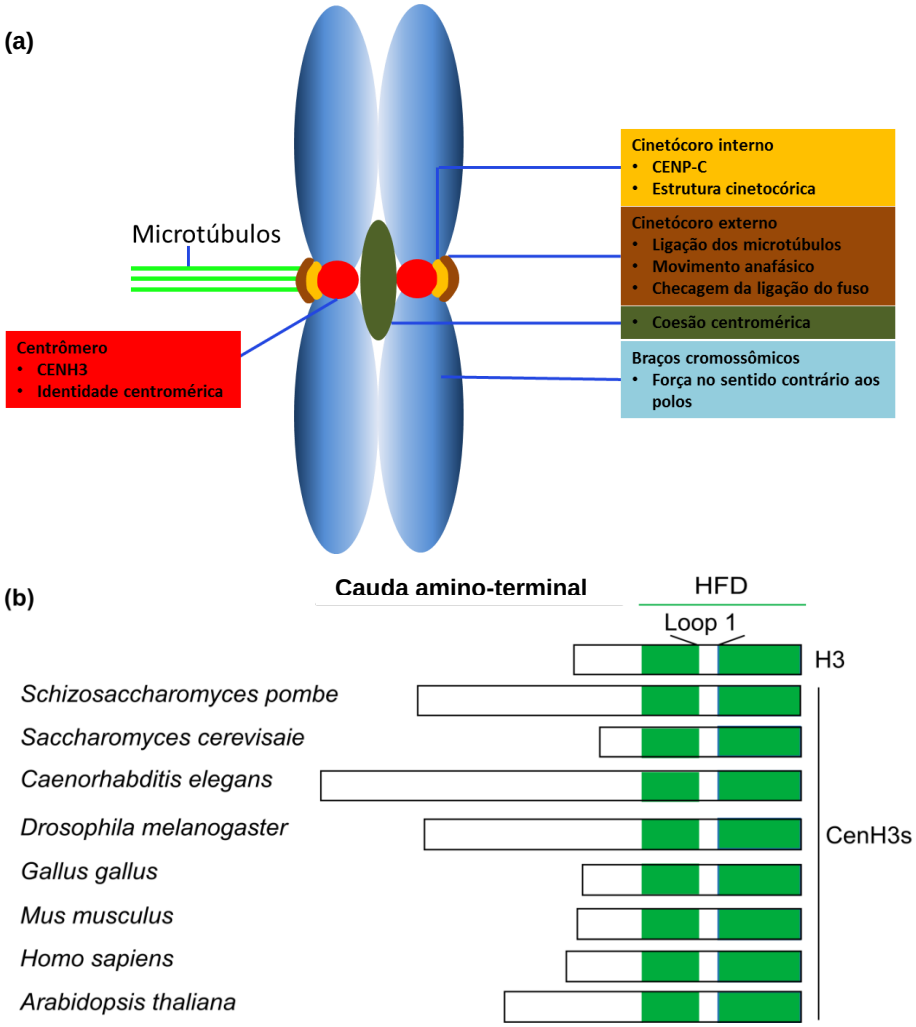

Figura 1. (a) Elementos estruturais e funcionais do centrômero mitótico. Modificado de SULLIVAN et al. (2001). (b) Alinhamento das CENH3s de diferentes espécies. A cauda amino-terminal não é conservada em tamanho e sequência nas diferentes linhagens. HFD = *histone fold domain*. Modificado de (HENIKOFF; DALAL, 2005).

A função do centrômero é extremamente conservada em eucariotos (HOUBEN; SCHUBERT, 2003; OEGEMA; HYMAN, 2006), no entanto a composição do DNA centromérico é altamente variável e, exceto em leveduras em que existe uma identidade centromérica dependente da sequência de DNA (CLARKE; CARBON, 1985), sequências de DNA centromérico não são nem necessárias nem suficientes para que haja a formação do centrômero (KALITSIS; CHOO, 2012; HENIKOFF; SMITH, 2015). No entanto, BASSETT et al. (2010) sugeriram que uma eventual aquisição de sequências repetitivas de DNA e concomitante formação de heterocromatina seria um mecanismo simples para garantir a função centromérica, fornecendo um ambiente favorável para a estabilização do centrômero ao longo do tempo.

2.1.1. Sequências de DNA centroméricas: conceito, identificação e validação

A heterocromatina dos genomas eucariotos é normalmente caracterizada pela presença de sequências repetitivas. Essas podem ser geralmente classificadas em dois tipos: 1) sequências de DNA satélite (satDNA), que são sequências de DNA repetidas em tandem no genoma (também chamadas de *tandem repeats*) formando blocos de heterocromatina (PLOHL et al., 2008; PLOHL et al., 2012); 2) elementos transponíveis (DNA *transposons*, retroelementos LTR, SINE, LINE, etc.), que são sequências evolutivamente derivadas de elementos virais que se acumulam no genoma por mecanismos de transposição, ocasionando uma distribuição dispersa uniformemente distribuída no genoma ou enriquecida em determinado domínio cromossômico (BÖHNE et al., 2008).

Os centrômeros da maioria das espécies de plantas analisadas possuem famílias distintas de satDNA e também frequentemente uma família de retrotransposons LTR *Ty3/gypsy* do clado CRM (*centromeric retrotransposon of maize*) associados à cromatina centromérica (NEUMANN et al., 2011; PLOHL et al., 2014). Essas sequências são denominadas sequências específicas dos centrômeros (cenDNA) e são normalmente inseridas em blocos de heterocromatina (peri)centromérica, em arranjos de mega pares de base (Mb) de satDNA. Esses arranjos se estendem em geral por

regiões muito mais longas do que o necessário para a função centromérica. Por exemplo, em *Arabidopsis thaliana* (L.) Heynh. e milho (*Zea mays* L.) foi constado que somente aproximadamente 15% e 38%, respectivamente, do cenDNA identificado nessas espécies está associado com os centrômeros funcionais (ZHONG et al., 2002; NAGAKI et al., 2003). Além disso, em espécies com cromossomos monocêntricos a especificidade do cenDNA pode variar, podendo ocorrer desde apenas um par cromossômico até todos os cromossomos do complemento (CHENG et al., 2002; PLOHL et al., 2014; ZHANG et al., 2014). Em um estudo recente foi reportado para ervilha (*Pisum sativum* L.), a interessante descoberta de cromossomos com múltiplos domínios centroméricos (3-5) em cada cromossomo. A caracterização do cenDNA dessa espécie revelou 13 famílias distintas de DNA satélite e um retrotransposon centromérico distribuídos desigualmente nesses domínios (NEUMANN et al., 2012).

Com o avanço de tecnologias de sequenciamento de nova geração (NGS), ficou cada vez mais acessível a realização de sequenciamentos genômicos de baixa cobertura para a identificação de sequências repetitivas. Dessa forma, um novo campo se abriu para o desenvolvimento de metodologias e programas que facilitem a análise desse montante de sequências geradas. Dentre essas, um programa que vem revelando grande potencial e uso na identificação de sequências repetitivas é o RepeatExplorer (NOVAK et al., 2010; NOVAK et al., 2013). Através de uma análise por agrupamento (ou *clustering*) de sequências semelhantes, esse programa forma *clusters* que são agrupamentos de sequências repetitivas e abundantes no genoma de uma dada espécie. Dessa forma, esse programa pode ser facilmente utilizado através de uma plataforma *online* (repeatexplorer.org) ou até mesmo por linha de comando em Linux e oferece uma caracterização e identificação global das principais sequências repetitivas presentes em um dado genoma. Diversos trabalhos recentes demonstram a versatilidade e utilidade desse programa na identificação e caracterização de sequências repetitivas com diferentes interesses (GONG et al., 2012; MARTIS et al., 2012; NEUMANN et al., 2012; HECKMANN et al., 2013; KLEMME et al., 2013; ZHANG et al., 2014).

A descrição de cenDNA baseada somente na sua localização (peri)centromérica não define se essa sequência está de fato associada com os centrômeros funcionais de uma espécie. Dessa forma, experimentos de colocalização de sequências candidatas com a proteína centromérica CENH3 e imunoprecipitação da cromatina (ChIP) centromérica tem sido aceitos como as formas mais convincentes de validação de cenDNAs (NAGAKI et al., 2003; NAGAKI et al., 2004; NEUMANN et al., 2012; MELTERS et al., 2013). Experimentos de CENH3-ChIP seguidos de PCR ou sequenciamento podem, além de confirmar sequências candidatas, identificar novos cenDNAs que ainda não tinham sido descobertos, sendo uma ferramenta importante na caracterização dos centrômeros funcionais (ver, por exemplo, GONG et al., 2012).

2.2. Cromossomos holocêntricos

A maioria dos organismos estudados possui um único centrômero por cromossomo, formando a constrição primária, sendo referidos como cromossomos monocêntricos (Figura 2a). No entanto, os cromossomos de alguns animais invertebrados e plantas apresentam a formação de cinetócoros dispersos ao longo de quase toda a extensão de cada uma das cromátides-irmãs, sendo chamados de cromossomos holocêntricos (ou holocinéticos) (Figura 2b). Esses cromossomos são identificados normalmente pela ausência de constrição primária e migração paralela das cromátides durante anáfase mitótica (TANAKA; TANAKA, 1977; VANZELA et al., 1996; LUCEÑO et al., 1998). A ocorrência de cromossomos holocêntricos em diversos grupos não relacionados sugere que a “holocentricidade” surgiu independentemente várias vezes por homoplasia (DERNBURG, 2001; GUERRA et al., 2010; MELTERS et al., 2012). Exemplos de organismos que apresentam cromossomos holocêntricos podem ser encontrados em diferentes taxa de animais e vegetais. Entre os animais, esses cromossomos ocorrem em nematoides e em diversas ordens de Arthropoda, como Heteroptera, Homoptera, Odonata, Lepidoptera e na família Buthidae (Arachnida), entre outros exemplos (NOKKALA, 1987; SHANAHAN, 1989; NOKKALA et al., 2002; BONGIORNI et al., 2004; LANZONE; DE SOUZA, 2006). Embora vertebrados sejam um dos grupos mais bem estudado, até o momento não foram encontrados

cromossomos holocêntricos nesses organismos. Em angiospermas, cromossomos holocêntricos são encontrados entre as eudicotiledôneas, tais como *Cuscuta* L. subgênero *Cuscuta* (Convolvulaceae) (PAZY; PLITMANN, 1987; GUERRA; GARCIA, 2004), *Drosera* L. (Droseraceae) (SHEIKH et al., 1995), e em *Myristica fragrans* Houtt. (Myristicaceae) (noz-moscada) (FLACH, 1966), bem como nas monocotiledôneas *Chionographis* (Willd.) Maxim. (Melanthiaceae) (TANAKA; TANAKA, 1977), Juncaceae Juss. e Cyperacae Juss. (MALHEIROS et al., 1947; HAKANSSON, 1958).

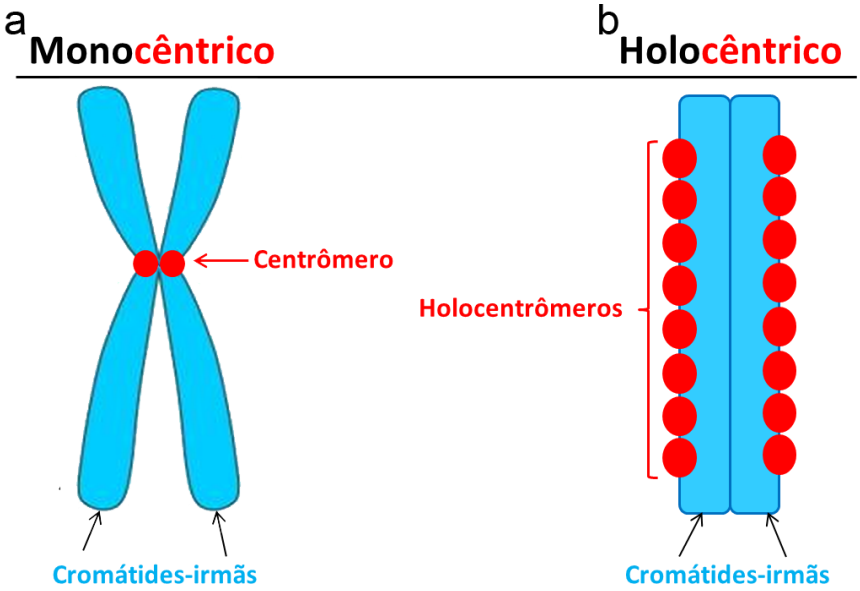

Figura 2. Modelo esquemático de um cromossomo monocêntrico e um holocêntrico

2.2.1. Estrutura dos cromossomos e organização do genoma de espécies com cromossomos holocêntricos

Com o avanço de técnicas citomoleculares e o desenvolvimento de anticorpos específicos, foi possível visualizar que os cromossomos holocêntricos também são caracterizados por apresentarem ligação dos microtúbulos de maneira difusa ao longo de cada cromátide e distribuição da proteína centromérica CENH3 formando uma linha cinetocórica na sua face exterior (BUCHWITZ et al., 1999; STEAR; ROTH, 2004; NAGAKI et al., 2005; GUERRA et al., 2006; HECKMANN et al., 2011). Apenas em insetos foi verificada a perda da CENH3 independentemente em algumas linhagens

(DRINNENBERG et al., 2014). No geral, essas observações mais recentes explicam as observações clássicas da ausência de constrição primária e migração paralela das cromátides-irmãs em anáfase mitótica. Interessantemente, a presença de um sulco cinetocórico em cada uma das cromátides de cromossomos holocêntricos metafásicos co-localizando com a distribuição da CENH3 foi visualizada até o momento somente em espécies do gênero *Luzula* DC. (NAGAKI et al., 2005; HECKMANN et al., 2011), não sendo observada em cromossomos holocêntricos de animais (BUCHWITZ et al., 1999; MADDOX et al., 2004) e de outras plantas (VANZELA et al., 1998; DA SILVA, C. R. M. et al., 2010).

Apesar da observação de uma organização distinta nesses cromossomos, poucos estudos têm sido realizados em plantas com cromossomos holocêntricos. A maioria destes se refere à morfologia cromossômica e sua cinética durante a mitose e meiose, bem como às propriedades da cromatina (GUERRA; GARCIA, 2004; DA SILVA, C. R. M. et al., 2010; GUERRA et al., 2010; HECKMANN et al., 2011). No entanto, pouco se sabe sobre a organização genômica de cromossomos holocêntricos em espécies vegetais. Recentemente, a primeira análise genômica de uma espécie vegetal holocêntrica foi conduzida em *Luzula elegans* Lowe (HECKMANN et al., 2013). Nesse trabalho foi verificado que *L. elegans* apresenta 61% do seu genoma composto por sequências repetitivas, com mais de 30 famílias de sequências distintas e uma alta diversidade de DNA satélite (satDNA). Interessantemente, não foi encontrada nenhuma sequência de DNA, satDNA e/ou retrotransposons centroméricos, com distribuição centromérica. Os autores propuseram um modelo com ausência de cenDNA em cromossomos holocêntricos.

A ausência de cenDNA é proposta mesmo em animais com cromossomos holocêntricos que apresentam seus genomas completamente sequenciados, como é o caso de *Caenorhabditis elegans* Maupas (CONSORTIUM, 1998; GASSMANN et al., 2012; STEINER; HENIKOFF, 2014) e *Bombyx mori* L. (INTERNATIONAL SILKWORM GENOME, 2008; D'ALENCON et al., 2010). Em *C. elegans* foi verificado por CENH3-ChIP que nucleossomos centroméricos não mostram uma associação enriquecida com sequências específicas de DNA (GASSMANN et al., 2012; STEINER; HENIKOFF,

2014). Assim, foi sugerido que sequências específicas centroméricas não existiriam em cromossomos holocêntricos (HECKMANN; HOUBEN, 2013; PLOHL et al., 2014).

A organização do genoma é normalmente evidenciada pela distribuição de marcas epigenéticas, ou seja, modificações pós-traducionais de histonas ou metilação do DNA. Diferentes marcas de histonas, particularmente isoformas metiladas distintas da histona H3, estão associadas à eu- ou heterocromatina (FUCHS et al., 2006). Por exemplo, H3K9me2 é uniformemente distribuída em cromossomos monocêntricos de espécies de plantas com genomas grandes (1C maior que 500 Mbp), enquanto genomas menores como o de *A. thaliana* mostram enriquecimento de H3K9me2 na heterocromatina preferencialmente pericentromérica. Em geral independentemente do tamanho do genoma, H3K4me2 está associado com eucromatina normalmente nas regiões mais distais dos braços cromossômicos na maioria das espécies vegetais. Assim, em cromossomos monocêntricos o tamanho do genoma influencia a distribuição de metilação das histonas associadas com as regiões transcricionalmente menos ativas (HOUBEN et al., 2003; FUCHS et al., 2006). Além do mais, cromossomos mitóticos de *Luzula* (NAGAKI et al., 2005) e de *Rhynchospora tenuis* Link. (GUERRA et al., 2006) se apresentam inteiramente marcados com a histona H3S10/S28 fosforilada de uma forma dependente do ciclo celular, indicando que esses cromossomos apresentam uma estrutura semelhante à região pericentromérica de monocêntricos (HOUBEN et al., 2007). No entanto, estudos sobre a distribuição de marcas de histonas típicas de eu- e heterocromatina em genomas de plantas com cromossomos holocêntricos são escassos. Somente recentemente HECKMANN et al. (2013) realizaram uma caracterização ampla da organização da eu- e heterocromatina nos cromossomos holocêntricos de *L. elegans*. Foi verificado que o genoma dessa espécie apresenta uma distribuição intercalada de modificações de histonas específicas de eu- e heterocromatina. Dessa forma, foi sugerida que a organização centromérica holocinética seria um fator determinante na organização do genoma em curtos trechos de eu- e heterocromatina para espécies com cromossomos holocêntricos. Embora tenha sido sugerido que essa organização seria típica de cromossomos holocêntricos em plantas, os autores destacam que mais estudos comparativos são necessários para

um melhor entendimento da organização do genoma de espécies com cromossomos holocêntricos.

2.3. Meiose em espécies com cromossomos monocêntricos e holocêntricos

Na meiose um único evento de replicação do DNA é seguido por dois eventos de segregação dos cromossomos para gerar produtos haplóides. Em espécies monocêntricas, a coesão das cromátides-irmãs deve ser desfeita em duas etapas durante a meiose: i) ao longo dos braços cromossômicos, liberando os quiasmas e permitindo a segregação reducional durante a meiose I, ii) nas regiões centroméricas-irmãs, permitindo a segregação das cromátides-irmãs durante a anáfase II da meiose. Durante a meiose I, ao contrário da divisão mitótica, o centrômero localizado de cromossomos monocêntricos favorece a coesão dos centrômeros-irmãos que serve para co-orientar as cromátides-irmãs na meiose I e proteger as coesinas contra a degradação antes da anáfase II (SAKUNO; WATANABE, 2009). Dessa forma, durante a anáfase I ocorre a segregação dos cromossomos homólogos para polos opostos, enquanto as cromátides-irmãs migram para o mesmo lado devido à coesão dos centrômeros-irmãos (Figura 3a).

Organismos com cromossomos holocêntricos não possuem um centrômero localizado para regular a co-orientação das cromátides-irmãs e as duas etapas de perda de coesão durante a meiose. Por isso, cromossomos holocêntricos apresentariam problemas durante a meiose, se a mesma fosse semelhante à de cromossomos monocêntricos (MELTERS et al., 2012; HECKMANN; HOUBEN, 2013) (Figura 3b-e). A conexão física mediada pelo *crossing-over* entre homólogos precisa ser resolvida adequadamente para permitir a divisão reducional de bivalentes. Em monocêntricos, durante a meiose I, a proteção da coesão entre os centrômeros de cromátides-irmãs é realizada por membros da família de proteínas MEI-S332/Shugoshin e Spo13. Essas proteínas estão associadas aos domínios peri- e/ou centroméricos dos cromossomos, onde inibem a degradação da Rec8, uma coesina específica da meiose, durante a transição metáfase I/anáfase I. A resolução dos quiasmas e separação dos

homólogos baseia-se na liberação da coesina ao longo dos braços cromossômicos, permitindo então a separação dos cromossomos homólogos na anáfase I. Durante a meiose II a coesão entre os cinetócoros-irmãos ainda é mantida pelo complexo MEI-S332/Shugoshin e Spo13, que previnem a degradação da coesina Rec8 residual. Finalmente, em anáfase II com a dissociação do complexo MEI-S332/Shugoshin, a coesão centromérica garantida pela Rec8 fica exposta à degradação pela separase, levando à separação das cromátides-irmãs (MARSTON; AMON, 2004; ISHIGURO; WATANABE, 2007; DURO; MARSTON, 2015). Nos cromossomos holocêntricos, entretanto, as fibras do fuso de polos diferentes se ligariam em cada lado de um quiasma e puxariam cada cromátide recombinada para ambos os polos. Para lidar com este problema, as espécies com cromossomos holocêntricos exibem apenas um ou dois quiasmas por bivalente (NOKKALA et al., 2004), preferencialmente em posições distais, e modificações na sequência dos eventos da meiose (MELTERS et al., 2012). Além do mais, a dificuldade de se obter a co-orientação dos centrômeros-irmãos na meiose I exige que adaptações apareçam durante a meiose de organismos com cromossomos holocêntricos (Figura 3).

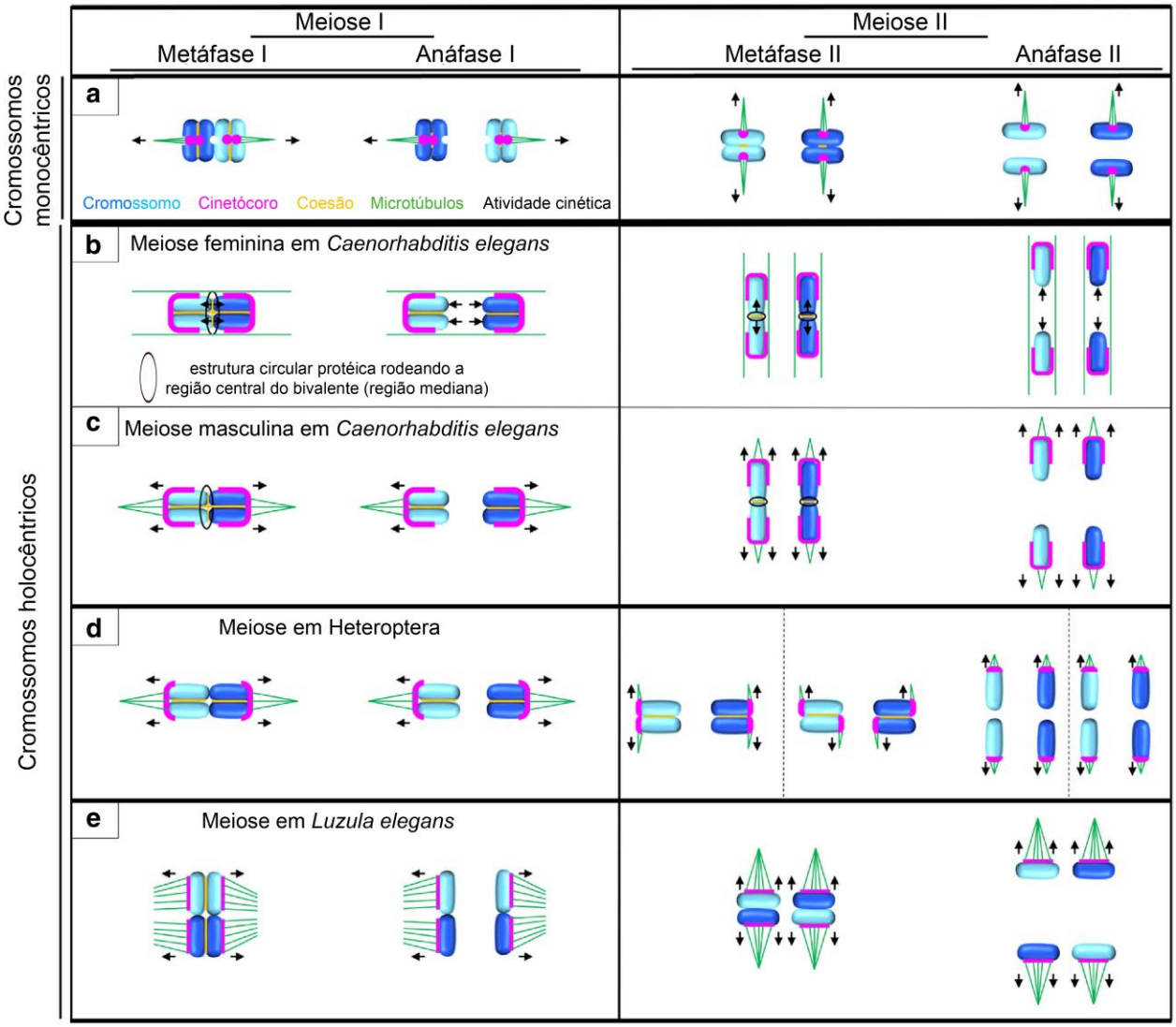

Figura 3. Modelo esquemático da meiose em espécies com cromossomos monocêntricos e de adaptações meióticas em espécies com cromossomos holocêntricos. (a) Cromossomos monocêntricos: cromátides irmãs mono-orientadas em metáfase I via cinetócoros irmãos fundidos, permitindo a segregação dos cromossomos homólogos, ao passo que na metáfase II cromátides irmãs bi-orientadas segregam uma das outras. (b-e) Cromossomos holocêntricos: Existem várias opções para lidar com uma arquitetura holocêntrica durante a meiose: (b, c) remodelação cromossômica, (d) cromossomos funcionalmente monocêntricos e (e) “segregação invertida de cromátides”. Modelo adaptado de HECKMANN et al. (2014).

2.3.1. Tipos de meiose observada em espécies com cromossomos holocêntricos

O que se sabe sobre meiose em espécies com cromossomos holocêntricos é principalmente baseado em descrições de microscopia clássica em algumas plantas, como em *L. elegans* (NORDENSKIÖLD, 1962; KUSANAGI, 1973), *Rhynchospora pubera* (Vahl) Boeckeler (GUERRA et al., 2010), *Eleocharis* R. Br. (HAKANSSON, 1954; DA SILVA, C. R. M. et al., 2005; DA SILVA, C. R. et al., 2008), diferentes espécies do gênero *Cuscuta* (PAZY; PLITMANN, 1987; GUERRA; GARCIA, 2004), *Chionographis* (TANAKA; TANAKA, 1980) e *Carex* L. (HOSHINO; OKAMURA, 1994; HOSHINO; WATERWAY, 1994), bem como em espécies animais (NOKKALA et al., 2004; VIERA et al., 2009). Estudos moleculares na meiose de espécies com cromossomos holocêntricos foram realizados principalmente em nematoides, como em *C. elegans* (HOWE et al., 2001; MONEN et al., 2005; WIGNALL; VILLENEUVE, 2009; SCHVARZSTEIN et al., 2010; LUI; COLAIACOVO, 2013). Somente recentemente foi realizado um estudo mais aprofundado na meiose de uma espécie vegetal com cromossomos holocêntricos (HECKMANN et al., 2014). Nesse estudo, foi verificado que os holocentrômeros em forma de linha de *L. elegans* persistem durante toda a meiose e que a ausência de co-orientação dos centrômeros-irmãos na metáfase I/anáfase I faz com que as cromátides-irmãs separem durante a anáfase I e somente ocorrendo segregação dos homólogos durante a anáfase II.

Existem algumas maneiras para a meiose ocorrer em espécies com cromossomos holocêntricos (ver Tabela 1). Em *C. elegans*, cromossomos holocêntricos sofrem uma remodelagem cromossômica (*chromosome remodelling*) durante a meiose. Cromossomos formam um único quiasma por bivalente, o qual causa a redistribuição de proteínas ao longo do eixo do bivalente, criando subdomínios que definem a região de remoção e proteção da coesão durante a meiose I (MARTINEZ-PEREZ et al., 2008). Os componentes cinetocóricos cobrem uniformemente cada metade do bivalente, mas são excluídos da região quiasmática mediana. Os bivalentes são então cercados por feixes de microtúbulos ao longo de suas laterais, no entanto a densidade de microtúbulos é extremamente baixa nos terminais cromossômicos embora haja uma alta concentração de proteínas cinetocóricas nessas regiões (WIGNALL; VILLENEUVE, 2009). Durante

anáfase I da meiose feminina microtúbulos se formam na região mediana dos bivalentes entre os cromossomos homólogos de forma independente de proteínas cinetocóricas (DUMONT et al., 2010). Cromátides-irmãs permanecem ligadas por um terminal cromossômico e são separadas durante a segunda divisão meiótica (ALBERTSON; THOMSON, 1993; MARTINEZ-PEREZ et al., 2008; DUMONT et al., 2010) (Figura 3b-c). Na meiose de insetos Heteroptera, cromossomos holocêntricos agem como monocêntricos, em que os microtúbulos se ligam a uma região terminal restrita no cromossomo (VIERA et al., 2009). Assim, ocorre uma separação dos cromossomos homólogos durante a meiose I e das cromátides-irmãs durante a meiose II (Figura 3d).

Alternativamente, para algumas espécies com cromossomos holocêntricos bivalentes alinhariam em metáfase I de tal forma que as cromátides-irmãs separariam em anáfase I. Assim, a primeira divisão meiótica seria equacional e a segunda [depois de associação *de novo* das cromátides homólogas (também denominadas de "cromátides homólogas não-irmãs")] seria reducional (Figura 3e). Isto representa uma sequência invertida de eventos meióticos comparado com a sequência reducional-equacional típica observada em organismos com cromossomas monocêntricos (MELTERS et al., 2012). Diferentes evidências têm levado autores a sugerirem a ocorrência de meiose invertida em organismos com cromossomos holocêntricos. Por exemplo, a observação de um número cromossômico diploide depois da primeira divisão meiótica e/ou ausência de bivalentes tem sido utilizada como indicação de meiose invertida em espécies de Cyperaceae (VANZELA et al., 1996; DA SILVA, C. R. M. et al., 2005). Em espécies do gênero *Luzula* (Juncaceae), a observação de uma separação precoce das cromátides-irmãs e migração paralela em anáfase I também foi um indicativo de meiose invertida (NORDENSKIÖLD, 1962). Em espécies de Odonota a indicação de meiose invertida se baseou principalmente na presença de um par heteromórfico de cromossomos sexuais e a observação de orientação equatorial desses bivalentes em metáfase I e a conseguinte presença de cromátides heteromórficas em metáfase II (MOLA, 1995). Uma combinação das evidências descritas acima foi observada na cochonilha *Planococcus citri* e levaram BONGIORNI

et al. (2004) a concluir que a meiose feminina e masculina dessa espécie também é invertida ou pós-reducional. Além dessas espécies, meiose invertida também é sugerida para vários outros organismos com cromossomos holocêntricos (Tabela 1 e recentemente revisado por MELTERS et al., 2012).

MALHEIROS et al. (1947) observaram em *Luzula purpurea* (sinonímia para *L. elegans*), uma espécie de Juncaceae que possui apenas três pares de cromossomos grandes, que as cromátides parecem ser puxadas para os polos pelas extremidades, tanto na meiose I quanto na meiose II. No entanto, em outro trabalho posterior utilizando a mesma espécie, esse comportamento não foi observado e as cromátides-irmãs parecem separar paralelamente em anáfase I, apresentando uma sequência invertida dos eventos meióticos (KUSANAGI, 1973). Nos últimos anos, o estudo dos cromossomos holocêntricos em animais tem avançado bastante, principalmente em relação à meiose (SCHVARZSTEIN et al., 2010). Em vegetais, esses estudos têm se restringido à análise mitótica, estando relacionados principalmente à estrutura cromossômica (NAGAKI et al., 2005; GUERRA et al., 2006; HECKMANN et al., 2011). Recentemente, foi possível verificar em *Luzula elegans* um comportamento holocêntrico dos cromossomos durante toda a meiose I e II e, em contraste com a orientação monopolar de centrômeros-irmãos, os holocentrômeros não-fusionados se comportam como duas unidades funcionais distintas durante meiose I, resultando na separação das cromátides-irmãs. Cromátides-homólogas permanecem terminalmente conectadas depois de metáfase I até metáfase II, separando-se somente em anáfase II (HECKMANN et al., 2014). Assim, os autores concluíram que ocorre uma sequência invertida dos processos meióticos nessa espécie. Entretanto, ainda restam dúvidas se a meiose invertida seria um evento comum entre organismos com cromossomos holocêntricos (NOKKALA et al., 2002), tendo em vista que teria surgido independentemente em diferentes linhagens com cromossomos holocêntricos.

Tabela 1. Tipos de adaptações meióticas e organização cinetocórica durante a mitose e meiose de espécies com cromossomos holocêntricos.

Grupo	Nome científico	Tipo de meiose	Organização cinetocórica na mitose	Organização cinetocórica na meiose	Referência
Juncaceae	*Luzula*	pós-reducional (invertida)	placa cinetocórica estendida	placa cinetocórica estendida, similar à mitose	BRASELTON, (1971; 1981), HECKMANN et al. (2014)
Cyperaceae	*Cyperus*	-	placa cinetocórica estendida	-	BRASELTON (1971)
	Rhynchospora	pós-reducional (invertida) ?	-	-	CABRAL (2010)
Nematoda	*Caenorhabditis elegans*	remodelagem cromossômica - reducional	placa cinetocórica estendida	ausência de placa cinetocórica	ALBERTSON; THOMSON (1982; 1993), MONEN et al. (2005)
	Parascaris univalens	meiose telocinética - reducional	placa cinetocórica estendida	ausência de placa cinetocórica	GODAY et al. (1985), GODAY; PIMPINELLI (1989)
Insetos*					
Hemiptera	*Planococcus citri* (**Homoptera**)	pós-reducional (invertida)	-	-	BONGIORNI et al. (2004)
	Puto albicans (**Homoptera**)	pós-reducional (invertida)	-	-	BROWN; CLEVELAND (1968)
	Oncopeltus fasciatus (**Heteroptera**)	meiose telocinética - reducional, pós-reducional somente para os cromossomos sexuais	placa cinetocórica estendida	ausência de placa cinetocórica	WOLFE; JOHN (1965), COMINGS; OKADA (1972)
	Graphosoma italicum (**Heteroptera**)	meiose telocinética - reducional, pós-reducional somente para os cromossomos sexuais	placa cinetocórica estendida	ausência de placa cinetocórica	RUFAS; GIMENEZ-MARTIN (1986), GONZÁLEZ-GARCÍA et al. (1996)
	Triatoma infestans (**Heteroptera**)	meiose telocinética - reducional, pós-reducional somente para os cromossomos sexuais	-	-	PEREZ et al. (1997), PEREZ et al. (2000)
Odonata	*Aeshna*	pós-reducional (invertida)	-	-	MOLA (1995)
	Somatochlora metallica	reductional	-	-	NOKKALA et al. (2002)
Lepdoptera	*Bombyx mori*	-	-	ausência de placa cinetocórica	FRIEDLANDER; WAHRMAN (1970), MURAKAMI; IMAI (1974)
Arachnida	*Tityus bahiensis*	-	placa cinetocórica estendida	evidência de placa cinetocórica	BENAVENTE (1982)

*Insetos com cromossomos holocêntricos são desprovidos de CENH3 e CENP-C (DRINNENBERG et al., 2014)

2.4. Estrutura centromérica durante a meiose em espécies com cromossomos holocêntricos

Durante a meiose, foi encontrada em várias espécies com cromossomos holocêntricos uma estrutura centromérica diferente (Tabela 1). Em *C. elegans*, os cromossomos mitóticos apresentam formação de uma placa cinetocórica trilaminar que se estende ao longo de cada cromátide (ALBERTSON; THOMSON, 1982). No entanto, durante a meiose não é observado formação de placa cinetocórica (ALBERTSON; THOMSON, 1993) e a segregação dos homólogos envolve um mecanismo de remodelagem cromossômica independente de CENH3 e CENP-C (MONEN et al., 2005) em que os cromossomos são envolvidos por feixes de microtúbulos que correm lateralmente ao longo dos lados de cada cromátide (WIGNALL; VILLENEUVE, 2009; SCHVARZSTEIN et al., 2010). O nematoide holocêntrico *Parascaris univaIens* Hertwig sofre restrição da atividade cinética somente nas regiões heterocromáticas terminais durante a meiose masculina. Essas regiões carecem de placas cinetocóricas longas, mas interagem diretamente com os feixes de microtúbulos (GODAY; PIMPINELLI, 1989; PIMPINELLI; GODAY, 1989). Em insetos holocêntricos da ordem Heteroptera, foi reportada uma atividade cinética localizada durante a meiose I e II, em contraste com a atividade dispersa observada em mitose (PEREZ et al., 2000; PAPESCHI et al., 2003). No hemiptera *Oncopeltus fasciatus* Dallas, a presença de uma placa cinetocórica holocinética durante a mitose, mas a sua ausência durante a meiose, foi concluída baseado em estudos de microscopia eletrônica. Múltiplos sítios de ligação de microtúbulos foram observados diretamente na cromatina dos cromossomos meióticos dessa espécie (COMINGS; OKADA, 1972).

Achados similares foram reportados para outros organismos com cromossomos holocêntricos, como por exemplo, para os nematoides *Ascaris lumbricoides* L. (GOLDSTEIN, 1977) e *P. univalens* (GODAY; PIMPINELLI, 1989; PIMPINELLI; GODAY, 1989), os hemipteras *Rhodnius prolixus* Stal (BUCK, 1967) e *Graphosoma italicum* L. (RUFAS; GIMENEZ-MARTIN, 1986) e o lepdoptera *Bombyx mori* (FRIEDLANDER; WAHRMAN, 1970). Adicionalmente, no escorpião holocêntrico *Tityus bahiensis* Perty uma placa cinetocórica foi encontrada durante toda a meiose, enquanto

nas aranhas *Dysdera crocata* C. L. Koch e *Segestria florentina* Rossi placas cinetocóricas foram observadas somente durante a meiose II (BENAVENTE, 1982). Assim, a ausência de uma placa cinetocórica durante a meiose parece ocorrer frequentemente dentre organismos com cromossomos holocêntricos e foi postulado como sendo relacionado à restrição da atividade cinetocórica e à terminalização dos quiasmas nesses organismos (COMINGS; OKADA, 1972; PIMPINELLI; GODAY, 1989). No entanto, na espécie de planta *Luzula elegans* foi reportado uma estrutura holocinética dos cromossomos não somente em mitose, mas também durante toda a meiose I e II (BRASELTON, 1971;1981; HECKMANN et al., 2014). É interessante notar que em *L. elegans* a meiose é invertida ao contrário das espécies anteriormente citadas (Tabela 1). Dessa forma, a organização dos centrômeros na meiose de espécies com cromossomos holocêntricos parece estar relacionada com tipo de adaptação meiótica apresentado por esses organismos.

2.5. Citogenética do gênero *Rhynchospora*

O gênero *Rhynchospora* Vahl, assim como outros gêneros da família Cyperaceae, caracteriza-se pela presença de cromossomos holocêntricos e tem sido bem estudado citogeneticamente há mais de duas décadas (GUERRA, 1993; VANZELA et al., 1996; LUCEÑO et al., 1998; VANZELA et al., 1998; VANZELA, 2000; VANZELA; GUERRA, 2000; VANZELA et al., 2003; GUERRA et al., 2006; GUERRA et al., 2010; ARGUELHO et al., 2012). A descrição e caracterização dos cromossomos holocêntricos deste grupo foi baseada principalmente na ausência de constrição primária, migração paralela das cromátides-irmãs em anáfase e distribuição dos microtúbulos do fuso mitótico ao longo de cada cromátide-irmã (VANZELA et al., 1996; LUCEÑO et al., 1998; GUERRA et al., 2006). O número cromossômico básico proposto para o gênero é $x = 5$, havendo números básicos secundários $x = 9$ e $x = 6$ ou 12 (LUCEÑO et al., 1998).

Dentre as espécies do gênero, *R. tenuis* Vahl, por ter o menor número cromossômico da família ($2n = 4$), e *R. pubera* (Vahl) Böckeler, por apresentar cromossomos grandes ($2n = 10$) (VANZELA et al., 1996; LUCEÑO et al., 1998), podem

ser consideradas como bons modelos citológicos. *Rhynchospora tenuis* possui um par cromossômico de maior tamanho (6,8 µm) e um menor (4,4 µm) (VANZELA et al., 1996), com sítios de DNA ribossomal (DNAr) 45S em uma das regiões terminais do par menor e sítios intersticiais de DNAr 5S no par maior (VANZELA et al., 2003; SOUSA et al., 2011). *Rhynchospora pubera* possui cromossomos com tamanho variando de 3.8 µm a 6.3 µm (LUCEÑO et al., 1998), com sítios de DNAr 45S uma das regiões terminais de três pares e sítios de DNAr 5S terminais e intersticiais em quatro pares cromossômicos (VANZELA et al., 1998; SOUSA et al., 2011).

2.5.1 A meiose de *Rhynchospora*

Estudos anteriores observaram a ausência de bivalentes em *R. tenuis* (*n* = 2), ocorrendo apenas univalentes em ambos os citótipos diploide e tetraploide (VANZELA et al., 1996; CABRAL, 2008;2010), o que, no entanto, não foi observado em outras espécies do gênero (LUCEÑO et al., 1998). Além disso, algumas características até agora únicas em plantas com holocêntricos também foram observadas em *R. tenuis* (CABRAL, 2008;2010). A associação ponta-a-ponta entre cromossomos homólogos no paquíteno/zigóteno e a presença de univalentes de diplóteno a metáfase I sugerem que a meiose de *R. tenuis* seja assináptica e aquiasmática. Durante a metáfase I, os quatro univalentes se reuniram na placa equatorial em conformação cruzada. Na anáfase I, foi observada a divisão longitudinal dos quatro univalentes, resultando em dois grupos de quatro cromátides migrando de forma espelhar para cada pólo, sugerindo a segregação de cromátides-irmãs (CABRAL, 2008;2010). A orientação bipolar das cromátides-irmãs nos univalentes evidenciada pela ligação dos microtúbulos, vindo de lados opostos, reforça essa interpretação (CABRAL, 2010). A conformação cruzada foi observada novamente durante prófase II e metáfase II. Finalmente, em anáfase II ocorreu a separação de duas cromátides para cada polo (CABRAL, 2008;2010). A ausência de quiasmas e a formação de univalentes na meiose de *R. tenuis* sugere que a meiose desta espécie seja invertida, uma vez que os quiasmas são essenciais à orientação monopolar dos cinetócoros-irmãos.

A meiose de *R. pubera* (*n* = 5) apresentou uma prófase I semelhante à prófase I de cromossomos monocêntricos, enquanto que a partir de metáfase I em diante há várias diferenças em relação à meiose monocêntrica (CABRAL, 2008;2010; GUERRA et al., 2010). Nos núcleos zigotênicos, os cromossomos homólogos pareceram intimamente pareados, com apenas pequenos trechos despareados, o que sugere um pareamento regular entre os homólogos. A meiose de *R. pubera* foi do tipo quiasmática e durante a diacinese foi observada a formação de cinco bivalentes, cada um com um a dois quiasmas terminais ou subterminais, assumindo forma de bastão ou anel. Na metáfase I, os bivalentes apresentaram forma globosa a ovalada ou então a forma de haltere. A orientação dos bivalentes no plano equatorial foi variável, tendo sido encontrados bivalentes em haltere com orientação equatorial (eixo maior paralelo ao plano equatorial) ou axial (eixo maior perpendicular ao plano equatorial) (GUERRA et al., 2010). As cromátides-irmãs apresentaram ligação anfitélica com o fuso na metáfase I aparentemente em uma região intersticial, indicando a ocorrência de segregação equacional na anáfase I e consequentemente de meiose invertida (CABRAL, 2010). Durante anáfase I, as cromátides apresentaram frequentemente forma alongada, sugerindo que a atividade cinetocórica estaria ocorrendo em uma região restrita da cromátide. Em anáfase I, as duas cromátides que migraram para polos opostos não estavam fortemente associadas e fios de ligação conectando algumas cromátides foram observados. Na prófase II, 10 cromátides individualizadas foram distinguidas em cada polo, que foram reunidas novamente em metáfase II. Na anáfase II, ocorreu a separação dos pares de cromátides, migrando cinco cromátides para cada polo. Esses cinco cromossomos foram ainda observados em cada um dos quatro núcleos da telófase II (CABRAL, 2008;2010; GUERRA et al., 2010). As peculiaridades observadas na meiose de *R. pubera* sugerem que esta espécie possua meiose invertida. No entanto, devido à dificuldade de se distinguir cromátides-irmãs de cromátides-homólogas, a validação dessa hipótese permaneceu em aberto. Além do mais, a falta de marcas centroméricas limitou uma caracterização compreensiva dos cromossomos mitóticos e meióticos nas espécies desse gênero.

3. Referências

AKIYOSHI, B.; GULL, K. Discovery of unconventional kinetochores in kinetoplastids. **Cell,** v. 156, n. 6, p. 1247-58, 2014.

ALBERTSON, D. G.; THOMSON, J. N. The kinetochores of *Caenorhabditis elegans*. **Chromosoma,** v. 86, n. 3, p. 409-28, 1982.

_____. Segregation of holocentric chromosomes at meiosis in the nematode, *Caenorhabditis elegans*. **Chromosome Research,** v. 1, n. 1, p. 15-26, 1993.

ARGUELHO, E. G. et al. New chromosome counts in Brazilian species of *Rhynchospora* (Cyperaceae). **Caryologia,** v. 65, p. 140-146, 2012.

BASSETT, E. A. et al. Epigenetic centromere specification directs aurora B accumulation but is insufficient to efficiently correct mitotic errors. **Journal of Cell Biology,** v. 190, n. 2, p. 177-85, 2010.

BENAVENTE, R. Holocentric chromosomes of arachnids: Presence of kinetochore plates during meiotic divisions. **Genetica,** v. 59, n. 1, p. 23-27, 1982.

BLACK, B. E. et al. Structural determinants for generating centromeric chromatin. **Nature,** v. 430, n. 6999, p. 578-82, 2004.

BÖHNE, A. et al. Transposable elements as drivers of genomic and biological diversity in vertebrates. **Chromosome Research,** v. 16, n. 1, p. 203-15, 2008.

BONGIORNI, S. et al. Inverted meiosis and meiotic drive in mealybugs. **Chromosoma,** v. 112, n. 7, p. 331-341, 2004.

BRASELTON, J. P. Ultrastructure of non-localized kinetochores of *Luzula* and *Cyperus*. **Chromosoma,** v. 36, n. 1, p. 89-99, 1971.

_____. The ultrastructure of meiotic kinetochores of *Luzula*. **Chromosoma,** v. 82, n. 1, p. 143-151, 1981.

BROWN, S. W.; CLEVELAND, C. Meiosis in the male of *Puto albicans* (Coccoidea-Homoptera). **Chromosoma,** v. 24, n. 2, p. 210-232, 1968.

BUCHWITZ, B. J. et al. A histone-H3-like protein in *C. elegans*. **Nature,** v. 401, n. 6753, p. 547-8, 1999.

BUCK, R. C. Mitosis and meiosis in *Rhodnius prolixus*: the fine structure of the spindle and diffuse kinetochore. **Journal of Ultrastructural Research,** v. 18, n. 5, p. 489-501, 1967.

BURES, P.; ZEDEK, F.; MARKOVA, M. Holocentric chromosomes. In: GREILHUBER, J.;DOLEZEL, J.*, et al* (Ed.). **Plant Genome Diversity**. Vienna: Springer-Verlag Wien, v.Volume 2, 2013. ISBN 978-3-7091-1160-4.

CABRAL, C. C. G. **Comportamento dos cromossomos holocinéticos em espécies de *Rhynchospora* (Cyperaceae) com meiose quiasmática e aquiasmática**. 2008. 71 Graduação (Graduação). Departamento de Botânica, Universidade Federal de Pernambuco, Recife.

_____. **Meiose invertida quiasmática e aquiasmática em plantas com cromossomos holocinéticos**. 2010. 64 Mestrado (Mestrado). Departamento de Botânica, Universidade Federal de Pernambuco, Recife.

CARROLL, C. W.; MILKS, K. J.; STRAIGHT, A. F. Dual recognition of CENP-A nucleosomes is required for centromere assembly. **Journal of Cell Biology,** v. 189, n. 7, p. 1143-55, 2010.

CHEERAMBATHUR, D. K.; DESAI, A. Linked in: formation and regulation of microtubule attachments during chromosome segregation. **Current Opinion in Cell Biology,** v. 26, p. 113-22, 2014.

CHEN, Y. et al. The N terminus of the centromere H3-like protein Cse4p performs an essential function distinct from that of the histone fold domain. **Molecular and Cell Biology,** v. 20, n. 18, p. 7037-48, 2000.

CHENG, Z. et al. Functional rice centromeres are marked by a satellite repeat and a centromere-specific retrotransposon. **Plant Cell,** v. 14, n. 8, p. 1691-704, 2002.

CLARKE, L.; CARBON, J. The structure and function of yeast centromeres. **Annual Reviews of Genetics,** v. 19, p. 29-55, 1985.

COMINGS, D. E.; OKADA, T. A. Holocentric chromosomes in *Oncopeltus*: kinetochore plates are present in mitosis but absent in meiosis. **Chromosoma,** v. 37, n. 2, p. 177-92, 1972.

CONSORTIUM, T. *C. E.* S. Genome sequence of the nematode *C. elegans*: A platform for investigating biology. **Science,** v. 282, n. 5396, p. 2012-2018, 1998.

D'ALENCON, E. et al. Extensive synteny conservation of holocentric chromosomes in Lepidoptera despite high rates of local genome rearrangements. **Proceedings of the National Academy of Sciences of the USA,** v. 107, n. 17, p. 7680-5, 2010.

DA SILVA, C. R.; GONZALEZ-ELIZONDO, M. S.; VANZELA, A. L. L. Chromosome reduction in *Eleocharis maculosa* (Cyperaceae). **Cytogenetic and Genome Research,** v. 122, n. 2, p. 175-80, 2008.

DA SILVA, C. R. M.; GONZALEZ-ELIZONDO, M. S.; VANZELA, A. L. L. Reduction of chromosome number in *Eleocharis subarticulata* (Cyperaceae) by multiple translocations. **Botanical Journal of the Linnean Society,** v. 149, n. 4, p. 457-464, 2005.

DA SILVA, C. R. M.; QUINTAS, C. C.; VANZELA, A. L. L. Distribution of 45S and 5S rDNA sites in 23 species of *Eleocharis* (Cyperaceae). **Genetica,** v. 138, n. 9-10, p. 951-957, 2010.

DERNBURG, A. F. Here, there, and everywhere: kinetochore function on holocentric chromosomes. **Journal of Cell Biology,** v. 153, n. 6, p. 33-38, 2001.

DORN, J. F.; MADDOX, P. S. Kinetochore dynamics: how protein dynamics affect chromosome segregation. **Current Opinion in Cell Biology,** v. 24, n. 1, p. 57-63, 2012.

DRINNENBERG, I. A. et al. Recurrent loss of CenH3 is associated with independent transitions to holocentricity in insects. **Elife,** v. 3, p. e03676, 2014.

DUMONT, J.; OEGEMA, K.; DESAI, A. A kinetochore-independent mechanism drives anaphase chromosome separation during acentrosomal meiosis. **Nature Cell Biology,** v. 12, n. 9, p. 894-901, 2010.

DURO, E.; MARSTON, A. L. From equator to pole: splitting chromosomes in mitosis and meiosis. **Genes and Development,** v. 29, n. 2, p. 109-22, 2015.

EARNSHAW, W. C. Discovering centromere proteins: from cold white hands to the A, B, C of CENPs. **Nature Reviews Molecular Cell Biology,** v. 16, n. 7, p. 443-9, 2015.

EARNSHAW, W. C. et al. Esperanto for histones: CENP-A, not CenH3, is the centromeric histone H3 variant. **Chromosome Research,** v. 21, n. 2, p. 101-6, 2013.

FALK, S. J. et al. CENP-C reshapes and stabilizes CENP-A nucleosomes at the centromere. **Science,** v. 348, n. 6235, p. 699-703, 2015.

FLACH, M. Diffuse centromeres in a dicotyledonous plant. **Nature,** v. 209, n. 5030, p. 1369-&, 1966.

FRIEDLANDER, M.; WAHRMAN, J. The spindle as a basal body distributor. A study in the meiosis of the male silkworm moth, *Bombyx mori*. **Journal of Cell Science,** v. 7, n. 1, p. 65-89, 1970.

FUCHS, J. et al. Chromosomal histone modification patterns--from conservation to diversity. **Trends in Plant Science,** v. 11, n. 4, p. 199-208, 2006.

GASSMANN, R. et al. An inverse relationship to germline transcription defines centromeric chromatin in *C. elegans*. **Nature,** v. 484, n. 7395, p. 534-7, 2012.

GODAY, C.; CIOFI-LUZZATTO, A.; PIMPINELLI, S. Centromere ultrastructure in germ-line chromosomes of *Parascaris*. **Chromosoma,** v. 91, n. 2, p. 121-125, 1985.

GODAY, C.; PIMPINELLI, S. Centromere organization in meiotic chromosomes of *Parascaris univalens*. **Chromosoma,** v. 98, n. 3, p. 160-6, 1989.

GOLDSTEIN, P. Spermatogenesis and spermiogenesis in *Ascaris lumbricoides* Var. suum. **Journal of Morphology,** v. 154, n. 3, p. 317-37, 1977.

GONG, Z. et al. Repeatless and repeat-based centromeres in potato: implications for centromere evolution. **Plant Cell,** v. 24, n. 9, p. 3559-74, 2012.

GONZÁLEZ-GARCÍA, J. M. et al. Meiosis in holocentric chromosomes: kinetic activity is randomly restricted to the chromatid ends of sex univalents in *Graphosoma italicum* (Heteroptera). **Chromosome Research,** v. 4, n. 2, p. 124-32, 1996.

GUERRA, M. Cytogenetics of Rutaceae V: High chromosomal variability in *Citrus* species revealed by CMA/DAPI staining. **Heredity,** v. 71, p. 234-241, 1993.

GUERRA, M. et al. Mitotic microtubule development and histone H3 phosphorylation in the holocentric chromosomes of *Rhynchospora tenuis* (Cyperaceae). **Genetica,** v. 126, n. 1-2, p. 33-41, 2006.

GUERRA, M. et al. Neocentrics and holokinetics (holocentrics): chromosomes out of the centromeric rules. **Cytogenetic and Genome Research,** v. 129, n. 1-3, p. 82-96, 2010.

GUERRA, M.; GARCIA, M. A. Heterochromatin and rDNA sites distribution in the holocentric chromosomes of *Cuscuta approximata* Bab. (Convolvulaceae). **Genome,** v. 47, n. 1, p. 134-40, 2004.

HAIZEL, T. et al. Molecular analysis of holocentric centromeres of *Luzula* species. **Cytogenetic and Genome Research,** v. 109, n. 1-3, p. 134-143, 2005.

HAKANSSON, A. Meiosis and pollen mitosis in X-rayed and untreated spikelets of *Eleocharis palustris*. **Hereditas,** v. 40, n. 3-4, p. 325-345, 1954.

_____. Holocentric Chromosomes in *Eleocharis*. **Hereditas,** v. 44, n. 4, p. 531-540, 1958.

HECKMANN, S.; HOUBEN, A. Holokinetic centromeres. In: JIANG, J. e BIRCHLER, J. A. (Ed.). **Plant Centromere Biology**. Oxford, UK: Wiley-Blackwell, 2013. cap. 7, p.83-94. ISBN 978-1-119-94921-3.

HECKMANN, S. et al. Alternative meiotic chromatid segregation in the holocentric plant *Luzula elegans*. **Nature Communications,** v. 5, p. 4979, 2014.

HECKMANN, S. et al. The holocentric species *Luzula elegans* shows interplay between centromere and large-scale genome organization. **Plant Journal,** v. 73, n. 4, p. 555-65, 2013.

HECKMANN, S. et al. Holocentric chromosomes of *Luzula elegans* are characterized by a longitudinal centromere groove, chromosome bending, and a terminal nucleolus organizer region. **Cytogenetic and Genome Research,** v. 134, n. 3, p. 220-228, 2011.

HENIKOFF, S.; DALAL, Y. Centromeric chromatin: what makes it unique? **Current Opinion in Genetics and Development,** v. 15, n. 2, p. 177-84, 2005.

HENIKOFF, S.; SMITH, M. M. Histone variants and epigenetics. **Cold Spring Harbor Perspectives Biology,** v. 7, n. 1, p. a019364, 2015.

HIPP, A. L.; ESCUDERO, M.; CHUNG, K.-S. **Holocentric chromosomes**. Brenner's Encyclopedia of Genetics. BRENNER, S. e MILLER, J. H.: Elsevier. 3**:** 499-501 p. 2013.

HOSHINO, T.; OKAMURA, K. Cytological studies on meiotic configurations of intraspecific aneuploids of *Carex blepharicarpa* (Cyperaceae) in Japan. **Journal of Plant Research,** v. 107, n. 1, p. 1-8, 1994.

HOSHINO, T.; WATERWAY, M. J. Cytogeography and meiotic chromosome configurations of six intraspecific aneuploids of *Carex conica* Boott (Cyperaceae) in Japan. **Journal of Plant Research,** v. 107, n. 2, p. 131-138, 1994.

HOUBEN, A. et al. Phosphorylation of histone H3 in plants - a dynamic affair. **Biochimica et Biophysica Acta,** v. 1769, n. 5-6, p. 308-315, 2007.

HOUBEN, A. et al. Methylation of histone H3 in euchromatin of plant chromosomes depends on basic nuclear DNA content. **Plant Journal,** v. 33, n. 6, p. 967-973, 2003.

HOUBEN, A.; SCHUBERT, I. DNA and proteins of plant centromeres. **Current Opinion in Plant Biology,** v. 6, n. 6, p. 554-60, 2003.

HOWE, M. et al. HIM-10 is required for kinetochore structure and function on *Caenorhabditis elegans* holocentric chromosomes. **Journal of Cell Biology,** v. 153, n. 6, p. 1227-38, 2001.

INTERNATIONAL SILKWORM GENOME, C. The genome of a lepidopteran model insect, the silkworm *Bombyx mori*. **Insect Biochemistry and Molecular Biology,** v. 38, n. 12, p. 1036-45, 2008.

ISHIGURO, K.; WATANABE, Y. Chromosome cohesion in mitosis and meiosis. **Journal of Cell Science,** v. 120, n. Pt 3, p. 367-9, 2007.

KALITSIS, P.; CHOO, K. H. The evolutionary life cycle of the resilient centromere. **Chromosoma,** v. 121, n. 4, p. 327-40, 2012.

KATO, H. et al. A conserved mechanism for centromeric nucleosome recognition by centromere protein CENP-C. **Science,** v. 340, n. 6136, p. 1110-3, 2013.

KLEMME, S. et al. High-copy sequences reveal distinct evolution of the rye B chromosome. **New Phytologist,** v. 199, n. 2, p. 550-8, 2013.

KUSANAGI, A. Preferential orientation of interchange multiples in *Luzula elegans*. **Japanese Journal of Genetics,** v. 48, n. 3, p. 175-183, 1973.

LAMB, J. C.; BIRCHLER, J. A. The role of DNA sequence in centromere formation. **Genome Biology,** v. 4, n. 5, p. 214, 2003.

LANZONE, C.; DE SOUZA, M. J. C-banding, fluorescent staining and NOR location in holokinetic chromosomes of bugs of the Neotropical genus *Antiteuchus* (Heteroptera : Pentatomidae : Discocephalinae). **European Journal of Entomology,** v. 103, n. 1, p. 239-243, 2006.

LERMONTOVA, I. et al. Loading of *Arabidopsis* centromeric histone CENH3 occurs mainly during G2 and requires the presence of the histone fold domain. **Plant Cell,** v. 18, n. 10, p. 2443-51, 2006.

LUCEÑO, M.; VANZELA, A. L. L.; GUERRA, M. Cytotaxonomic studies in Brazilian *Rhynchospora* (Cyperaceae), a genus exhibiting holocentric chromosomes. **Canadian Journal of Botany-Revue Canadienne De Botanique,** v. 76, n. 3, p. 440-449, 1998.

LUI, D. Y.; COLAIACOVO, M. P. Meiotic development in *Caenorhabditis elegans*. **Advances in Experimental Medicine and Biology,** v. 757, p. 133-70, 2013.

MADDOX, P. S. et al. "Holo"er than thou: chromosome segregation and kinetochore function in *C. elegans*. **Chromosome Research,** v. 12, n. 6, p. 641-53, 2004.

MALHEIROS, N.; CASTRO, D.; CÂMARA, A. Cromosomas sem centrómero localizado: O caso de *Luzula purpurea* Link. . **Agronomia Lusitana** v. 9, p. 51-74 1947.

MARSTON, A. L.; AMON, A. Meiosis: cell-cycle controls shuffle and deal. **Nature Reviews Molecular Cell Biology,** v. 5, n. 12, p. 983-97, 2004.

MARTINEZ-PEREZ, E. et al. Crossovers trigger a remodeling of meiotic chromosome axis composition that is linked to two-step loss of sister chromatid cohesion. **Genes and Development,** v. 22, n. 20, p. 2886-901, 2008.

MARTIS, M. M. et al. Selfish supernumerary chromosome reveals its origin as a mosaic of host genome and organellar sequences. **Proceedings of the National Academy of Sciences of the USA,** v. 109, n. 33, p. 13343-13346, 2012.

MELTERS, D. P. et al. Comparative analysis of tandem repeats from hundreds of species reveals unique insights into centromere evolution. **Genome Biology,** v. 14, n. 1, p. R10, 2013.

MELTERS, D. P. et al. Holocentric chromosomes: convergent evolution, meiotic adaptations, and genomic analysis. **Chromosome Research,** v. 20, n. 5, p. 579-93, 2012.

MESTROVIC, N. et al. Conserved DNA motifs, including the CENP-B box-like, are possible promoters of satellite DNA array rearrangements in nematodes. **PLoS One,** v. 8, n. 6, p. e67328, 2013.

MOLA, L. M. Post-reductional meiosis in *Aeshna* (Aeshnidae, Odonata). **Hereditas,** v. 122, p. 47-55, 1995.

MONEN, J. et al. Differential role of CENP-A in the segregation of holocentric *C. elegans* chromosomes during meiosis and mitosis. **Nature Cell Biology,** v. 7, n. 12, p. 1248-1255, 2005.

MOORE, L. L.; MORRISON, M.; ROTH, M. B. HCP-1, a protein involved in chromosome segregation, is localized to the centromere of mitotic chromosomes in *Caenorhabditis elegans*. **Journal of Cell Biology,** v. 147, n. 3, p. 471-479, 1999.

MURAKAMI, A.; IMAI, H. T. Cytological evidence for holocentric chromosomes of the silkworms, *Bombyx mori* and *B. mandarina*, (Bombycidae, Lepidoptera). **Chromosoma,** v. 47, n. 2, p. 167-178, 1974.

NAGAKI, K. et al. Sequencing of a rice centromere uncovers active genes. **Nature Genetics,** v. 36, n. 2, p. 138-45, 2004.

NAGAKI, K.; KASHIHARA, K.; MURATA, M. Visualization of diffuse centromeres with centromere-specific histone H3 in the holocentric plant *Luzula nivea*. **Plant Cell,** v. 17, n. 7, p. 1886-1893, 2005.

NAGAKI, K. et al. Chromatin immunoprecipitation reveals that the 180-bp satellite repeat is the key functional DNA element of *Arabidopsis thaliana* centromeres. **Genetics,** v. 163, n. 3, p. 1221-5, 2003.

NEUMANN, P. et al. Plant centromeric retrotransposons: a structural and cytogenetic perspective. **Mobile DNA,** v. 2, n. 1, p. 4, 2011.

NEUMANN, P. et al. Stretching the rules: monocentric chromosomes with multiple centromere domains. **PLoS Genetics,** v. 8, n. 6, p. e1002777, 2012.

NOKKALA, S. Cytological characteristics of chromosome behavior during female meiosis in *Sphinx ligustri* L (Sphingidae, Lepidoptera). **Hereditas,** v. 106, n. 2, p. 169-179, 1987.

NOKKALA, S. et al. Holocentric chromosomes in meiosis. I. Restriction of the number of chiasmata in bivalents. **Chromosome Research,** v. 12, n. 7, p. 733-9, 2004.

NOKKALA, S.; LAUKKANEN, A.; NOKKALA, C. Mitotic and meiotic chromosomes in *Somatochlora metallica* (Cordulidae, Odonata). The absence of localized centromeres and inverted meiosis. **Hereditas,** v. 136, n. 1, p. 7-12, 2002.

NORDENSKIÖLD, H. Studies of meiosis in *Luzula purpurea*. **Hereditas,** v. 48, n. 3, p. 503-519, 1962.

NOVAK, P.; NEUMANN, P.; MACAS, J. Graph-based clustering and characterization of repetitive sequences in next-generation sequencing data. **BMC Bioinformatics,** v. 11, p. 378, 2010.

NOVAK, P. et al. RepeatExplorer: a Galaxy-based web server for genome-wide characterization of eukaryotic repetitive elements from next-generation sequence reads. **Bioinformatics,** v. 29, n. 6, p. 792-3, 2013.

OEGEMA, K.; HYMAN, A. A. Cell division. **WormBook**, p. 1-40, 2006.

OHKURA, H. Meiosis: An overview of key differences from mitosis. **Cold Spring Harbor Perspectives in Biology,** v. 7, n. 5, 2015.

PAPESCHI, A. G. et al. Behaviour of ring bivalents in holokinetic systems: alternative sites of spindle attachment in *Pachylis argentinus* and *Nezara viridula* (Heteroptera). **Chromosome Research,** v. 11, n. 8, p. 725-33, 2003.

PAZY, B.; PLITMANN, U. Persisting demibivalents: a unique meiotic behavior in *Cuscuta babylonica* Choisy. **Genome,** v. 29, n. 1, p. 63-66, 1987.

PEREZ, R. et al. Meiotic behaviour of holocentric chromosomes: orientation and segregation of autosomes in *Triatoma infestans* (Heteroptera). **Chromosome Research,** v. 5, n. 1, p. 47-56, 1997.

PEREZ, R. et al. Meiosis in holocentric chromosomes: orientation and segregation of an autosome and sex chromosomes in *Triatoma infestans* (Heteroptera). **Chromosome Research,** v. 8, n. 1, p. 17-25, 2000.

PIMPINELLI, S.; GODAY, C. Unusual kinetochores and chromatin diminution in *Parascaris*. **Trends in Genetics,** v. 5, n. 9, p. 310-315, 1989.

PLOHL, M. et al. Satellite DNAs between selfishness and functionality: structure, genomics and evolution of tandem repeats in centromeric (hetero)chromatin. **Gene,** v. 409, n. 1-2, p. 72-82, 2008.

PLOHL, M.; MESTROVIC, N.; MRAVINAC, B. Satellite DNA evolution. **Genome Dynamics,** v. 7, p. 126-52, 2012.

_____. Centromere identity from the DNA point of view. **Chromosoma,** v. 123, n. 4, p. 313-25, 2014.

RUFAS, J. S.; GIMENEZ-MARTIN, G. Ultrastructure of the kinetochore in *Graphosoma italicum* (Hemiptera, Heteroptera). **Protoplasma,** v. 132, n. 3, p. 142-148, 1986.

SAKUNO, T.; WATANABE, Y. Studies of meiosis disclose distinct roles of cohesion in the core centromere and pericentromeric regions. **Chromosome Research,** v. 17, n. 2, p. 239-49, 2009.

SCHVARZSTEIN, M.; WIGNALL, S. M.; VILLENEUVE, A. M. Coordinating cohesion, co-orientation, and congression during meiosis: lessons from holocentric chromosomes. **Genes and Development,** v. 24, n. 3, p. 219-228, 2010.

SHANAHAN, C. M. Cytogenetics of Australian scorpions .1. Interchange polymorphism in the family Buthidae. **Genome,** v. 32, n. 5, p. 882-889, 1989.

SHEIKH, S. A.; KONDO, K.; HOSHI, Y. Study of diffused centromeric nature of *Drosera* chromosomes. **Cytologia** v. 60, p. 43-47, 1995.

SOUSA, A. et al. Distribution of 5S and 45S rDNA sites in plants with holokinetic chromosomes and the "chromosome field" hypothesis. **Micron,** v. 42, n. 6, p. 625-31, 2011.

STEAR, J. H.; ROTH, M. B. The *Caenorhabditis elegans* kinetochore reorganizes at prometaphase and in response to checkpoint stimuli. **Molecular Biology of the Cell,** v. 15, n. 11, p. 5187-96, 2004.

STEINER, F. A.; HENIKOFF, S. Holocentromeres are dispersed point centromeres localized at transcription factor hotspots. **Elife,** v. 3, p. e02025, 2014.

_____. Diversity in the organization of centromeric chromatin. **Curr Opin Genet Dev,** v. 31, p. 28-35, 2015.

SUBIRANA, J. A.; MESSEGUER, X. A satellite explosion in the genome of holocentric nematodes. **PLoS One,** v. 8, n. 4, p. e62221, 2013.

SULLIVAN, B. A.; BLOWER, M. D.; KARPEN, G. H. Determining centromere identity: cyclical stories and forking paths. **Nature Reviews Genetics,** v. 2, n. 8, p. 584-96, 2001.

TANAKA, N.; TANAKA, N. Chromosome studies in *Chionographis* (Liliaceae) I. Holokinetic nature of chromosomes in *Chionographis japonica* Maxim. **Cytologia,** v. 42, n. 3-4, p. 753-763, 1977.

_____. Chromosome studies in *Chionographis* (Liliaceae) III. The mode of meiosis. **Cytologia,** v. 45, p. 809-817, 1980.

VANZELA, A. L. L. Karyotype evolution and cytotaxonomy in Brazilian species of *Rhynchospora* Vahl (Cyperaceae). **Botanical Journal of the Linnean Society,** v. 134, n. 4, p. 557-566, 2000.

VANZELA, A. L. L.; CUADRADO, A.; GUERRA, M. Localization of 45S rDNA and telomeric sites on holocentric chromosomes of *Rhynchospora tenuis* Link (Cyperaceae). **Genetics and Molecular Biology,** v. 26, n. 2, p. 199-201, 2003.

VANZELA, A. L. L. et al. Multiple locations of the rDNA sites in holocentric chromosomes of *Rhynchospora* (Cyperaceae). **Chromosome Research,** v. 6, n. 5, p. 345-349, 1998.

VANZELA, A. L. L.; GUERRA, M. Heterochromatin differentiation in holocentric chromosomes of *Rhynchospora* (Cyperaceae). **Genetics and Molecular Biology,** v. 23, n. 2, p. 453-456, 2000.

VANZELA, A. L. L.; GUERRA, M.; LUCEÑO, M. *Rhynchospora tenuis* Link (Cyperaceae), a species with the lowest number of holocentric chromosomes. **Cytobios,** v. 88, n. 355, p. 219-228, 1996.

VIERA, A.; PAGE, J.; RUFAS, J. S. Inverted meiosis: the true bugs as a model to study. **Genome Dynamics,** v. 5, p. 137-56, 2009.

WANG, G. et al. Characterization of CENH3 proteins and centromere-associated DNA sequences in diploid and allotetraploid *Brassica* species. **Chromosoma,** v. 120, n. 4, p. 353-65, 2011.

WIGNALL, S. M.; VILLENEUVE, A. M. Lateral microtubule bundles promote chromosome alignment during acentrosomal oocyte meiosis. **Nature Cell Biology,** v. 11, n. 7, p. 839-44, 2009.

WOLFE, S. L.; JOHN, B. The organization and ultrastructure of male meiotic chromosomes in *Oncopeltus fasciatus*. **Chromosoma,** v. 17, n. 2, p. 85-103, 1965.

ZHANG, H. et al. Boom-bust turnovers of megabase-sized centromeric DNA in *Solanum* species: Rapid evolution of DNA sequences associated with centromeres. **Plant Cell,** v. 26, n. 4, p. 1436-1447, 2014.

ZHONG, C. X. et al. Centromeric retroelements and satellites interact with maize kinetochore protein CENH3. **Plant Cell,** v. 14, n. 11, p. 2825-36, 2002.

Capítulo 1: Chiasmatic and achiasmatic inverted meiosis of plants with holocentric chromosomes

Artigo publicado no periódico *Nature Communications*

nature COMMUNICATIONS

ARTICLE

Received 19 Mar 2014 | Accepted 25 Aug 2014 | Published 8 Oct 2014

DOI: 10.1038/ncomms6070 OPEN

Chiasmatic and achiasmatic inverted meiosis of plants with holocentric chromosomes

Gabriela Cabral[1,2,*], André Marques[1,*], Veit Schubert[3], Andrea Pedrosa-Harand[1] & Peter Schlögelhofer[2]

Meiosis is a specialized cell division in sexually reproducing organisms before gamete formation. Following DNA replication, the canonical sequence in species with monocentric chromosomes is characterized by reductional segregation of homologous chromosomes during the first and equational segregation of sister chromatids during the second meiotic division. Species with holocentric chromosomes employ specific adaptations to ensure regular disjunction during meiosis. Here we present the analysis of two closely related plant species with holocentric chromosomes that display an inversion of the canonical meiotic sequence, with the equational division preceding the reductional. In-depth analysis of the meiotic divisions of *Rhynchospora pubera* and *R. tenuis* reveals that during meiosis I sister chromatids are bi-oriented, display amphitelic attachment to the spindle and are subsequently separated. During prophase II, chromatids are connected by thin chromatin threads that appear instrumental for the regular disjunction of homologous non-sister chromatids in meiosis II.

[1] Department of Botany, Laboratory of Plant Cytogenetics and Evolution, Federal University of Pernambuco, Rua Nelson Chaves s/n, Recife, Pernambuco 50670-420, Brazil. [2] Department of Chromosome Biology, Max F. Perutz Laboratories, University of Vienna, Dr Bohr-Gasse 9, Vienna A-1030, Austria. [3] Leibniz Institute of Plant Genetics and Crop Plant Research, Corrensstraße 3, Gatersleben 06466, Germany. * These authors contributed equally to this work. Correspondence and requests for materials should be addressed to P.S. (email: peter.schloegelhofer@univie.ac.at).

Meiosis is a special type of cell division that occurs in sexually reproducing organisms and results in the formation of gametes. DNA replication is followed by two rounds of chromosome segregation, thereby halving the genomic content. The canonical sequence of events is characterized by sister centromeres segregating together during the first (reductional) division and then separating during the second meiotic (equational) division. Regular chromosome disjunction during meiosis I depends on physical connections between homologous non-sister chromatids. These connections, termed chiasmata, correspond to regions that have undergone interhomologue recombination. Recombined DNA strands together with sister chromatid cohesion hold the homologous chromosomes together until the transition from metaphase I to anaphase I. At anaphase I onset, cohesion of chromosome arms is released but maintained in proximity of sister centromeres. The sister centromeres are co-oriented and attached to the same spindle. In contrast, in metaphase II, sister centromeres are oriented in a bipolar manner and are attached to different spindles resulting in sister centromere separation[1,2].

Meiotic recombination is initiated by the formation of DNA double-strand breaks (DSBs) catalysed by the conserved Spo11 protein (together with additional factors)[3,4]. The break ends are subsequently processed into single-stranded DNA overhangs, which invade an intact DNA duplex of the homologous chromosome. This repair process is mediated by RecA-like proteins (Rad51 and Dmc1). Only some of these interhomologue interactions lead to mutual exchange of chromosome parts, thereby re-shuffling genetic information as well as generating physical links (chiasmata)[5,6]. The interhomologue interactions support pairing of homologous chromosomes. Stabilization of chromosome pairing is achieved during synapsis, a process in which the axes of homologous chromosomes, comprising meiosis-specific proteins such as Hop1 (named ASY1 in higher plants), are linked together by proteins of the central element such as Zip1 (known as ZYP1 in higher plants) giving rise to a proteinaceous structure, named synaptonemal complex (SC)[7].

Several studies provided evidence that there is an interdependent relationship between the process of DSB formation, meiotic recombination, chromosome pairing and synapsis in most organisms[8,9]. In this sense, DSB formation and subsequent repair have been found to be important for both pairing and synapsis in yeast, mouse and plants such as maize and *Arabidopsis*. In contrast, pairing and synapsis in the worm *Caenorhabidits elegans* and the fly *Drosophila melanogaster* are independent of DSB formation[10,11]. In *C. elegans* these processes rely on specific chromosomal regions that associate with chromosome-specific zinc-finger proteins[12,13]. Interestingly, in *Drosophila* males, chromosomes segregate reductionally even without the formation of chiasmata (and also chromosome 4 in *Drosophila* females), which has been explained by interactions of heterochromatic regions, at least in the case of sex chromosomes and the autosome 4 (refs 14–16).

The reductional segregation of homologous chromosomes in anaphase I also relies on monopolar attachment of sister kinetochores to the spindle. Together with cohesion maintenance at the centromeric region, monopolar attachment of sister kinetochores promotes the joint migration of sister chromatids to the same pole at anaphase I[17–19]. In plants and budding yeast, monopolar attachment is promoted by specific kinetochore proteins that bridge the two sister kinetochores during meiosis I (refs 20,21). Cohesion loss along the chromosome arms but not at the centromeric region allows homologues to segregate at anaphase I, while preserving sister chromatid–centromere association. Protection of cohesion at the centromeric region during meiosis I depends on a specific protein that localizes to centromeres and prevents the cleavage of a cohesin subunit and therefore ensures that sister chromatids remain attached to each other until anaphase II (ref. 22).

On the basis of the extension of the kinetochore region, chromosomes are classified into two major types: monocentric chromosomes with a clearly localized and restricted kinetochore region, and holocentric chromosomes with a more diffused kinetochore that spans the length of condensed chromosomes. Holocentric chromosomes are present in a number of taxa, including nematode worms, such as *Parascaris* and *Caenorhabditis,* several insects orders, such as Odonata and Heteroptera, and higher plants, such as the Cyperaceae and Juncaceae families[23–25]. While neutral for mitotic divisions, the presence of a holocentric kinetochore could impose obstacles to the particular dynamics of cohesion loss in meiosis I that releases chromosome arms but keeps sister centromeres together[26,27]. In *C. elegans* female meiosis, this problem is circumvented in the following way: crossovers are restricted to form only a single chiasma per bivalent, which then triggers the redistribution of proteins along the bivalent axis, creating subdomains that define the region of cohesin removal and protection during meiosis I (ref. 28). Kinetochore components uniformly coat each half bivalent but are excluded from the midbivalent region. The chromosomes are embedded in massive microtubule bundles, and during anaphase I homologous chromosomes are segregated to the poles by microtubule forces pushing from the midbivalent regions towards the poles[29,30]. Sister chromatids remain attached via the other bivalent axes and are separated during the second meiotic division[28,29,31].

Some other organisms with holocentric chromosomes, including plants (for example, *Luzula campestris* or *Cuscuta babylonica*), may circumvent the problem of meiosis by a different strategy. They were reported to display a diploid number of individualized chromatids at prophase II, indicating complete loss of sister chromatid cohesion in meiosis I. Accordingly, several authors have suggested that sister chromatids may segregate at anaphase I leading to the concept of inverted meiosis in which the order of reductional and equational division is inverted and separation of homologous non-sister chromatids follows sister chromatid segregation[23,32–39]. For successful generation of haploid generative cells via inverted meiosis, at least three requirements have to be met: (1) bipolar orientation of sister kinetochores and their attachment to microtubules from opposite spindle poles in meiosis I (amphitelic attachment); (2) segregation of sister chromatids to opposite poles in anaphase I (equational division); and (3) a mechanism to align and distribute homologous non-sister chromatids during the second meiotic division. So far, the occurrence of inverted meiosis has received strongest support by studies of a mealybug species (*Hemiptera*) in which a diploid individual with a heteromorphic chromosome pair was analysed[33,38]. Further evidence for inverted meiosis and also for its occurrence in the plant kingdom is still absent.

Here we present an in-depth analysis on the meiotic behaviour of two Cyperaceae species with holocentric chromosomes, *Rhynchospora pubera* ($n=5$) and *R. tenuis* ($n=2$). Our data support the occurrence of inverted meiosis in plants based on the observation that sister chromatids display amphitelic attachment to the spindle, that sister chromatids are subsequently separated during meiosis I and that homologous non-sister chromatids display mostly regular disjunction in anaphase II. Furthermore, the availability of a *R. pubera* individual with a heteromorphic chromosome pair allows the non-ambiguous reconstruction of the inverted meiotic sequence. The analyses of both species are complementary, since *R. pubera* displays chiasmatic meiosis, which is most commonly found among plants with holocentric chromosomes, while *R. tenuis* represents an exceptional case with achiasmatic meiosis.

Results

Chiasmatic meiosis of *R. pubera*. An overview of *R. pubera* meiosis has been described previously[24]. Briefly, in early prophase I chromosomes pair and synapse, inferred by the change in thickness of the filamentous chromosomes in the transition from zygotene to pachytene (Fig. 1a,b). Following condensation, five bivalents were observed in diakinesis (Fig. 1c), bearing most frequently one chiasma (71.3%, $n=1,379$ diakinesis and metaphase bivalents). Bivalents with two chiasmata and univalents were also observed, but with lower frequencies (25.2% and 3.5%, respectively; Supplementary Fig. 1a,b). Chiasmata were mostly positioned close to the chromosome ends ($n=342$ diakinesis bivalents). We infer that several aspects of *R. pubera* are similar to meiotic progression of other plants (for example, *Arabidopsis* or maize). First, we see deposition of the axial element protein ASY1 (refs 40,41), indicating conservation of axis architecture (Supplementary Fig. 1d). Second, we observed RAD51 foci in prophase I cells (but not in mitotic cells), indicating that meiotic DSBs are formed and processed[42] (Supplementary Fig. 1e). Third, despite the fact that we observe numerous RAD51 foci (indicative for numerous DSBs), only very few crossovers are formed. The small number of crossovers per bivalent and their preferential terminal localization in case of bivalents with two crossovers indicate strong CO interference. At metaphase I, bivalents with a single chiasma typically assumed a dumbbell shape (Fig. 1d). At anaphase I, mostly individualized chromatids are pulled to the poles (Fig. 1e). During anaphase I and prophase II, many cells contain (up to 10) individualized chromatids, instead of the five pairs of chromatids that would be expected for a canonical meiosis (Fig. 1f). In many cases thin chromatin threads, connecting the individualized 4′,6-diamidino-2-phenylindole (DAPI)-stained bodies (in some instances more than two are connected), can be observed (Fig. 1g). At metaphase II, chromatids associate into pairs (Fig. 1h) and segregation of five chromatids to each pole occurs in anaphase II (Fig. 1i). These observations were intriguing, since they suggested that meiosis in *R. pubera* does not follow the canonical meiotic steps but rather that sister chromatids are separated in anaphase I and that the thin chromatin threads represent connections of homologous non-sister chromatids.

We quantified our observations and found that 9% of all prophase II cells had eight or more isolated chromatids (class I), 20% had four to six isolated chromatids (class II), 45.5% had only two isolated chromatids (class III) and 25.5% had no isolated chromatids (class IV, $n=55$; Fig. 2a,b). Chromatids were counted as pairs when they were in close proximity or at least connected by a chromatin thread (Fig. 2c). In all, 21.5% of all chromatids were not connected by threads, 10.7% were connected by threads and 67.8% appeared in close proximity ($n=270$ pairs of chromatids). We were interested whether chromatid association

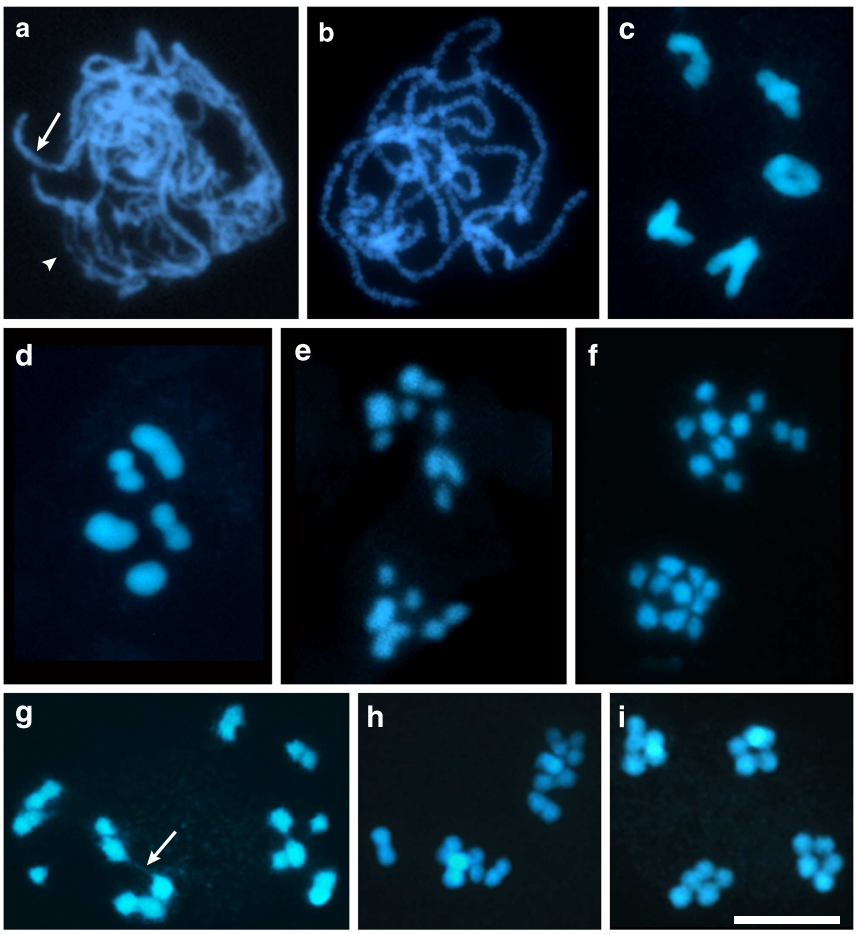

Figure 1 | *R. pubera* meiosis. DAPI images representing different stages of meiosis. (**a**) Zygotene with paired (arrow) and unpaired (arrowhead) chromosomal regions. (**b**) Pachytene with completely paired chromosomes. (**c**) Diakinesis with one ring bivalent and four bivalents with one terminal/subterminal chiasma. (**d**) Metaphase I. (**e**) Anaphase I showing some individualized chromatids being pulled to either pole. (**f**) Prophase II with 10 individualized chromatids at each pole. (**g**) Prophase II showing chromatid pairs visibly connected by chromatin threads (arrow). (**h**) Metaphase II. (**i**) Late anaphase II. Size bar corresponds to 10 μm.

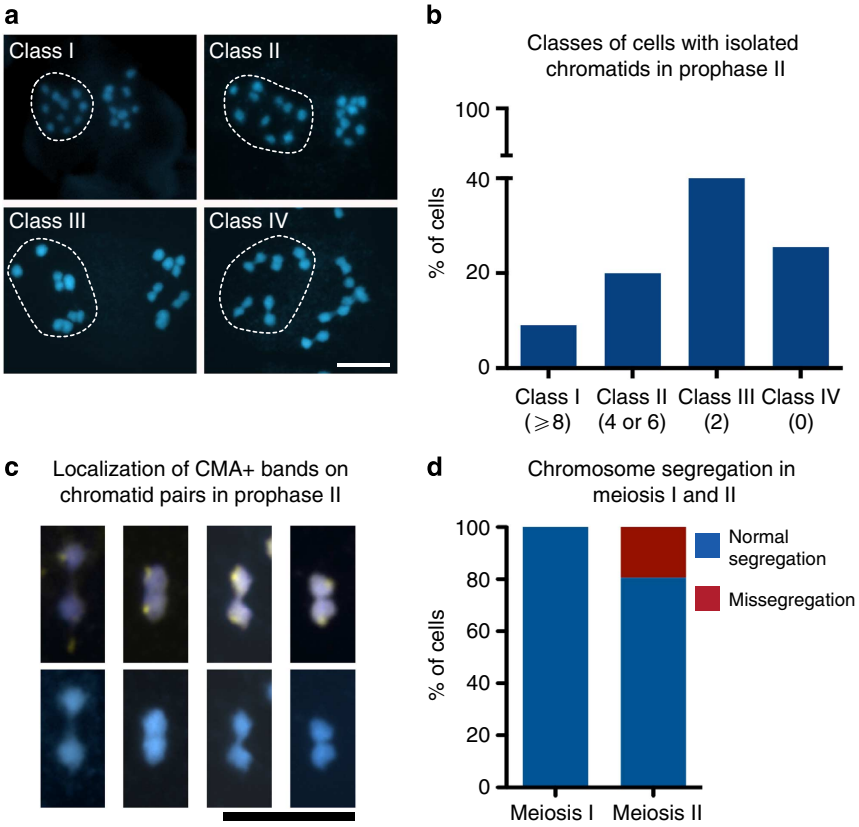

Figure 2 | Association of chromatids in meiosis II of *R. pubera*. (**a**) Different classes of cells with individualized chromatids in prophase II. Class I comprises cells with eight or more individualized chromatids, Class II cells have four or six, class III have two and class IV represents cells without individualized chromatids. Daughter cells exemplifying each class are highlighted. (**b**) Frequency of the different classes of cells with isolated chromatids during prophase II ($n=55$). (**c**) Pairs of chromatids of prophase II cells connected with a thin DAPI (blue)-stained thread or in close association. CMA staining (yellow) indicates regions of 45S rDNA. (**d**) Quantification of chromosome mis-segregation in meiosis I and II ($n=37$ and 36 cells, respectively). Size bars correspond to 10 μm.

would be directed by 45S rDNA repeat regions (to be found on 3 of the 5 chromosomes of *R. pubera*)[43] as described for the sex chromosome of *D. melanogaster*. We performed chromomycin A3 (CMA) staining that labels the 45S rDNA clusters in many plant species[43–45] and also in *R. pubera* (Supplementary Fig. 2a). It is evident that 45S rDNA is not involved in mediating the interactions of chromatids during prophase II in *R. pubera*, since in none of the observed cases ($n=63$) the parts of the chromatids that face each other or the chromatin threads are associated with CMA staining (Fig. 2c). Since the rDNA clusters are located terminally on the *R. pubera* chromosomes[46], terminal associations would either involve the 45S rDNA regions, which is not the case, or position them at the other end of the paired or associated chromatids. Interestingly, during metaphase I, those rod bivalents with 45S rDNA or CMA labelling were always arranged with the 45S rDNA clusters pointing outwards ($n=141$; Supplementary Fig. 2b).

During prophase II, chromatids were predominantly connected to a partner (Fig. 2a–c), yet some chromatids were clearly not. As outlined above, chromatids (either sister chromatids, in case of a canonical meiosis, or homologous non-sister chromatids, in case of an inverted meiosis) have to be connected at metaphase II to ensure regular disjunction. Since we observed some univalents in meiosis I and isolated chromatids in prophase II, we investigated mis-segregation in meiosis I and meiosis II. Indeed, we observed that 19.5% ($n=36$) of all meiosis II products had incorrect numbers of chromosomes (Fig. 2d; Supplementary Fig. 2c); however, none of the analysed cells showed mis-segregation during meiosis I ($n=37$). We assume that segregation of chromatids during meiosis II not only yielded ~80% of products with the correct number of chromatids but also with the correct set, since we only observed limited pollen abortion in anthers (Supplementary Fig. 2d). This indicates that (a) the occasional univalents (observed in diakinesis) do not lead to unbalanced chromatid numbers in telophase I/prophase II and that (b) those isolated DAPI-stained bodies observed in prophase II may actually represent single sister chromatids, which separated during meiosis I from their respective sister, but have failed to connect to a homologous non-sister chromatid and are therefore mis-segregating in meiosis II.

While our observations depict meiotic peculiarities not described for other organisms so far, they do not provide direct evidence for an equational first meiotic division and a reductional second division. To further investigate the nature of *R. pubera* meiosis, we analysed the meiotic spindle and its attachment to chromosomes since we envisaged that knowing the mode of spindle attachment to meiotic chromosomes would allow drawing conclusions about chromosome/chromatid segregation during meiosis I. In mitotic cells (Fig. 3a; Supplementary Movie 1), 10 holocentric chromosomes align along the metaphase axis and each is attached to the spindle at various sites in a bipolar manner (amphitelic attachment). The kinetochores can be visualized all along the chromosome as parallel axes of CENH3 labelling (Fig. 3b). In meiosis I, the five bivalents are highly condensed and (especially well visible in dumbbell/rod bivalents) are aligned on the metaphase plate with their longitudinal axes perpendicular to

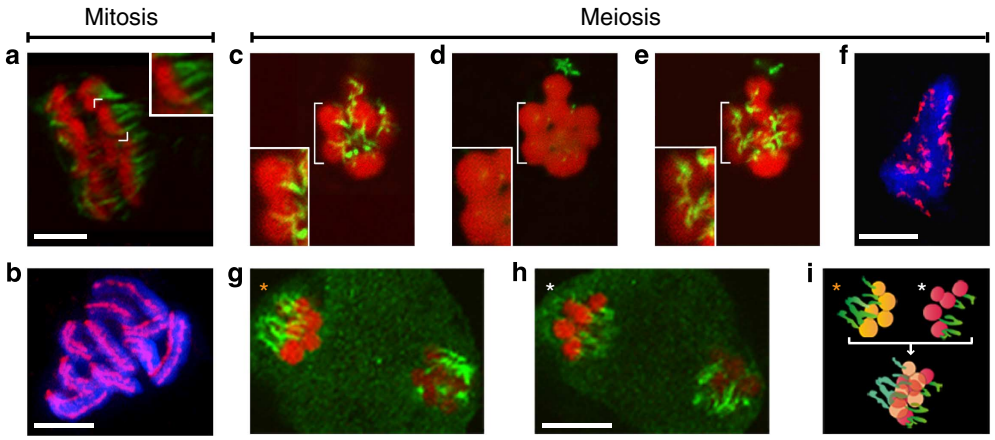

Figure 3 | Microtubule attachment on chromosomes of *R. pubera*. (**a**) Mitotic metaphase with one chromosome highlighted in the upper corner. Note the multiple sites of microtubule attachment. (**b**) Mitotic metaphase with chromosomes labelled with an antibody directed against CENH3, which localizes in two parallel lines along each chromosome. (**c**–**e**) Polar view of meiotic metaphase I with one bivalent highlighted. The same cell is viewed in an upper focal plane (**c**), a medium focal plane (**d**) and a lower focal plane (**e**). (**f**) Chromosomes at meiotic metaphase I labelled with an antibody directed against CENH3, which localizes in distinct patches along both sides of each bivalent. (**g**–**h**) Metaphase II. Upper (**g**) and lower (**h**) focal planes of the same cell. (**i**) Scheme of orientation of metaphase chromosomes marked with * in **g**,**h** representing the five chromatids attached to microtubules from each spindle pole and an overlay showing the bipolar orientation. (**a**,**c**–**e**,**g**,**h**) Chromosomes in red, microtubules in green. (**b**,**f**) Chromosomes in blue, CENH3 in magenta. Size bars correspond to 5 μm.

the spindle. Microtubules are attached to the central regions and on both sides of each half bivalent, resulting in multiple spindle attachment regions per bivalent ($n = 20$; Fig. 3c–e; Supplementary Movies 2 and 3). Each half of such a (dumbbell) bivalent is assumed to consist of two sister chromatids (see Supplementary Fig. 3a and Fig. 7 for schematic representations). This assumption is based on observations in *C. elegans*, which shows bivalents with a dumbbell shape bearing a single subterminal chiasma, resembling the bivalents of *R. pubera*[27]. To confirm the localization of microtubules in the central region of the 'half bivalents', the 45S rDNA clusters, localized at the termini of three chromosomes in *R. pubera*[43], were visualized with fluorescent *in situ* hybridization (FISH; Supplementary Fig. 2b). As mentioned above, in all dumbbell-shaped bivalents containing the 45S rDNA cluster, these regions were localized at the chromosome termini opposite to the associated regions and not at the central region where microtubules attach. The microtubule immunostaining also revealed that there are several microtubule attachment sites in metaphase I chromosomes, similar to the less condensed mitotic chromosomes. These observations correlate well with the localization of CENH3 on the highly condensed metaphase I bivalents, showing multiple patches of labelling in two parallel lines (Fig. 3f). It is interesting to note that the distribution of the mitotic centromere marker H2AThr120ph gives a diffuse staining around the meiotic metaphase chromosomes, while in mitotic chromosomes its localization resembles CENH3, indicating substantial reorganization of the meiotic centromeres (Supplementary Fig. 3b). In metaphase II, each chromatid was associated with microtubules from one cell pole ($n = 48$; Fig. 3g–i; Supplementary Movie 4).

In comparison with a regular meiosis, as described for the holocentric organism *C. elegans*, multiple differences have been identified in *R. pubera*. In *C. elegans* the meiotic spindle forms microtubule bundles that surround the bivalents (female meiosis) or shows terminal associations to bivalents (male meiosis) at metaphase I, and, importantly, bivalents orient themselves with the long axis parallel to the spindle[29]. In *R. pubera*, bivalents are oriented with the longer axis perpendicular to the spindle and they appear to have several microtubule attachment sites with kinetochores of sister chromatids attached independently to microtubules emanating from opposite poles (amphitelic attachment). At anaphase I, *C. elegans* homologues are separated, while in *R. pubera* sister chromatids are separated from each other and pulled to different poles. At this stage, sister chromatids of *C. elegans* are still held together by cohesins and, in contrast, the non-sister chromatids of *R. pubera* appear individualized, with some being connected with thin chromatin threads. Importantly, the diploid number of DAPI-stained bodies can clearly be visualized in each half of the dyad in prophase II, following the expectations of sister separation during meiosis I in *R. pubera*. In *C. elegans* at metaphase II/anaphase I, sister chromatids align and are subsequently separated. In *R. pubera*, chromatids associate with the help of an unknown mechanism and subsequently undergo disjunction during anaphase II. These observations are in strong favour of sister separation during meiosis I in *R. pubera* (Supplementary Fig. 3).

We gained further evidence of the independent orientation and separation of sister kinetochores in meiosis I by analysing chromosome segregation of a *R. pubera* individual with an apparent chromosome breakage in chromosome 2 (Fig. 4a,b). As observed for other species[47], fragments of holocentric chromosomes can acquire new telomeric sequences and be stably transmitted in *R. pubera* as well. This heteromorphic chromosome pair provided an ideal test system for the analysis of chromosome segregation during meiosis. In case sister chromatids are separated during the first meiotic division (equational division), each of the two cells of the resulting dyad should contain the same number of DAPI-stained bodies (chromatids and chromatid fragments). In contrast, if homologous chromosomes are separated then the number of DAPI-stained bodies (chromatids and chromatid fragments) is not expected to be the same, with one cell of the dyad receiving the intact chromosome 2 and the other one the two parts of the fragmented chromosome 2 (A schema for the two different scenarios can be found in Supplementary Fig. 4). The plants were phenotypically normal and fertile; however, during prophase of meiosis I a heteromorphic bivalent was visible. The heteromorphic bivalent formed terminal chiasmata involving both broken parts ($n = 45$; a non-associated chromatid fragment was never observed), visible during diakinesis (Fig. 4c,d) and

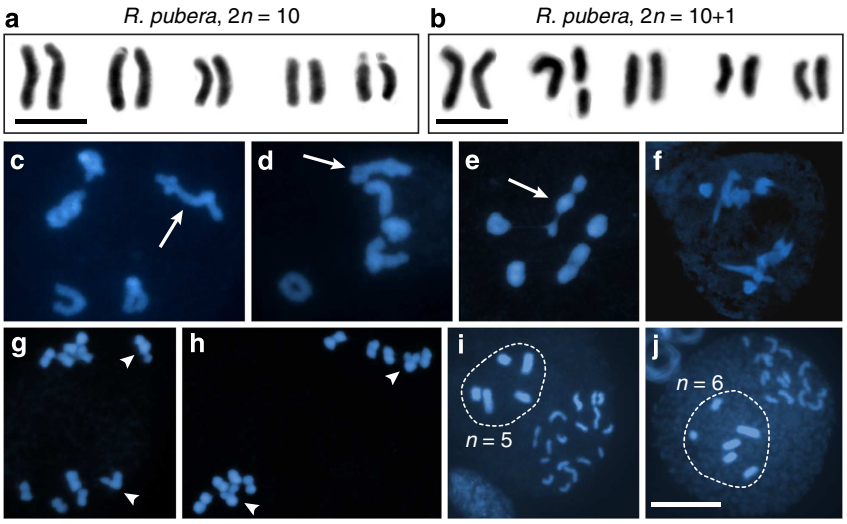

Figure 4 | Meiosis of *R. pubera* (2*n* = 10 + 1). (**a**) Karyotype of *R. pubera* 2*n* = 10. (**b**) Karyotype of *R. pubera* 2*n* = 10 + 1. (**c**–**j**) DAPI images representing different stages of meiosis. (**c**,**d**) Cells in diakinesis showing the pairing behaviour of the heteromorphic bivalent (arrows). (**e**) Metaphase I. Arrow points to heteromorphic bivalent. (**f**) Anaphase I. (**g**,**h**) Cells in prophase II/metaphase II showing equational segregation of chromatids of the heteromorphic bivalent (arrowheads). (**i**,**j**) Microsporogenesis showing examples of pseudomonads in which the nucleus with (**i**) *n* = 5 or (**j**) *n* = 6 (highlighted) is centrally positioned and will give rise to a pollen grain. Size bars correspond to 10 μm.

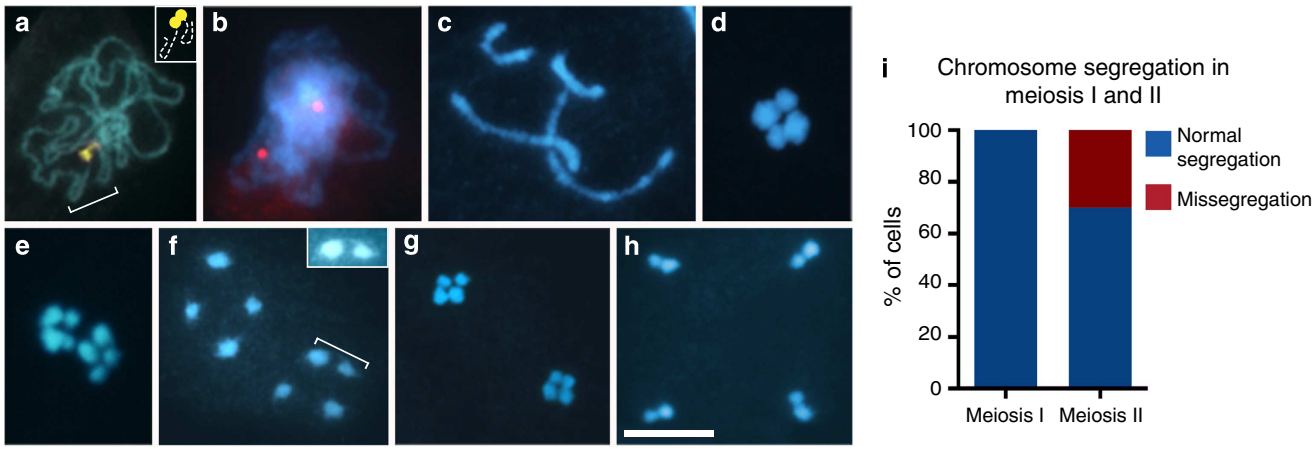

Figure 5 | Meiosis of *R. tenuis*. DAPI Images representing different stages of meiosis. (**a**) Zygotene showing end-to-end association of chromosomes carrying the CMA$^+$ bands (yellow). (**b**) Zygotene showing unpaired 5S rDNA sites (in red). (**c**) Diplotene/diakinesis with four univalents. (**d**) Metaphase I with univalents organized in a cross-like shape. (**e**) Lateral view of anaphase I. (**f**) Prophase II. The inset shows the highlighted chromatids with adjusted brightness and contrast to enhance visibility of chromatin threads. (**g**) Metaphase II. (**h**) Late anaphase II. (**i**) Quantification of chromosome mis-segregation in meiosis I and II (*n* = 107 and 80 cells, respectively). Size bar corresponds to 10 μm.

metaphase I (Fig. 4e). All post anaphase I and prophase II cells analysed (*n* = 24) clearly showed mirror images of the heteromorphic chromosome pair, demonstrating that meiosis I in *R. pubera* is indeed equational (Fig. 4f–h). In *R. pubera* three of the four microspores generated are degraded[48] and the individual plant with the broken chromosome 2 seems not to be different in this respect, showing pollen grains with five or six DAPI-stained bodies (Fig. 4i,j).

Achiasmatic meiosis of *R. tenuis*. *R. tenuis* (*n* = 2) is closely related to *R. pubera*, and its analysis provides further support for the occurrence of inverted meiosis in the *Cyperaceae* family. An advantage for analysis is that the two chromosomes differ in their size and can easily be distinguished. To analyse chromosome pairing and synapsis during *R. tenuis* early prophase, the small chromosome pair was specifically labelled with CMA (anticipated to label the nucleolus-organizing region[45,49]). The second chromosome pair was identified by *in situ* hybridization of the 5S rDNA cluster, localizing to the interstitial region of the chromosome lacking the CMA$^+$ signal[46]. The CMA-chromosome primarily displayed end-to-end associations (71%, *n* = 90) during early prophase I (Fig. 5a), while lateral alignment, indicative of pairing, was less often observed. The 5S rDNA marker on the second chromosome pair appeared unpaired in 80% of the cells analysed (zygotene/pachytene stage; *n* = 33) suggesting the absence of pairing also for this chromosome (Fig. 5b).

Interestingly, other aspects of meiosis seemed conserved, since deposition of the meiosis-specific axial element protein ASY1 indicates that the overall meiotic chromosome organization is similar compared with other plant species including *R. pubera*

(Supplementary Fig. 5a). We also observed RAD51 foci in meiotic cells (but not in mitotic cells) of *R. tenuis* and believe that they indicate programmed meiotic DSB formation and processing (Supplementary Fig. 5b). Yet, when chromosomes condensed further in diplotene/diakinesis four univalents could be clearly distinguished and chiasmata were never observed ($n = 210$; Fig. 5c). This indicates that the DSBs formed earlier during prophase are repaired via non-crossover pathways. At metaphase I, these four non-paired univalents aligned at the equatorial plane forming a cross-like figure (Fig. 5d). In anaphase I, four chromatids (two of each size) are pulled to each pole indicating segregation of sister chromatids ($n = 107$; Fig. 5e; Supplementary Fig. 6). It is interesting to note that in prophase II the four chromatids are associated via thin chromatin threads, forming connections between two or more chromatids (Fig. 5f). At metaphase II the four chromatids in each part of the dyad were again arranged in a cross-like configuration (Fig. 5g) and separated in anaphase II with two chromatids of different size segregating (Fig. 5h) to the respective poles.

While segregation of sister chromatids appears error-free during the first meiotic division, 30% of the post-anaphase II stages ($n = 80$) had an irregular genomic content (Fig. 5i; Supplementary Fig. 5c). It is interesting to note that this mostly concerned the type of chromatids (for example, two large or two small chromatids together; 25%) and only in few cases aneuploidy (5%). In agreement with the meiosis II segregation defects, we also observed some nonviable pollens (Supplementary Fig. 5d). Taken together, this indicates that sister chromatid cohesion in *R. tenuis* is completely lost during the first, achiasmatic meiotic division and, furthermore, that during the second meiotic division homologous non-sister chromatids have only a partially functional compensatory mechanism to enhance regular disjunction.

To further corroborate the finding of an equational nature during the first meiotic division in *R. tenuis*, we performed immunostaining of microtubules. In metaphase I, each univalent associates with microtubules emanating from opposite poles of the cell, thereby displaying an amphitelic attachment to the spindle ($n = 22$; Fig. 6a–d). During metaphase II ($n = 142$) and anaphase II ($n = 54$; Fig. 6e–g), each chromatid appears to be associated with microtubules from only one cell pole. The described results are intriguing since the predictions for achiasmatic meiosis embedded in either a regular or inverted pathway are very different. In the canonical meiotic pathway, non-paired univalents are expected to be randomly distributed at anaphase I. In contrast, in case of inverted meiosis, sister chromatids of each univalent are expected to become individually attached to the spindle and to be separated during anaphase I. Therefore, the expectation for inverted meiosis is, to see four chromatids in both parts of the resulting dyad and also error-free, reliable disjunction. Indeed, these expectations are always met ($n = 107$). In metaphase II, chromatids align and subsequently undergo disjunction during anaphase II. In the case of achiasmatic meiosis, following the canonical pathway, the second meiotic division is expected to resemble an equational, error-free division. In contrast, the second division of an inverted meiosis is expected to face the problem of distributing homologous non-sister chromatids. Depending on the accuracy of a hypothetical mechanism to promote regular disjunction, errors during chromatid disjunction are expected in the second meiotic division of an inverted meiosis. Indeed, about 30% of all meiotic products of *R. tenuis* show irregularities. These results strongly support the claim of inverted meiotic events in *R. tenuis* (Supplementary Fig. 6).

Discussion

The occurrence of a diploid number of individualized chromatids in prophase II has been the principal indication for inverted meiosis in several species dating from very early studies on meiosis of holocentric chromosomes[32,34,37,38]. However, this deviation from the canonical progression through meiosis could be ascribed to either separation of sister chromatids in anaphase I (equational division) or to disjunction of homologous chromosomes followed by loss of sister chromatid cohesion (reductional division with premature cohesion loss). To our understanding, and as outlined above, genuine inverted meiosis has to meet at least the criteria of: (1) bipolar orientation of sister chromatids and their attachment to opposite spindle poles in meiosis I; (2) segregation of sister chromatids to opposite poles in anaphase I (equational division); and (3) a mechanism to align and distribute homologous non-sister chromatids during meiosis II.

Here we present robust evidence for inverted meiosis in two related plant species of the *Cyperaceae* family, *R. pubera* and *R. tenuis*. We found that *R. tenuis* separates sister chromatids equationally during the first meiotic division. Meiosis in *R. tenuis* is achiasmatic, which means that the homologous chromosomes do not exchange genetic material and that they do not become connected during meiotic prophase I via chiasmata. The connection of sister chromatids is apparently completely lost at the end of meiosis I, yet chromatids are not distributed randomly during anaphase II.

Does meiosis in *R. tenuis* fulfil all criteria to be defined as 'inverted meiosis'? Certainly, sister chromatids have a bipolar orientation and are attached to opposite spindle poles (amphitelic attachment) in meiosis I. Furthermore, sister chromatid cohesion at the onset of anaphase I is lost and sister chromatids segregate

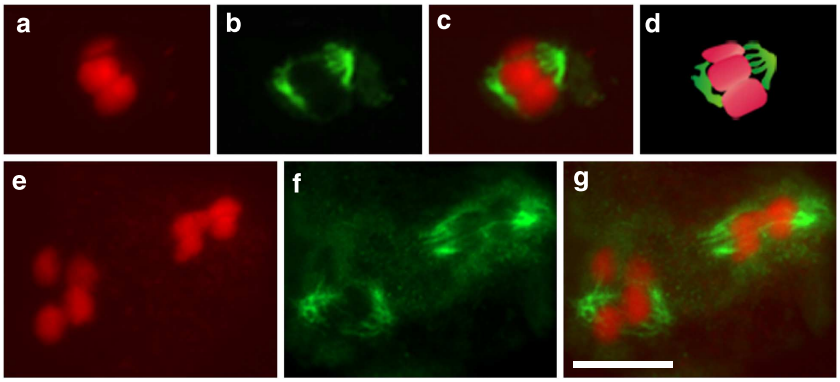

Figure 6 | Microtubule attachment in *R. tenuis* meiosis. (**a**–**c**) Lateral view of metaphase I chromosomes (**a**, red) showing microtubules (**b**, green) attached to both sides of each univalent. Only three out of four univalents are visible. (**d**) Scheme of the overlay shown in **c**. (**e**–**g**) Early anaphase II with chromatids (**e**, red) individually attached to microtubules **(f**, green). (**g**) Overlay of **e**,**f.** Size bar corresponds to 5 μm.

to opposite poles. It should be noted that the haploid genome complement of *R. tenuis* comprises only two chromatids[50]. In this sense, the extreme reduction of chromosome number could be seen as an adaptation to the inverted, achiasmatic meiotic sequence with a good stochastic chance to end up with the correct set of chromosomes in a generative cell. Interestingly, we observed that 70% of all meiosis II products contained the correct set, which is well above the expected 25% if chromatids would be distributed randomly in anaphase II. In the light of the given numbers, the thin chromatin threads visible in *R. tenuis* prophase II, which connect chromatids with each other, could be instrumental to support regular disjunction. Although we do not have indication of their sequence composition, these threads could be of heterochromatic nature and resemble those found to connect achiasmatic chromosomes during meiosis I in *D. melanogaster*. It is important to note that in *R. tenuis* these connections cannot be the remnants of recombination, since this species displays achiasmatic meiosis. Pradillo *et al.*[51] suggest that SC components may enhance regular disjunction of univalents during meiosis I in *Arabidopsis* mutants with impaired DSB formation or interhomologue bias. Certainly one can also envisage that in *R. pubera* and *R. tenuis*, SC-related proteins may support regular segregation of homologous non-sister chromatids during meiosis II.

We believe that the chromatin threads are part of a mechanism to associate the four chromatids during prophase II and align them during metaphase II. Even though a specific mechanism to link corresponding homologous non-sister chromatids may not be in place, the presumably nonspecific association of the chromatids would allow balancing of the force exerted by the metaphase II spindle. Since the chromatids in *R. tenuis* are of very different size and would, therefore, according to their holocentric nature accommodate more or less microtubule attachment sites, we envisage a model of balanced spindle forces only in case one large and one small chromosome is connected to each spindle pole, thereby promoting regular chromatid disjunction (Fig. 7). In fact, with the single assumption that the spindle is organized such that there is indeed a preference for only two chromatids connecting to one pole, then even random segregation would result in a correct genome complement in ~66% of all meiosis II division events. This number is in good agreement with the experimental data.

Meiotic progression is more complex in *R. pubera*. First, *R. pubera* has five chromosomes and homologous chromosomes pair and form chiasmata in meiosis I. Interestingly, univalents have been observed infrequently during prophase I; yet no unequal segregation was observed during anaphase I. This is intriguing as it suggests that, similar to cases described earlier[52–54], also in *R. pubera* univalents are segregated equationally during meiosis I. Furthermore, during anaphase I, 10 isolated DAPI-stained bodies (a diploid number of isolated chromatids) moved towards each pole. Together, this indicates loss of sister chromatid cohesion and equational division.

Further evidence to support the idea of sister chromatid segregation during meiosis I is the observation that in *R. pubera* each bivalent has multiple microtubule attachment sites. These sites are in the central region of each half bivalent, with sister chromatids being attached to spindles from different poles (Fig. 7). This amphitelic attachment is one of the prerequisites for inverted meiosis. It would certainly be ideal to distinguish sister chromatids and homologous non-sister chromatids directly (for example, with FISH probes specific for only one of the two homologues or LacO arrays inserted only in one of the two homologues). Unfortunately, advanced tools are not available for the two non-model plants investigated in this study. Nonetheless, the availability of a plant

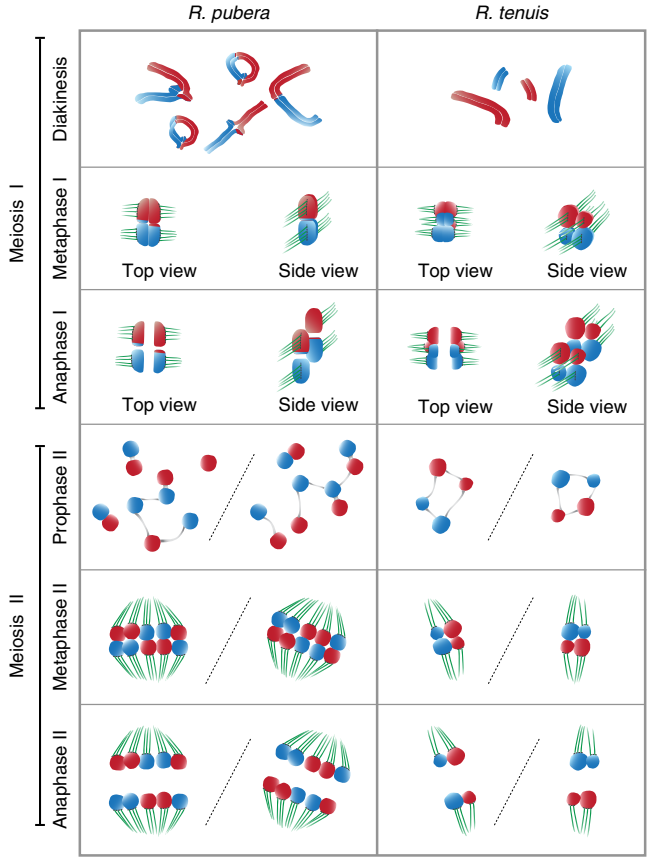

Figure 7 | Model for meiotic events in *R. pubera* and *R. tenuis*. During meiosis I chromosomes of *R. pubera* recombine, pair and bivalents with chiasmata become visible in diakinesis. In contrast, chromosomes of *R. tenuis* do not form chiasmata and univalents become visible. In metaphase I (only one, rod-shaped bivalent of *R. pubera* is shown; all four chromosomes of *R. tenuis* are shown), chromosomes align at the metaphase plate and sister chromatid show amphitelic attachment to the spindle. In anaphase I (only one, rod-shaped bivalent of *R. pubera* is shown; all four chromosomes of *R. tenuis* are shown), sister chromatids are separated from each other and pulled to different poles. For prophase II, each half of the dyad is shown. While chromatids of *R. pubera* appear mostly in pairs, with some chromatids being connected with thin chromatin threads, all four chromatids of *R. tenuis* appear interconnected by thin chromatin threads. In metaphase II, chromatids align and subsequently undergo regular disjunction during anaphase II. Note, the model idealizes regular disjunction in meiosis II but actually 19.5 and 30% of all meiotic products of *R. pubera* and *R. tenuis*, respectively, show irregularities. Refer to text for further details. Parental chromosomes/chromatids are in red and blue, the spindle in green and chromatin threads in grey.

with a heteromorphic chromosome pair allowed to nonambiguously define segregation of sister chromatids during meiosis I in *R. pubera*, similar to earlier studies in the homopteran *Planococcus citri*[38].

Does meiosis in *R. pubera* fulfil all criteria to be defined as 'inverted meiosis'? As outlined above, the kinetic activity centres of the sister chromatids are in bipolar orientation. During anaphase I, sister chromatid cohesion seems to be lost and isolated chromatids segregate to opposite poles. In this sense, two of the three criteria for genuine inverted meiosis are satisfied. The question how homologous non-sister chromatids find each other during meiosis II to promote regular disjunction remains open.

In *R. pubera* prophase II, the chromatids resulting from anaphase I separation appear mostly as pairs or with DAPI-

stained threads connecting them. Some of the chromatid pairs are at a greater distance to each other, connected by a thin chromatin thread and, in some cases, individualized chromatids are connected to more than one chromatids. As in the case for *R. tenuis*, we believe that these chromatin threads are instrumental for associating (homologous) non-sister chromatids in preparation for the second meiotic division.

These threads could be heterochromatin; however, in contrast to *D. melanogaster*, which employs in some instances heterochromatic 45S rDNA repeat containing regions to connect achiasmatic chromosomes during meiosis I (ref. 16), the *R. pubera* 45S rDNA regions are not involved in these interactions. We do not believe that these threads are connected by maintained cohesion proteins, since bivalents with two crossovers (25% of all bivalents in *R. pubera*) would eventually have one sister chromatid connected to two different non-sister chromatids that would subsequently interfere with chromosome segregation; however, anaphase bridges have not been observed ($n = 30$). The idea of chromatin connections between non-sister chromatids finds further support by the results presented above for the achiasmatic meiosis in the closely related plant *R. tenuis* and by a parallel study performed in the holocentric plant *Luzula elegans*[55]. It appears unlikely that different solutions to cope with holocentricity have evolved in these closely related species. In case of *R. pubera*, we envisage a similar model as outlined for *R. tenuis*, with the addition that during prophase II chromatin connections may preferentially form between homologous non-sister chromatids since they originated from the same bivalent and were therefore in closer proximity.

Nevertheless, alternative ways to ensure proper chromosome segregation during meiosis emerged in other organisms with holocentric chromosomes. For instance, in *C. elegans* the chiasma position defines the orientation of bivalents to the spindle and thus how they attach to spindle microtubules[29,31] as also the regions for cohesin maintainance in meiosis I (ref. 28). Importantly, regions of sister chromatid cohesion maintenance also display synthetic attachment to the spindle in *C. elegans*. It appears that *R. pubera* and *R. tenuis* have adapted a different mode to deal with the holocentric nature of chromosomes during meiosis characterized by (I) amphitelic sister chromatid attachment in metaphase I, by (II) equational sister chromatid separation in anaphase I and (III) by employing a chromatin thread-mediated mechanism in prophase II to associate (homologous) non-sister chromatids for regular disjunction in meiosis II. Altogether, these meiotic alterations can be framed under the term 'inverted meiosis'.

Methods

Plant material. Individuals of *R. tenuis* were collected in Porto de Galinhas (Ipojuca, PE, Brazil) and individuals of *R. pubera* in Mata de Dois Irmãos (Recife, PE, Brazil). Both species were either cultivated in an open experimental garden or in a greenhouse. Vouchers are kept at the herbarium of the Federal University of Pernambuco.

Slide preparation, DAPI staining and CMA/DAPI banding. Anthers were fixed in ethanol-acetic acid (3:1 v/v) and stored in fixative at −20 °C. Anthers were digested in 4% cellulase, 4% pectolyase and 4% cytohelicase at 37 °C for 4 h, and meiocytes were squashed in a drop of 60% acetic acid. Coverslips were removed after freezing in liquid nitrogen and slides were kept at −20 °C before use. Slides were stained with DAPI, 1 μg ml^{-1}, for 30 min and mounted in glycerol/McIlvaine (1:1, v/v). The CMA/DAPI banding was performed as previously described[44]. For that, slides were aged for 3 days, stained with 0.5 mg ml^{-1} CMA for 1 h and restained with 2 μg ml^{-1} DAPI for 30 min more. Before analysis, slides were aged for 3 more days.

Fluorescent *in situ* hybridization. FISH was performed as described in ref. 56 with some modifications. In brief, slides were treated with pepsin (0.1 mg ml^{-1}) and denatured with 70% formamide for 10 min at 85 °C. Slides were then denatured once more together with the hybridization mix (50% (v/v) formamide, 10% (w/v) dextran sulfate, 2 × SSC, 10% (w/v) SDS, 2–5 ng μl^{-1} probe) for 10 min at 90 °C. After the stringency washes, slides were mounted with DAPI/Vectashield H-1000 (2 μg ml^{-1}). The 45S rDNA was detected using the probe R2, a 6.5-kb fragment of an 18S–5.8S–25S rDNA repeat unit from *Arabidopsis thaliana*[57], and the 5S rDNA was detected using the Rhy2 clone of *R. tenuis* as a probe[46]. The plasmid DNAs were isolated using the Plasmid Mini Kit (QIAGEN) and the 45S rDNA and 5S rDNA probes were labelled by nick translation (Invitrogen) with digoxigenin-11-dUTP (Roche Diagnostics) and Cy3-dUTP (GE Healthcare), respectively. The 45S rDNA probe was detected with sheep anti-digoxigenin fluorescein isothiocyanate (FITC) conjugate antibody (Roche) and amplified with rabbit anti-sheep FITC conjugate antibody (Dako).

Immunostaining. The immunostaining for ASY1 and H2AThr120ph (ref. 58) was performed as described in[59] with some modifications. Anthers were fixed in 4% paraformaldehyde in PBS buffer (1.3 M NaCl, 70 mM Na_2HPO_4, 30 mM NaH_2PO_4) for 40 min at room temperature (RT) and squashed in a drop of the same buffer. After coverslips were removed, slides were stained with DAPI/PBS (2 μg ml^{-1}) for selection of appropriate meiotic stages. Slides were then washed with PBS and blocked with 3% bovine serum albumin (BSA) for 10 min at RT. The antibodies used were rabbit anti-AtASY1 (ref. 41), diluted 1:250 in blocking solution, and goat anti-rabbit IgG FITC conjugated (Sigma, no. F9887), diluted 1:300. Slides were counterstained and mounted with DAPI/Vectashield H-1000 (2 μg ml^{-1}).

Immunostaining for RAD51 was performed as described in ref. 60 using a monoclonal mouse anti-Rad51 antibody (NeoMarkers, no. MS-988-P0), diluted 1:75, and goat anti-mouse IgG Alexa568 conjugated (Molecular Probes, no. A11031), diluted 1:300.

Immunolocalization of tubulin was performed as previously described[61] with some modifications. Anthers were pretreated with 0.1 mM m-maleimidobenzoic acid N-hydroxysuccinimide ester for 15 min at RT and fixed with 4% paraformaldehyde in PEM buffer (50 mM PIPES, 5 mM $MgSO_4$, 5 mM EGTA, 0.1% Triton X-100, pH 6.9) for 1 h at RT. Afterwards, anthers were squashed in the same buffer on a gelatin-coated slide. After coverslips were removed, slides were stained with DAPI/PEM (2 μg ml^{-1}) and selected under a fluorescence microscope. The best slides were washed in PEM, digested with 1.4% β-glucuronidase for 30 min at RT and blocked with 3% BSA for 1 h at RT. The antibodies used were mouse anti-β-tubulin (Sigma, no. T9026), diluted 1:40, and rabbit anti-mouse IgG TRITC conjugated (DAKO), diluted 1:25, or goat anti-mouse IgG Alexa568 conjugated (Molecular Probes, no. A11031), diluted 1:300.

For anti-grassCENH3 (ref. 62) immunostaining anthers undergoing meiosis were covered with ice-cold 100% methanol, allowing cells to fix for 30 min at −20 °C. The fixative was then aspirated and anthers were rinsed three times in PBS for 5 min each. Pollen mother cells were squeezed out from the anthers and squashed in a drop of 1 × PBS. The coverslips were removed following freezing in liquid nitrogen. The immunostaining procedure was conducted as described above.

Microscopy. Pictures of cells stained with DAPI or CMA/DAPI were taken with a Leica DMRB fluorescent microscope equipped with a Cohu digital camera and Leica Q-FISH programme. FISH pictures, together with RAD51 and ASY1 immunostaining pictures, were taken on a Carl Zeiss Axioplan 2 equipped with Photometrics Quantix camera and MetaMorph 7.1.4.0 software (Molecular Dynamics). Pictures of microtubule immunostaining were taken with the confocal microscope Carl Zeiss LSM 510 Meta using the LSM 510 programme. Image deconvolution was performed with the Auto Deblur 9.2.1 software (AutoQuant Imaging). Alternatively, pictures were taken with a Leica DM5500B microscope equipped with a deconvolution system and a Leica DFC345 FX camera. Further processing of images was made with HeliconFocus 5.0 and Adobe Photoshop CS4 softwares.

To analyse the substructures of immunosignals and chromatin beyond the classical Abbe/Raleigh limit at an optical resolution of ~120 nm (super resolution), structured illumination microscopy (SIM) was applied using a C-Apo × 63/1.2 W Korr objective of an Elyra microscope system and the software ZEN (Zeiss, Germany). Image stacks were captured separately for each fluorochrome using appropriate excitation and emission filters. Maximum intensity projections were generated from the stacks of optical SIM sections through the specimens by the ZEN software (three-dimensional-rendering based on SIM image stacks was carried out using the ZEN software).

References

1. Marston, A. L. Chromosome segregation in budding yeast: sister chromatid cohesion and related mechanisms. *Genetics* **196,** 31–63 (2014).
2. McNicoll, F., Stevense, M. & Jessberger, R. Cohesin in gametogenesis. *Curr. Top. Dev. Biol.* **102,** 1–34 (2013).
3. Keeney, S. Spo11 and the formation of DNA double-strand breaks in meiosis. *Genome Dyn. Stab.* **2,** 81–123 (2008).
4. Keeney, S. & Neale, M. J. Initiation of meiotic recombination by formation of DNA double-strand breaks: mechanism and regulation. *Biochem. Soc. Trans.* **34,** 523–525 (2006).

5. Edlinger, B. & Schlogelhofer, P. Have a break: determinants of meiotic DNA double strand break (DSB) formation and processing in plants. *J. Exp. Bot.* **62,** 1545–1563 (2011).
6. Page, S. L. & Hawley, R. S. Chromosome choreography: the meiotic ballet. *Science* **301,** 785–789 (2003).
7. de Boer, E. & Heyting, C. The diverse roles of transverse filaments of synaptonemal complexes in meiosis. *Chromosoma* **115,** 220–234 (2006).
8. Hamant, O., Ma, H. & Cande, W. Z. Genetics of meiotic prophase I in plants. *Annu. Rev. Plant Biol.* **57,** 267–302 (2006).
9. Hunter, N. in *Molecular Genetics of Recombination* 381–442 (Springer, 2007).
10. McKim, K. S. *et al.* Meiotic synapsis in the absence of recombination. *Science* **279,** 876–878 (1998).
11. Dernburg, A. F. *et al.* Meiotic recombination in C. elegans initiates by a conserved mechanism and is dispensable for homologous chromosome synapsis. *Cell* **94,** 387–398 (1998).
12. Phillips, C. M. *et al.* Identification of chromosome sequence motifs that mediate meiotic pairing and synapsis in *C. elegans*. *Nat. Cell. Biol.* **11,** 934–942 (2009).
13. Lake, C. M. & Hawley, R. S. The molecular control of meiotic chromosomal behavior: events in early meiotic prophase in *Drosophila* oocytes. *Annu. Rev. Physiol.* **74,** 425–451 (2012).
14. Hughes, S. E. *et al.* Heterochromatic threads connect oscillating chromosomes during prometaphase I in *Drosophila* oocytes. *PLoS Genet.* **5,** e1000348 (2009).
15. Tsai, J. H., Yan, R. & McKee, B. D. Homolog pairing and sister chromatid cohesion in heterochromatin in *Drosophila* male meiosis I. *Chromosoma* **120,** 335–351 (2011).
16. Tsai, J. H. & McKee, B. D. Homologous pairing and the role of pairing centers in meiosis. *J. Cell Sci.* **124,** 1955–1963 (2011).
17. Hauf, S. & Watanabe, Y. Kinetochore orientation in mitosis and meiosis. *Cell* **119,** 317–327 (2004).
18. Shao, T. *et al.* OsREC8 is essential for chromatid cohesion and metaphase I monopolar orientation in rice meiosis. *Plant Physiol.* **156,** 1386–1396 (2011).
19. Wang, M. *et al.* OsSGO1 maintains synaptonemal complex stabilization in addition to protecting centromeric cohesion during rice meiosis. *Plant J.* **67,** 583–594 (2011).
20. Monje-Casas, F., Prabhu, V. R., Lee, B. H., Boselli, M. & Amon, A. Kinetochore orientation during meiosis is controlled by Aurora B and the monopolin complex. *Cell* **128,** 477–490 (2007).
21. Li, X. X. & Dawe, R. K. Fused sister kinetochores initiate the reductional division in meiosis I. *Nat. Cell Biol.* **11,** 1103–U1122 (2009).
22. Ishiguro, T., Tanaka, K., Sakuno, T. & Watanabe, Y. Shugoshin-PP2A counteracts casein-kinase-1-dependent cleavage of Rec8 by separase. *Nat. Cell Biol.* **12,** 500–506 (2010).
23. Mola, L. M. & Papeschi, A. G. Holokinetic chromosomes at a glance. *J. Basic Appl. Genet.* **16,** 1–4 (2006).
24. Guerra, M. *et al.* Neocentrics and holokinetics (holocentrics): chromosomes out of the centromeric rules. *Cytogenet. Genome Res.* **129,** 82–96 (2010).
25. Melters, D. P., Paliulis, L. V., Korf, I. F. & Chan, S. W. Holocentric chromosomes: convergent evolution, meiotic adaptations, and genomic analysis. *Chromosome Res.* **20,** 579–593 (2012).
26. Dernburg, A. F. Here, there, and everywhere: kinetochore function on holocentric chromosomes. *J. Cell Biol.* **153,** F33–F38 (2001).
27. Schvarzstein, M., Wignall, S. M. & Villeneuve, A. M. Coordinating cohesion, co-orientation, and congression during meiosis: lessons from holocentric chromosomes. *Genes Dev.* **24,** 219–228 (2010).
28. Martinez-Perez, E. *et al.* Crossovers trigger a remodeling of meiotic chromosome axis composition that is linked to two-step loss of sister chromatid cohesion. *Genes Dev.* **22,** 2886–2901 (2008).
29. Wignall, S. M. & Villeneuve, A. M. Lateral microtubule bundles promote chromosome alignment during acentrosomal oocyte meiosis. *Nat. Cell Biol.* **11,** 839–U135 (2009).
30. Dumont, J., Oegema, K. & Desai, A. A kinetochore-independent mechanism drives anaphase chromosome separation during acentrosomal meiosis. *Nat. Cell Biol.* **12,** 894–901 (2010).
31. Albertson, D. G. & Thomson, J. N. Segregation of holocentric chromosomes at meiosis in the nematode, *Caenorhabditis elegans*. *Chromosome Res.* **1,** 15–26 (1993).
32. Malheiros, N., Castro, D. & Câmara, A. Cromosomas sem centrómero localizado. O caso de *Luzula purpurea* Link. *Agron. Lusit.* **9,** 51–73 (1947).
33. Chandra, H. S. Inverse meiosis in triploid females of mealy bug, *Planococcus citri*. *Genetics* **47,** 1441–1454 (1962).
34. Nordenskiold, H. Tetrad analysis and course of meiosis in three hybrids of *Luzula campestris*. *Hereditas* **47,** 203–237 (1961).
35. Pazy, B. & Plitmann, U. Persisting demibivalents - a unique meiotic behavior in *Cuscuta-babylonica choisy*. *Genome* **29,** 63–66 (1987).
36. Guerra, M. & Garcia, M. A. Heterochromatin and rDNA sites distribution in the holocentric chromosomes of *Cuscuta approximata Bab*. (Convolvulaceae). *Genome* **47,** 134–140 (2004).
37. Da Silva, C. R. M., Gonzalez-Elizondo, M. S. & Vanzela, A. L. L. Reduction of chromosome number in Eleocharis subarticulata (Cyperaceae) by multiple translocations. *Bot. J. Linn. Soc.* **149,** 457–464 (2005).
38. Bongiorni, S., Fiorenzo, P., Pippoletti, D. & Prantera, G. Inverted meiosis and meiotic drive in mealybugs. *Chromosoma* **112,** 331–341 (2004).
39. Kusanagi, A. Mechanism of post-reductional meiosis in *Luzula*. *Jpn. J. Genet.* **37,** 396–39 (1962).
40. Caryl, A. P., Armstrong, S. J., Jones, G. H. & Franklin, F. C. A homologue of the yeast HOP1 gene is inactivated in the Arabidopsis meiotic mutant asy1. *Chromosoma* **109,** 62–71 (2000).
41. Armstrong, S. J., Caryl, A. P., Jones, G. H. & Franklin, F. C. Asy1, a protein required for meiotic chromosome synapsis, localizes to axis-associated chromatin in Arabidopsis and Brassica. *J. Cell Sci.* **115,** 3645–3655 (2002).
42. Li, W. *et al.* The Arabidopsis AtRAD51 gene is dispensable for vegetative development but required for meiosis. *Proc. Natl Acad. Sci. USA* **101,** 10596–10601 (2004).
43. Vanzela, A. L. L., Cuadrado, A., Jouve, N., Luceno, M. & Guerra, M. Multiple locations of the rDNA sites in holocentric chromosomes of *Rhynchospora* (Cyperaceae). *Chromosome Res.* **6,** 345–349 (1998).
44. Vanzela, A. L. L. & Guerra, M. Heterochromatin differentiation in holocentric chromosomes of *Rhynchospora* (Cyperaceae). *Genet. Mol. Biol.* **23,** 453–456 (2000).
45. Guerra, M. Patterns of heterochromatin distribution in plant chromosomes. *Genet. Mol. Biol.* **23,** 1029–1041 (2000).
46. Sousa, A. *et al.* Distribution of 5S and 45S rDNA sites in plants with holokinetic chromosomes and the "chromosome field" hypothesis. *Micron* **42,** 625–631 (2011).
47. Fujiwara, H., Nakazato, Y., Okazaki, S. & Ninaki, O. Stability and telomere structure of chromosomal fragments in two different mosaic strains of the silkworm, *Bombyx mori*. *Zool. Sci.* **17,** 743–750 (2000).
48. San Martin, J. A. B., Andrade, C. G. T. D., Mastroberti, A. A., Mariath, J. E. D. & Vanzela, A. L. L. Asymmetric cytokinesis guide the development of pseudomonads in *Rhynchospora pubera* (Cyperaceae). *Cell Biol. Int.* **37,** 203–212 (2013).
49. Vanzela, A. L. L., Cuadrado, A. & Guerra, M. Localization of 45S rDNA and telomeric sites on holocentric chromosomes of *Rhynchospora tenuis* Link (Cyperaceae). *Genet. Mol. Biol.* **26,** 199–201 (2003).
50. Castiglione, M. R. & Cremonini, R. A fascinating island: $2n\frac{1}{4}4$. *Plant Biosyst.* **146,** 711–726 (2012).
51. Pradillo, M. *et al.* An analysis of univalent segregation in meiotic mutants of *Arabidopsis thaliana*: a possible role for synaptonemal complex. *Genetics* **175,** 505–511 (2007).
52. Pazy, B. Supernumerary chromosomes and their behaviour in meiosis of the holocentric *Cuscuta babylonica Choisy*. *Bot. J. Linn. Soc.* **123,** 173–176 (1997).
53. Viera, A., Page, J. & Rufas, J. in *Meiosis* Vol. 5, 137–156 (Karger, 2009).
54. Papeschi, A. G. & Mola, L. M. Meiotic studies in *Acanonicus-Hahni* (Stal) (Coreidae, Heteroptera).1. Behavior of univalents in desynaptic individuals. *Genetica* **80,** 31–38 (1990).
55. Heckmann, S. *et al.* Alternative meiotic chromatid segregation in the holocentric plant *Luzulaelegans*. *Nat. Commun.* **5,** 4979 (2014).
56. Pedrosa, A., Sandal, N., Stougaard, J., Schweizer, D. & Bachmair, A. Chromosomal map of the model legume *Lotus japonicus*. *Genetics* **161,** 1661–1672 (2002).
57. Wanzenbock, E. M., Schofer, C., Schweizer, D. & Bachmair, A. Ribosomal transcription units integrated via T-DNA transformation associate with the nucleolus and do not require upstream repeat sequences for activity in *Arabidopsis thaliana*. *Plant J.* **11,** 1007–1016 (1997).
58. Demidov, D. *et al.* Anti-phosphorylated histone H2AThr120: a universal microscopic marker for centromeric chromatin of mono- and holocentric plant species. *Cytogenet. Genome Res.* **143,** 150–156 (2014).
59. Manzanero, S., Arana, P., Puertas, M. J. & Houben, A. The chromosomal distribution of phosphorylated histone H3 differs between plants and animals at meiosis. *Chromosoma* **109,** 308–317 (2000).
60. Chelysheva, L. *et al.* An easy protocol for studying chromatin and recombination protein dynamics during *Arabidopsis thaliana* meiosis: immunodetection of cohesins, histones and MLH1. *Cytogenet. Genome Res.* **129,** 143–153 (2010).
61. Peirson, B. N., Bowling, S. E. & Makaroff, C. A. A defect in synapsis causes male sterility in a T-DNA-tagged *Arabidopsis thaliana* mutant. *Plant J.* **11,** 659–669 (1997).
62. Nagaki, K. *et al.* Sequencing of a rice centromere uncovers active genes. *Nat. Genet.* **36,** 138–145 (2004).

Acknowledgements

We thank Josef Loidl, Andreas Houben and Marie-Therese Kurzbauer for inspiring discussions and intellectual input and Pawel Pasierbek (IMP, Vienna) for his help with advanced imaging techniques. We are thankful to Chris Franklin for kindly providing the anti-ASY1 antibody. G.C. and A.P.-H. were supported by the Brazilian agency Conselho

Nacional do Desenvolvimento Científico e Tecnológico (CNPq) and A.M. by the Brazilian agency Coordenação de Aperfeiçoamento de Pessoal de Nível Superior. P.S. was supported by the Austrian Science Fund grant F19307 and by the Austrian Academy of Science grant APART11230.

Author contributions

G.C. and A.M. performed the experiments shown. P.S. and A.P.-H. conceived the experiments and G.C., A.M., A.P.-H. and P.S. analysed the data. P.S. wrote the manuscript with extensive contribution of all authors.

Additional information

Supplementary Information accompanies this paper at http://www.nature.com/naturecommunications

Competing financial interests: The authors declare no competing financial interests.

Reprints and permission information is available online at http://npg.nature.com/reprintsandpermissions/

How to cite this article: Cabral, G. *et al.* Chiasmatic and achiasmatic inverted meiosis of plants with holocentric chromosomes. *Nat. Commun.* 5:5070 doi: 10.1038/ncomms6070 (2014).

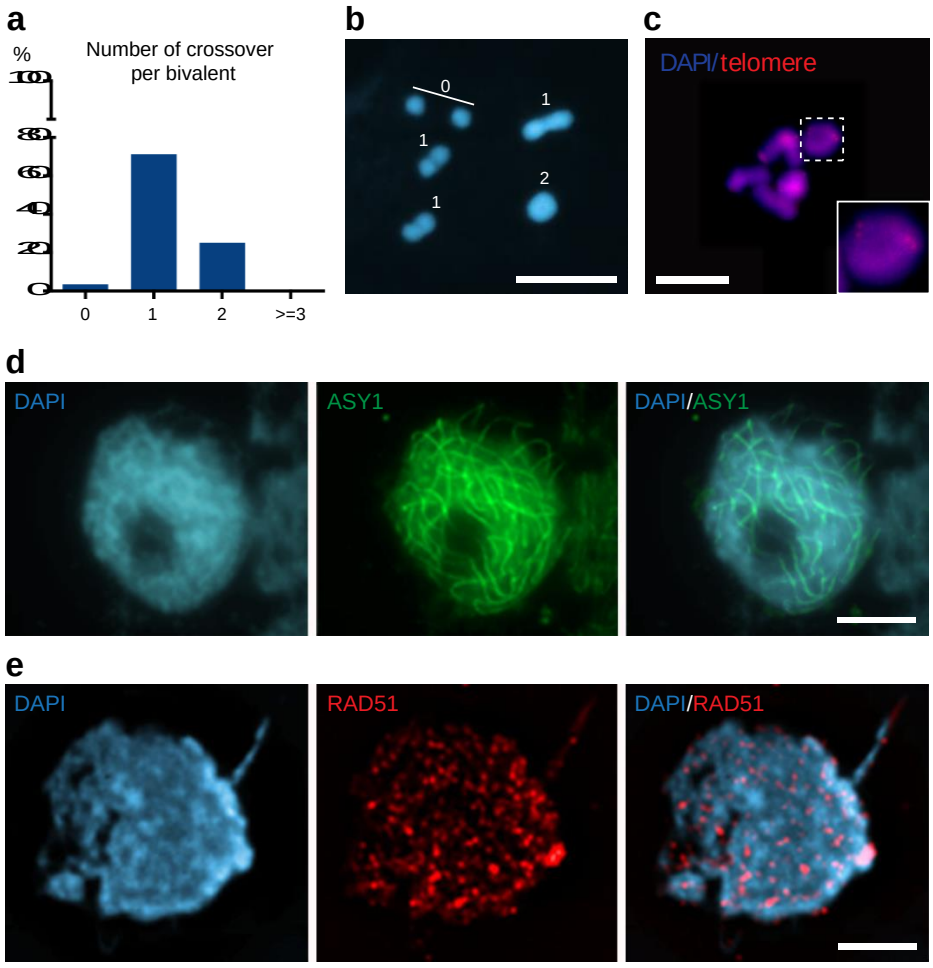

Supplementary Figure 1. Additional information on meiosis in *R. pubera*. a) The graph shows the distribution of chiasmata per bivalent/chromosome pair (n=1379) and the image in **b**) depicts a metaphase I cell showing one chromosome pair without a chiasma (0), three bivalents with one chiasma (1) and one bivalent with two chiasmata (2). **c**) Chiasmata have been observed at terminal positions. The panel highlights a ring bivalent with chiasmata located close to the telomere signals. **d**) Localization of ASY1 (green) in a leptotene nucleus indicates the formation of a meiotic chromosome axis. **e**) Leptotene nucleus with RAD51 (red) foci indicating the occurrence of DNA double strand breaks and subsequent processing. Size bars in (c), (d) and (e) correspond to 5µm and in (b) to 10µm.

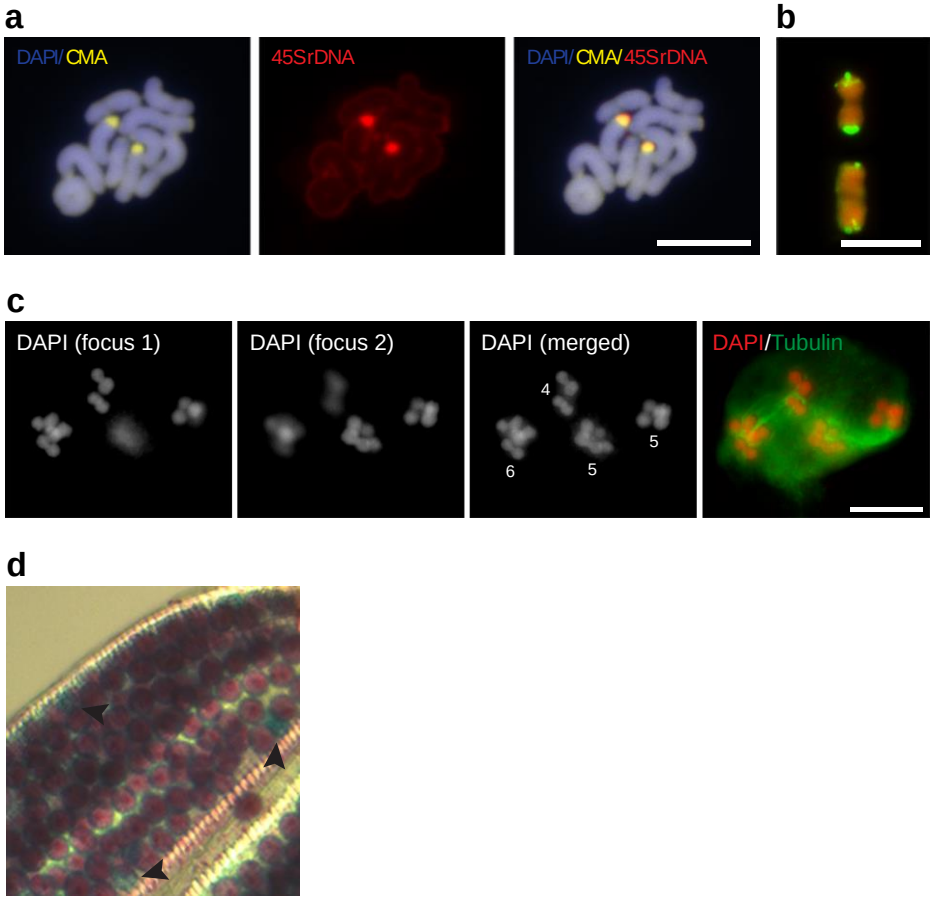

Supplementary Figure 2. 45S rDNA in *R. pubera*. **a**) Images show a mitotic metaphase cell of *R. pubera*. The CMA signal (yellow; left panel) and the 45S rDNA signal (red; middle panel) co-localize (right panel) at the telomeres of one chromosome pair. **b**) *in situ* hybridisation of 45S rDNA on rod bivalents in meiotic metaphase I to demonstrate the orientation of chromatids within the bivalent. 45S rDNA regions are located at the distal ends of rod bivalents. Chromosomes in red, 45S loci in green. **c**) Mis-segregation in meiosis II. Different focal planes of a late anaphase II stage with two unbalanced products (4 and 6 chromatids) and two balanced products (5 and 5 chromatids). Chromosomes in red, tubulin in green. **d**) Detail of an anther with viable pollen in magenta and non-viable pollen in green (arrowheads). Size bar in (b) corresponds to 5µm and in (a) and (c) to 10µm.

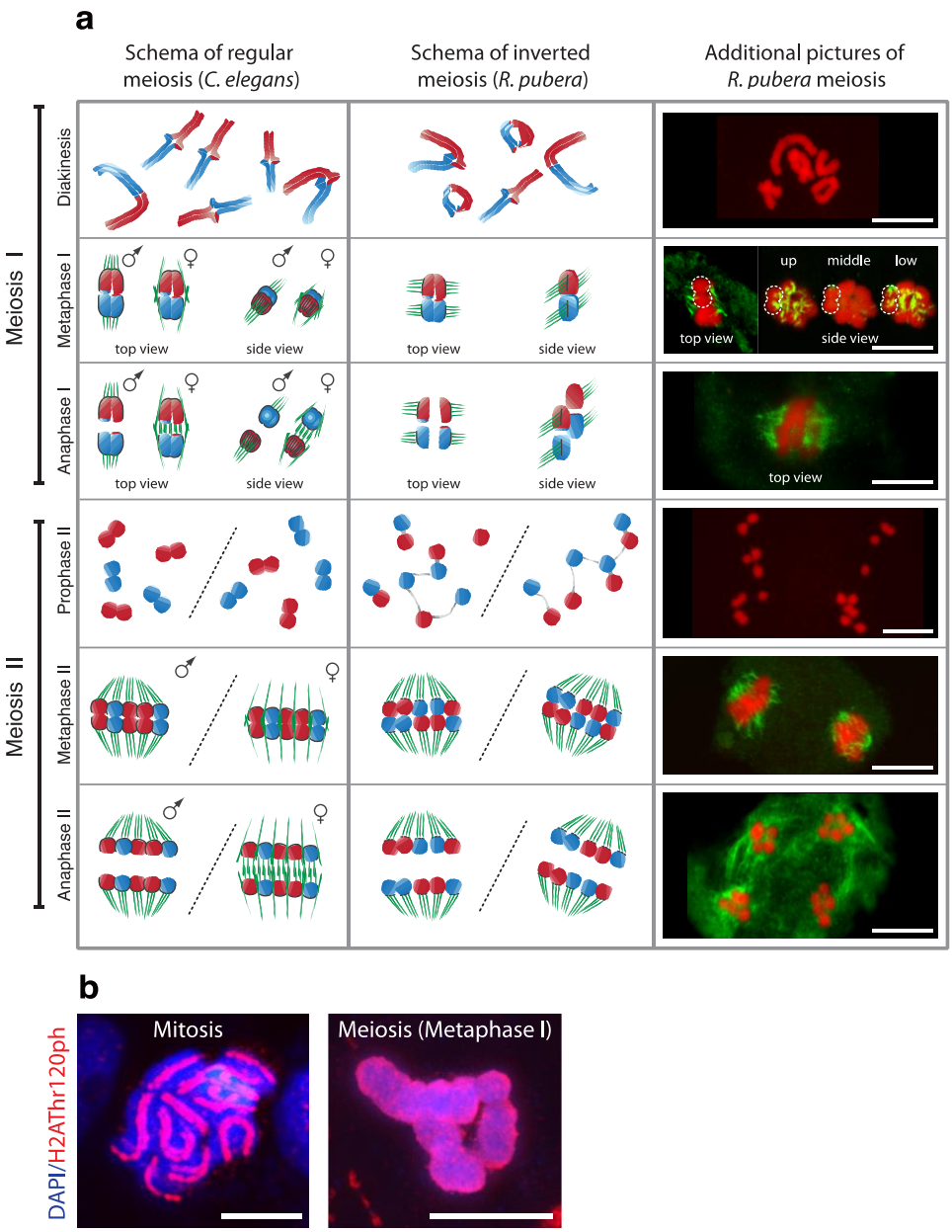

Supplementary Figure 3. Schema of regular and inverted meiosis. a) Illustration of regular meiotic progression in *C. elegans* (left row) and the inverted sequence of events in *R. pubera* (middle row). During meiosis I chromosomes recombine, pair and bivalents with chiasmata become visible in diakinesis. At metaphase I, (only one, rod-shaped bivalent is shown) chromosomes align at the metaphase plate. While in *C. elegans* sister chromatids are mono-oriented towards the same side of the spindle and

the meiotic spindle forms a barrel around the bivalents (female) or shows terminal associations (male), sister chromatids of *R. pubera* show amphitelic attachment to the spindle. At anaphase I, *C. elegans* homologs are separated while in *R. pubera* sister chromatids are separated from each other and pulled to different poles. At prophase II (each half of the dyad shown), sister chromatids of *C. elegans* are still held together by cohesins (not shown). In contrast, the non-sister-chromatids of *R. pubera* appear individualized with some being connected with thin chromatin threads. Importantly, the diploid number of DAPI stained bodies can clearly be visualized in each half of the dyad in prophase II, following the expectations of sister separation during meiosis I. In *C. elegans* at metaphase II/anaphase I, sister chromatids align and are subsequently separated. In *R. pubera*, chromatids associate with the help of an unknown mechanism and subsequently undergo disjunction during anaphase II. The model idealises regular disjunction in meiosis II but actually 19,5% of all meiotic products of *R. pubera* show irregularities. Chromosomes/chromatids are in red and blue, the spindle in green and chromatin threads in grey. Additional images of *R. pubera* meiosis, corresponding to the shown stages (right row), with chromosomes in red and tubulin in green. The size bars correspond to 10µm.

b) H2AThr120ph distribution in *R. pubera*. Mitotic (left panel) and meiotic (right panel) chromosomes (blue) stained with an antibody directed against H2AThr120ph (magenta). While during mitotic metaphase H2AThr120ph appears to be distributed along the chromosomes, defining holocentric kinetochore regions, its distribution during meiotic metaphase I is less specific. Size bar corresponds to 5µm for mitosis and 10µm for meiosis.

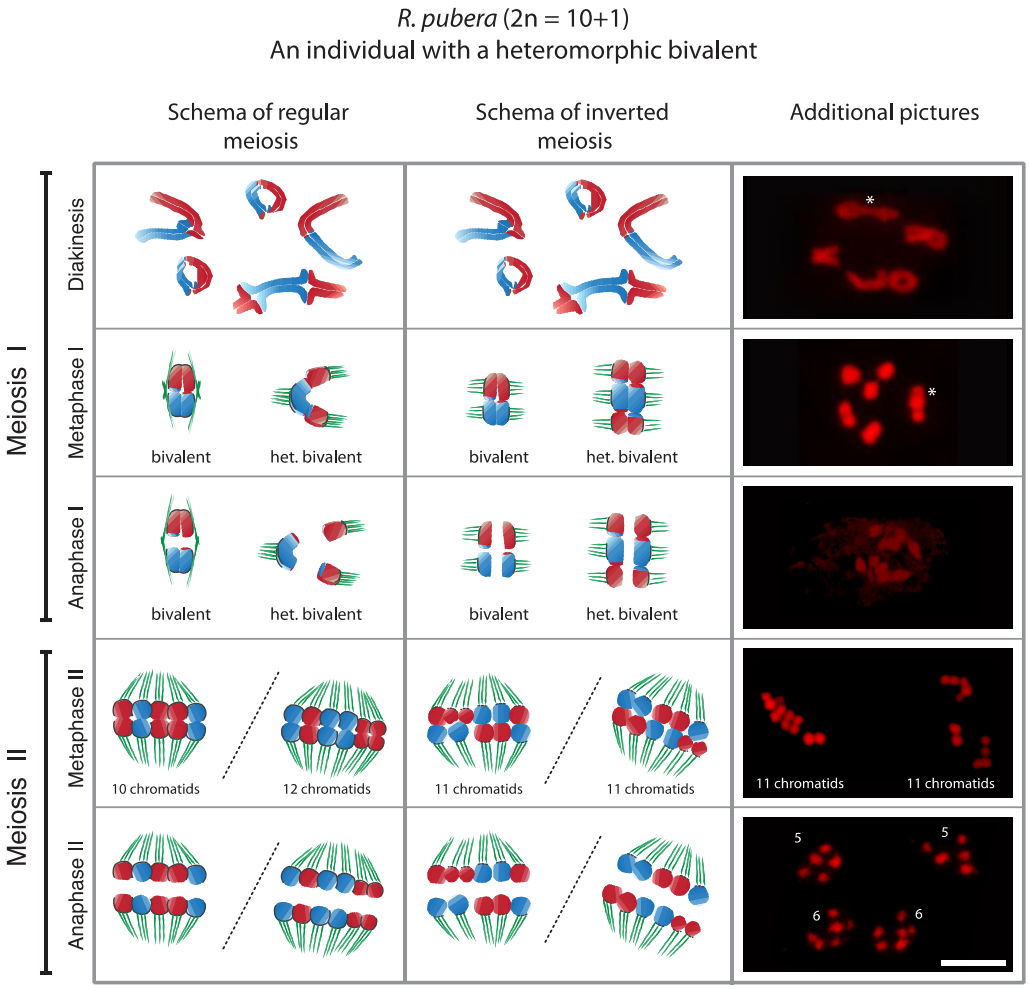

Supplementary Figure 4. *R. pubera* plant with heteromorphic chromosome pair. The figure compares a hypothetical, regular meiotic sequence (left row) with the predictions for an inverted meiotic sequence (middle row) in a *R. pubera* individual with a broken chromosome. During meiosis I chromosomes recombine and pair. At diakinesis, regular bivalents and also one heteromorphic bivalent (het. bivalent) become visible. The latter is comprised of the intact chromosome pairing with the two broken chromosome parts of the homolog (according to our observations, both fragments were always paired with the corresponding intact partner; n = 45). In metaphase I, (only one, rod-shaped, regular bivalent and the trivalent are shown)

chromosomes align at the metaphase plate. In a hypothetical regular meiosis the spindle will either attach to both parts of the broken chromosome (shown) or only to one part of the broken chromosome (not shown) and this will then lead to unequal numbers of chromosomes/fragments in the resulting dyad. In case of an inverted sequence of events in the holocentric plant *R. pubera*, both sisters of the broken chromosome fragments will be distributed to either part of the resulting dyad, yielding balanced numbers of chromatids/fragments. Additional images of *R. pubera* (2n= 10+1) meiosis, corresponding to the stages shown in the cartoon, are provided (right row). Chromosomes are shown in red and the heteromorphic bivalent is highlighted with an asterisk. Importantly, the expectations of inverted meiosis with segregation of sister chromatids at anaphase I (11 chromatids/fragment at each side of the dyad/metaphase II) are always met (n = 24). Refer to text for further details. Parental chromosomes/chromatids are in red and blue and the spindle in green. The size bar corresponds to 10µm.

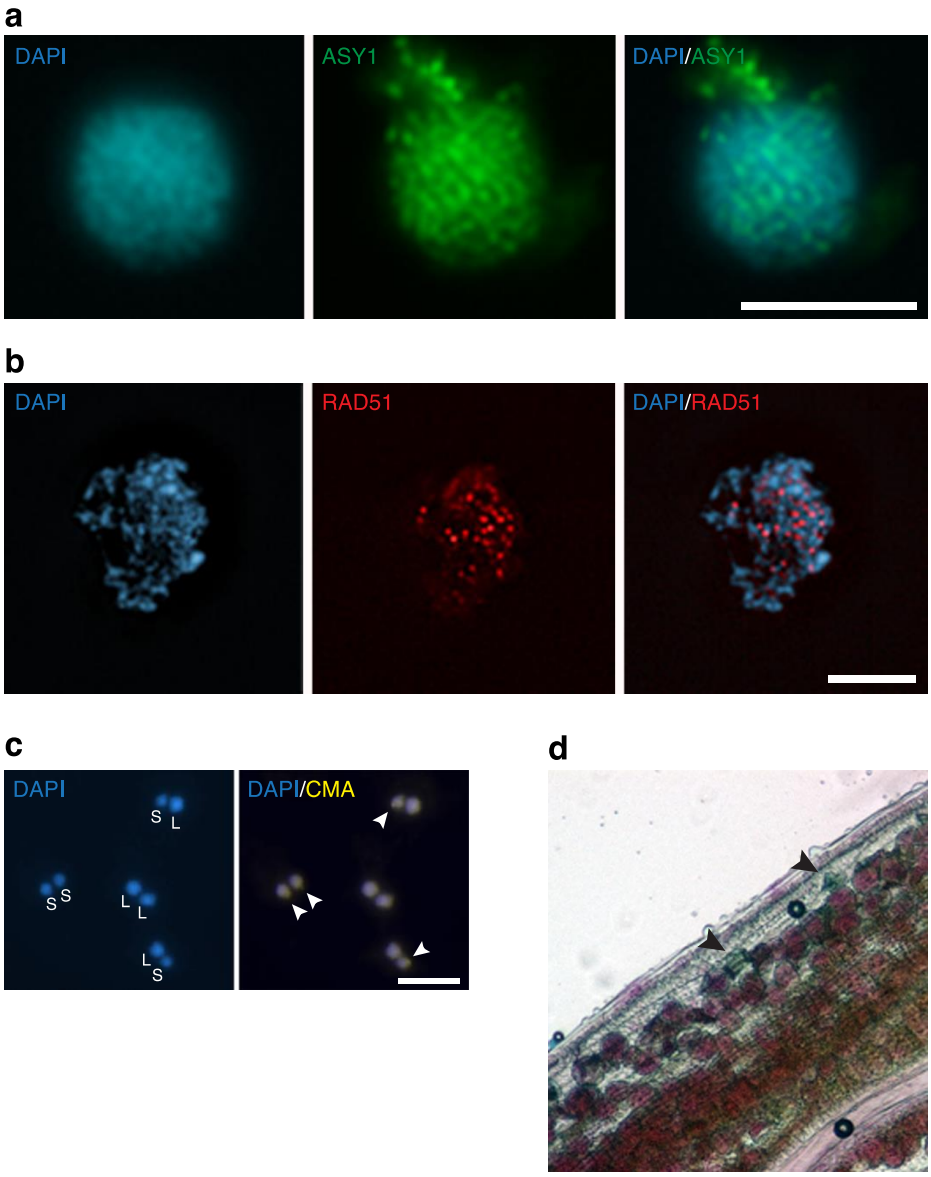

Supplementary Figure 5. Additional data for *Rhynchospora tenuis*. **a**) Localization of ASY1 (green) in a leptotene nucleus indicates the formation of a meiotic chromosome axis. **b**) Zygotene nucleus with RAD51 (red) foci indicating the occurrence of DNA double strand breaks and subsequent processing. **c**) Mis-segregation in meiosis II. Small (S) and large (L) chromatids are indicated and their identity further corroborated by CMA staining (arrowheads). Two meiosis II products with regular disjunction (SL) and two products with irregular disjunction (SS and LL,

respectively) are shown. **d**) Detail of an anther with viable pollen in magenta and non-viable pollen in green (arrowheads). Size bars in (a) and (b) correspond to 5µm and in (c) to 10µm.

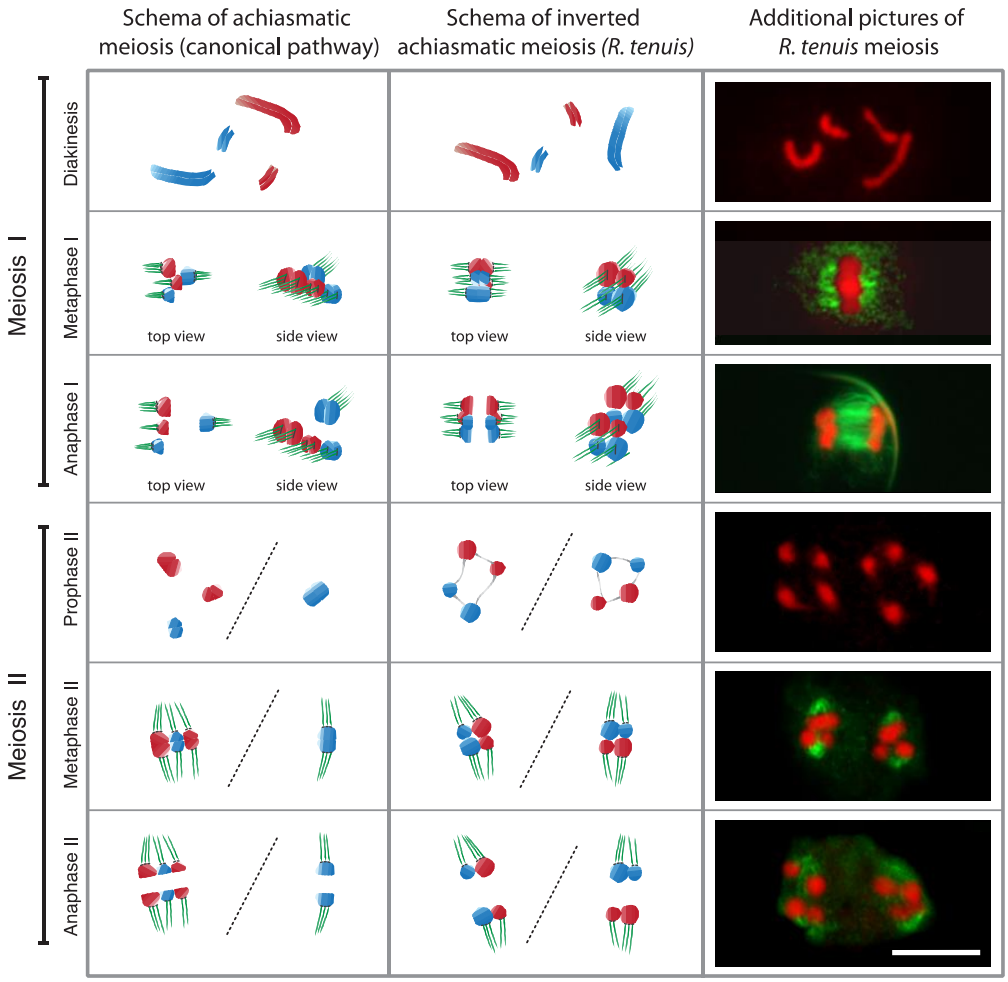

Supplementary Figure 6. Schema of achiasmatic meiotic division patterns. The figure compares a hypothetical achiasmatic meiotic progression embedded in a regular meiotic sequence (left row) with the predictions for an achiasmatic meiosis embedded in an inverted meiotic sequence (middle row). The 4 chromosomes of *R. tenuis* do not form chiasmata and univalents become visible at diakinesis. In the canonical meiotic pathway, univalent are expected to be randomly distributed at anaphase I. In contrast, in case of inverted meiosis sister chromatids become individually attached to the spindle and are separated during anaphase I. The expectation is, to see 4 chromatids in both parts of the resulting dyad and also error-

free, reliable disjunction. Indeed, these expectations are always met (n = 107) (compare with images in the right row at prophase II, and also with data presented in Fig. 5). All four chromatids of *R. tenuis* appear interconnected by thin chromatin threads. In metaphase II, chromatids align and subsequently undergo disjunction during anaphase II. In the case of achiasmatic meiosis, following the canonical pathway, the second meiotic division is expected to resemble an equational, error-free division. In contrast, the second division of an inverted meiosis is expected to face the problem of distributing homologous non-sister chromatids. Depending on the accuracy of a hypothetical mechanism to promote regular disjunction, errors during chromatid disjunction are expected in the second meiotic division of an inverted meiosis. Indeed, about 30% of all meiotic products of *R. tenuis* show irregularities. These results strongly support the claim of inverted meiotic events in *R. tenuis*. Refer to text for further details. Parental chromosomes/chromatids are in red and blue, the spindle in green and chromatin threads in grey. Additional images of *R. tenuis* meiosis, corresponding to the stages shown in the cartoon, are provided (right row), with chromosomes in red and tubulin in green. The size bar corresponds to 10µm.

Capítulo 2: Holocentromeres in *Rhynchospora* are associated with genome-wide centromere-specific repeat arrays interspersed among euchromatin

Artigo publicado no periódico *PNAS*

Holocentromeres in *Rhynchospora* are associated with genome-wide centromere-specific repeat arrays interspersed among euchromatin

André Marques[a,b], Tiago Ribeiro[a,b], Pavel Neumann[c], Jiří Macas[c], Petr Novák[c], Veit Schubert[b], Marco Pellino[b], Jörg Fuchs[b], Wei Ma[b], Markus Kuhlmann[b], Ronny Brandt[b], André L. L. Vanzela[d], Tomáš Beseda[e], Hana Šimková[e], Andrea Pedrosa-Harand[a,1], and Andreas Houben[b,1]

[a]Laboratory of Plant Cytogenetics and Evolution, Department of Botany, Federal University of Pernambuco, 50670-420 Recife, Pernambuco, Brazil; [b]Leibniz Institute of Plant Genetics and Crop Plant Research Gatersleben, 06466 Stadt Seeland, Germany; [c]Laboratory of Molecular Cytogenetics, Institute of Plant Molecular Biology, Biology Centre of the Academy of Sciences of the Czech Republic, 370 05 Ceske Budejovice, Czech Republic; [d]Laboratory of Cytogenetics and Plant Diversity, Department of General Biology, State University of Londrina, 86057-970, Londrina, Paraná, Brazil; and [e]Center of the Region Haná for Biotechnological and Agricultural Research, Institute of Experimental Botany, CZ-78371 Olomouc, Czech Republic

Edited by James A. Birchler, University of Missouri-Columbia, Columbia, MO, and approved September 11, 2015 (received for review June 23, 2015)

Holocentric chromosomes lack a primary constriction, in contrast to monocentrics. They form kinetochores distributed along almost the entire poleward surface of the chromatids, to which spindle fibers attach. No centromere-specific DNA sequence has been found for any holocentric organism studied so far. It was proposed that centromeric repeats, typical for many monocentric species, could not occur in holocentrics, most likely because of differences in the centromere organization. Here we show that the holokinetic centromeres of the Cyperaceae *Rhynchospora pubera* are highly enriched by a centromeric histone H3 variant-interacting centromere-specific satellite family designated "Tyba" and by centromeric retrotransposons (i.e., CRRh) occurring as genome-wide interspersed arrays. Centromeric arrays vary in length from 3 to 16 kb and are intermingled with gene-coding sequences and transposable elements. We show that holocentromeres of metaphase chromosomes are composed of multiple centromeric units rather than possessing a diffuse organization, thus favoring the polycentric model. A cell-cycle–dependent shuffling of multiple centromeric units results in the formation of functional (poly)centromeres during mitosis. The genome-wide distribution of centromeric repeat arrays interspersing the euchromatin provides a previously unidentified type of centromeric chromatin organization among eukaryotes. Thus, different types of holocentromeres exist in different species, namely with and without centromeric repetitive sequences.

centromere | satellite DNA | holokinetic | chromosome | evolution

The centromere is the chromosome region where the microtubules attach to the chromatids to enable their movement to the daughter cells during mitosis and meiosis. This region is often enriched in repetitive DNA families, with satellite DNAs (satDNAs) and transposable elements, such as *Ty3/gypsy*-like retrotransposons being the most frequent ones in plants. However, there is little sequence conservation among species (1, 2), and centromere-specific sequences are neither sufficient nor required for the centromere identity (3). Instead, the assembly site for the kinetochore complex of most active centromeres is epigenetically determined by the chromosomal location of the centromeric histone H3 variant CENH3, also known as "CENP-A" (4). Nevertheless, some evolutionary preferences seem to exist, and long-established centromeres are frequently formed on long arrays of satDNAs and/or transposable elements (1).

In certain independent eukaryotic lineages holocentric (also called "holokinetic") chromosomes occur. These holocentrics lack a primary constriction, and they form kinetochores distributed along almost the entire poleward surface of the chromatids, to which the spindle fibers attach (5, 6). The best-analyzed organisms possessing holocentric chromosomes are the nematode *Caenorhabditis elegans* (7, 8) and some species of the plant genus *Luzula* (9–11). In both cases, a longitudinal CENH3-positive centromere structure was observed during mitosis. In the rush *Luzula* (Juncaceae), the longitudinal centromere forms a groove (here referred as the "centromere groove") in each sister chromatid along almost the whole metaphase chromosome except for the most terminal regions (9–11). Recently, a similar centromere organization was found in the sedge species *Rhynchospora pubera* (12). The absence of CENH3 and the centromeric protein C (CENP-C) in some lineages of holocentric insects (13) challenges the general notion of a conserved molecular composition of centromeres in mono- and holokinetic chromosome species. Furthermore, no centromere-specific repeat has been identified thus

Significance

Holocentric chromosomes are characterized by kinetochore activity along each sister chromatid. Although the kinetochore structure seems to be well conserved, as in monocentric organisms, the organization of holocentromeres is still elusive, and no centromeric repeat has been found associated with centromeric histone H3 variant-positive centromeric nucleosomes for any holocentric organism studied hitherto. We demonstrate that holocentrics of the sedge (Cyperaceae) *Rhynchospora pubera* possess different classes of centromere-specific repeats. Holocentromeres are composed of multiple centromeric units interspersing the gene-containing chromatin, and, as a functional adaption, a cell-cycle–dependent shuffling of centromeric units results in the formation of functional (poly)centromeres during cell division. The genome-wide distribution of centromeric repeat arrays interspersing the euchromatin provides a previously unidentified type of centromere organization.

Author contributions: A.M., A.P.-H. and A.H. designed research; A.M., T.R., P. Neumann, J.M., P. Novák, V.S., M.P., J.F., W.M., M.K., R.B., A.L.L.V., T.B., and H.Š. performed research; A.M., P. Neumann, J.M., P. Novák, and V.S. analyzed data; and A.M., P. Neumann, J.M., A.P.-H., and A.H. wrote the paper.

The authors declare no conflict of interest.

This article is a PNAS Direct Submission.

Freely available online through the PNAS open access option.

Data deposition: Assembled BAC sequences are available through the iPlant Data Store and can be accessed via iPlant Discovery Environment or at https://de.iplantcollaborative.org/dl/d/8258A143-C5F5-4DF1-84F2-88C94BE8EA8F/R_pubera_holocentromeres_data.rar. Original ChIP-sequencing sample data, original Illumina sequencing data for the genomic DNA and BACs, and RNA-sequencing data have been deposited at the Sequence Read Archive (www.ebi.ac.uk/ena/) [accession nos. PRJEB9647 (ChIP-sequencing sample data), PRJEB9643 (Illumina sequencing data for genomic DNA), PRJEB9649 (Illumina sequencing data for BACs), and PRJEB9645 (RNA-sequencing data)]. CENH3 cDNA sequences variants were deposited in the GenBank database [accession nos. KR029618 (RpCENH3_1) and KR029619 (RpCENH3_2)].

[1]To whom correspondence may be addressed. Email: andrea.pedrosaharand@pesquisador.cnpq.br or houben@ipk-gatersleben.de.

This article contains supporting information online at www.pnas.org/lookup/suppl/doi:10.1073/pnas.1512255112/-/DCSupplemental.

far for any species possessing holocentric chromosomes (14–17). For instance, Heckmann, et al. (15) have characterized the high-copy fraction of the *Luzula elegans* genome in detail, and none of the identified repeats showed colocalization with the holokinetic centromere. Even in *C. elegans,* where robust studies [Chip-on chip (ChIP-chip) and ChIP sequencing (ChIP-seq)] were performed, no centromere-specific repeats were identified (14, 16).

ChIP-chip experiments suggested that nearly half of the *C. elegans* genome may be associated with CENH3 domains, although only 4% of them form the holocentromeres. Therefore, CENH3 nucleosomes may assemble at random positions (14). However, a recent study based on native CENH3 ChIP sequencing proposed that the holocentromeres in *C. elegans* consist of about 700 individual centromeric units distributed along the length of the chromosomes. Each of these units is formed by only one CENH3-containing nucleosome, where microtubules attach during cell division. These centromeric sites coincide with transcription factor hotspots which are occupied by many transcription factors, without having high binding affinity for any of them (16). The observation that any sequence of *C. elegans* can be propagated as an extrachromosomal array suggests that no specialized sequences are required for the segregation of holocentric chromosomes (18). On the other hand, that DNA arrays did not segregate with the same fidelity as normal chromosomes indicates that these extrachromosomal arrays lack certain features that promote mitotic stability of wild-type chromosomes (19).

To test the assumption that all holocentromeres are devoid of centromere-specific repeats, we analyzed *R. pubera* (12, 20–22). We report here on the first (to our knowledge) conserved centromere-specific repeats of a holocentric species and propose a model of chromosome organization for species with centromeric repeats distributed throughout the entire genome.

Results

Satellite Repeat Tyba Shows a Holocentromere-Specific Localization. To identify putative centromeric repeats in the genome of the holocentric plant *R. pubera*, with diploid chromosome number 2n = 10 and a genome size of the unreplicated reduced chromosome complement (1C) = 1.61 Gbp, we performed high-throughput shotgun sequencing. A randomly sampled proportion (8.89 million) of generated paired-end reads then was subjected to bioinformatic analysis, implemented within the clustering-based repeat identification pipeline (23, 24). This analysis resulted in thousands of clusters, or groups of reads, with overlapping sequences, each representing a single repeated element or part of it. After repeat classification within major clusters, the global repeat composition of the genome was determined by taking into account the sizes (number of reads) of individual clusters, which are proportional to the genomic abundance of the corresponding repeats.

The *R. pubera* genome was found to be relatively poor in repeated sequences, with highly and moderately repetitive elements represented by clusters with genome proportions of at least 0.01%, collectively making up 41.16% of the genome. The majority of these sequences were classified into the major classes of repetitive DNA. DNA transposons (8.81% of the genome), with more than half represented by miniature inverted-repeat transposable elements (MITEs), accounted for the most frequent repetitive elements, followed by *Ty1/copia* (8.68%) and *Ty3/gypsy* (5.14%) LTR retrotransposons. Other classes of repetitive DNA, such as non-LTR retrotransposons, pararetroviruses, *hAT* DNA transposons, and helitrons were found in much lower genomic proportions (*SI Appendix*, Table S1).

All satDNA reads were grouped into two highly abundant clusters, representing 2.24% and 1.36% of the genome. Because of the high similarity of reads (~70%) present in both clusters, they were considered as two subfamilies of the same satDNA repeat, named "Tyba" (meaning "abundance" in Tupi-Guarani, a language spoken by many Brazilian native tribes), and were designated "Tyba1" and "Tyba2." The consensus monomer length of Tyba1 and -2 is 172 bp (*SI Appendix*, Fig. S2*C*), which is in the range of

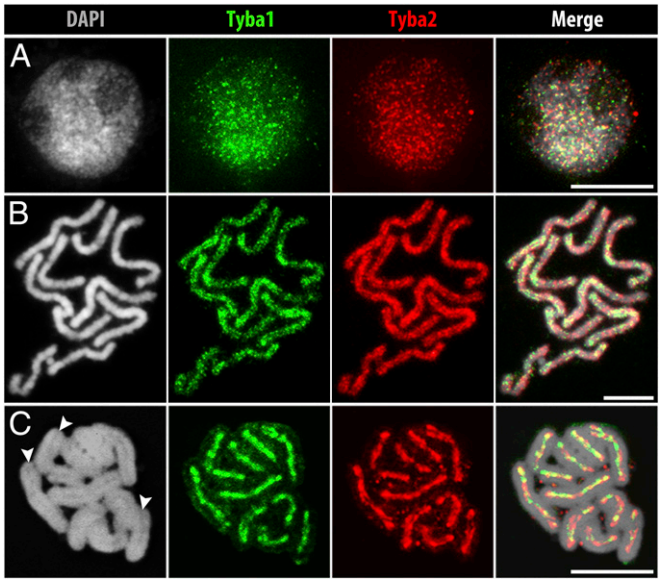

Fig. 1. FISH localization of Tyba1 and -2 in *R. pubera*. (*A*) Hybridization signals of both Tyba subfamilies in an interphase nucleus show a genome-wide dot-like labeling. (*B*) Prometaphase chromosomes show a line-like but dispersed labeling on the poleward surface of each chromatid and (*C*) a distinct labeling along the centromere groove of both sister chromatids during metaphase. Arrowheads in C indicate grooves. (Scale bars: 5 μm.)

monomer lengths of many other known centromeric satDNAs (1, 25, 26). After FISH with Tyba1- and Tyba2-specific probes, interphase nuclei showed dispersed dot-like signals (Fig. 1*A*), contrasting with the typical strong clustered distribution of satDNA in interphase nuclei of other species. With the onset of chromosome condensation, Tyba signals associate and form dot-like lines along the sister chromatids (Fig. 1*B* and *SI Appendix* Fig. S1*A*). At metaphase, all chromosomes showed line-like FISH signals colocalizing with the longitudinal DAPI-negative centromere groove (Fig. 1*C* and Movie S1). The hybridization intensity of Tyba1 and -2 probes varied along the chromatids, but only minor labeling was found outside the groove. Both the repetitive nature and the chromosomal distribution of Tyba1 and -2 indicate that this satDNA family is centromere specific in *R. pubera*. In contrast, other high-copy sequences, such as MITE DNA transposons, showed dispersed labeling throughout the chromosomes (*SI Appendix*, Fig. S1*B*).

Because no other high-copy satellite repeat other than Tyba was found in *R. pubera,* and no heterochromatic domains are visible throughout the cell cycle, we asked whether this genome is organized on a large scale into euchromatin- and heterochromatin-enriched subregions. Therefore, we applied antibodies against typical euchromatin- and heterochromatin-associated histone methylation marks (H3K4me3 and H3K9me2, respectively). In agreement with other holocentric species (15, 27) the euchromatin and heterochromatic domains in *R. pubera* were found dispersed along the entire chromosomes (*SI Appendix*, Fig. S1 *C* and *D*). Thus, on a large scale, euchromatin and heterochromatic domains are interspersed.

Tyba satDNA Interacts with CENH3-Containing Nucleosomes. The centromere specificity of Tyba repeats was tested by colocalization analysis and ChIP with a *R. pubera*-specific CENH3 antibody. First, the pollen mother cell transcriptome of *R. pubera* was determined, and assembled RNA-sequencing (RNA-seq) reads were used to identify *CENH3*. RT-PCR revealed, in addition to the 680-bp-long *CENH3*-like sequence (*RpCENH3_1*, GenBank accession no. KR029618), a second *CENH3*-like variant (*RpCENH3_2*, GenBank accession no. KR029619) of 708 bp, characterized by an insertion in the C-terminal tail after the stop codon (*SI Appendix*, Fig. S2*A*). Both are expressed mainly

in anthers and roots but less in leaf tissue, most likely because of the higher number of dividing cells in anthers and roots (*SI Appendix*, Fig. S2*D*). Alignment of the *R. pubera* CENH3 candidates with CENH3s of other plant species supported the correct identification (*SI Appendix*, Fig. S2*B*). Phylogenetic analysis grouped both RpCENH3s as a sister branch of Juncaceae and other monocot CENH3s (*SI Appendix*, Fig. S2*E*) (transcriptome assemblies, alignments, and trees are available through the iPlant Data Store and can be accessed via iPlant Discovery Environment or at https://de.iplantcollaborative.org/dl/d/8258A143-C5F5-4DF1-84F2-88C94BE8EA8F/R_pubera_holocentromeres_data.rar).

Next, an antibody (anti-RpCENH3) designed to recognize both CENH3 variants of *R. pubera* was generated and used for immunostaining. A specific labeling of the centromere groove was found at metaphase (*SI Appendix*, Fig. S3*A* and Movie S2). In interphase nuclei, a dispersed distribution of CENH3 foci was found, whereas prophase chromosomes displayed line-like signal arrangements (*SI Appendix*, Fig. S3 *B* and *C*). Colocalization experiments using the CENH3-specific antibody and a Tyba-specific FISH probe revealed a coincidence of both signal patterns along the holocentromeres of metaphase chromosomes (Fig. 2 *A* and *B* and Movie S3) and in interphase nuclei (Fig. 2*C*). Detailed analyses using super-resolution microscopy at a lateral resolution of ~120 nm quantified an overlap of 57.8% of CENH3 signals with Tyba signals and a 69.1% overlap of Tyba with CENH3 in interphase ($n = 4$). Within the holocentromeres of metaphase chromosomes ($n = 8$) these values amounted to 53.6% and 76.0%, respectively. Double-labeling experiments on extended chromatin fibers confirmed the segmental overlap of the two signal types (Fig. 2*D*). Hence, as in other species e.g., *Arabidopsis*, maize, rice, and humans (28–31), not all centromeric repeat copies interact with CENH3-containing chromatin, and vice versa. Finally, the association of the satDNA with functional centromeres was analyzed by CENH3-ChIP. Quantitative PCR showed a higher than fourfold enrichment of Tyba1 and -2 in the RpCENH3-ChIP-DNA compared to the input DNA (*SI Appendix*, Fig. S2*F*). Analysis of ChIP-seq reads demonstrated that Tyba1 and -2 showed the highest level of association in the immunoprecipitated fraction, with 10- and 15-fold enrichment, respectively (Fig. 3*A*). Thus, both members of the Tyba satDNA interact with CENH3-containing nucleosomes.

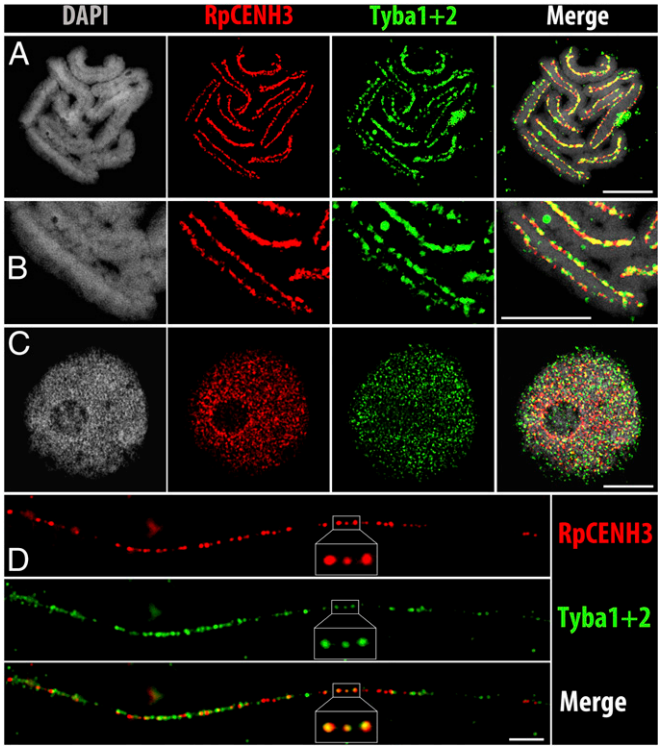

Fig. 2. Colocalization of RpCENH3 and Tyba1 and -2 on *R. pubera* holocentromeres. (*A*) Metaphase. (*B*) Enlarged metaphase chromosome. (*C*) Interphase nucleus. (*D*) Extended chromatin fiber. *A–C* are superresolution microscopy (SIM) images. (Scale bars: 5 μm.)

To validate the tandem-repeat organization and to check whether Tyba is present also in related species, we performed PCR and Southern hybridization using *DraI*-digested genomic DNA of different species of *Rhynchospora* and four other Cyperaceae genera. PCR using Tyba1-specific primers resulted in amplification products in all tested species. However, Southern hybridizations using Tyba1 from *Rhynchospora tenuis* exhibited only tandem repeat-typical ladder-like patterns in all *Rhynchospora* species (*SI Appendix*, Fig. S3*D*), indicating a conserved abundance of this repeat within this genus. Indeed, immuno-FISH using *R. pubera* Tyba probes and antibodies against CENH3 confirmed a colocalized holocentric signal distribution in *R. tenuis* and *R. ciliata* (*SI Appendix*, Fig. S3 *E* and *F*) similar to that in *R. pubera*. Additionally, as reported for other centromeric sequences (32), Tyba1 and -2 are transcriptionally active in all tissues of *R. pubera* analyzed by RT-PCR (*SI Appendix*, Fig. S3*G*) and RNA-seq search.

Although Tyba is clearly the most abundant centromeric repeat found in *R. pubera*, detailed analysis of ChIP-seq data revealed that CENH3-containing chromatin is also associated with at least three additional families of repetitive sequences: the *Ty3/gypsy* LTR retrotransposon CRRh and two different Tyba-containing repeats, hereafter referred to as "TCR1" and "TCR2" (Fig. 3*A*). The CRRh retrotransposon family, representing about 0.2% of the genome, was found to be heterogeneous, including two autonomous elements (CRRh-1 and CRRh-2) and three non-autonomous elements (noaCRRh-1, noaCRRh-2, and noaCRRh-3). Each autonomous element possessed a single ORF of 1,473 and 1,463 codons, respectively. The putative polyprotein sequences were relatively divergent (59.5% identity), but they both contained all the domains necessary for replication and integration (Gag, protease, reverse transcriptase, RNase H, and integrase) (*SI Appendix*, Fig. S4*A*). In contrast, the nonautonomous elements did not encode any of the protein domains found in the autonomous elements, but each of them possessed an ORF of unknown function (*SI Appendix*, Fig. S4*A*). Although the internal sequences of noaCRRh-1 and -2 had no significant similarity to either of the autonomous elements, their LTR sequences shared 73.3 and 72.7% similarity, respectively, with the LTR sequence of CRRh-1, suggesting that they are derivates of CRRh-1. On the other hand, noaCRRh-3 seemed to have originated from CRRh-2, because these elements shared significant similarities at both LTR termini and in a short region in the 5′ UTR. Phylogenetic analysis based on reverse transcriptase domain sequences revealed that the CRRh elements belong to the group B of the centromeric retrotransposon of maize (CRM) clade of chromoviruses (*SI Appendix*, Fig. S4*B*). Similar to other CRM chromoviruses of this group, both CRRh elements lacked the putative targeting domain at the C terminus of integrase (*SI Appendix*, Fig. S4*E*) (2). In-depth analysis of ChIP enrichment showed that only CRRh-1, noaCRRh-1, noaCRRh-2, and noaCRRh-3 elements are associated with CenH3-containing chromatin, but CRRh-2 is not (*SI Appendix*, Fig. S4*C*). Inspection of sequences at insertion sites further revealed that all four ChIP-enriched elements are frequently integrated into Tyba arrays (*SI Appendix*, Fig. S4*D*). The observed number of CRRh insertions into Tyba was 13- to 21-fold higher than expected (P value < 2.2e-6), implying preferential CRRh insertion into Tyba regions. This observation was confirmed experimentally by FISH, which detected CRRh-specific signals intermingled with Tyba signals within the longitudinal centromere groove (Fig. 3*B*), although the CRRh signals were less abundant. Thus, the holocentromeres of *R. pubera* are enriched in different types of repetitive sequences, with the satDNA Tyba being the main sequence contributing to the formation of active centromeric units, and CRRh showing only moderate enrichment.

Unlike CRRh, whose association with Tyba is clearly a result of its integration preferences, Tyba is a constituent of the repetitive

GENETICS

unit in both TCR1 and TCR2. The sequence of the repetitive element TCR1 could be reconstructed in part, because the ∼5-kb-long fragments represent around 0.14% of the genome. One end of the reconstructed consensus sequence likely represents the real boundary of the repetitive unit, because the analysis of this end in reads from different genomic loci revealed a high diversity in the flanking sequences, as is typical for insertion sites. The other end possessed a sequence with high similarity to Tyba. Because our attempts to bridge the Tyba region were not successful, the other boundary of the TCR1 repeat remained unknown. Nevertheless, the presence of putative insertion sites at the Tyba-lacking terminus strongly suggests that TCR1 is a transposable element. In contrast, the repetitive element TCR2 (0.02% of the genome) lacked any sign of insertion sites, and both ends of the in silico reconstructed fragment possessed sequences with high similarity to Tyba. PCR with primers designed from the Tyba-unrelated part of the repeat and directed outwards from the repetitive unit amplified three major fragments about 2.5, 5.0, and 7.5 kb in length, suggesting that TCR2 is a tandem repeat. Sequencing of four randomly selected clones revealed that the monomer of TCR2 is 2,551 bp long and possess nine monomers of Tyba.

Centromeric Sequences Are Composed of High-Order Tyba Tandem Repeats Interspersing the Gene-Containing Chromatin. The higher-order organization of centromeric DNA was analyzed using seven Tyba-containing genomic BACs of *R. pubera*. The identified Tyba arrays were found to be rather small, varying from 3 to 16 kb. As typical for centromeric satDNAs (25, 33), we found the Tyba arrays forming high-order repeat (HOR) structures. Pentamers (830–870 bp) were the most frequent HORs in all BACs analyzed, whereas dimers (∼344 bp) were found only occasionally in two BACs (8P1 and 23M1) (*SI Appendix*, Table S2). Tyba arrays occurred as a continuous array in five of the seven BACs; in BACs 17C8 and 23H8 the array was divided into subarrays (Fig. 3*C* and *SI Appendix*, Fig. S3*H*). The regions between these subarrays did not show similarity to any known sequence.

A close proximity between Tyba and putative centromeric retroelements was found in three BACs (17C8, 9H8, and 8P1). To confirm these elements as centromeric retroelements, their reverse transcriptase-domain sequences were analyzed phylogenetically. Only the element found in BAC 8P1 grouped within other centromeric retroelements, relatively close to the CRRh clade. The elements found in BACs 17C8 and 9H8 represent most likely a chromovirus of the Tekay clade and a pararetrovirus, respectively (*SI Appendix*, Fig. S3*H*). Interestingly, in BACs 17C8 and 9H8 Tyba arrays were found very close to the protein domain regions of these elements, but in BAC 8P1 the CRRh-like element was present ∼20 kb upstream of the Tyba array (Fig. 3*C* and *SI Appendix*, Fig. S3*H*). Thus, although we frequently detected CRRh elements integrated into Tyba arrays (*SI Appendix*, Fig. S4*D*), we did not observe this integration in the sequenced BACs.

In addition to a long Tyba array, BAC 23M1 showed a short Tyba-like cluster (∼700 bp) inserted into an LTR retrotransposon-like sequence (*SI Appendix*, Fig. S3*H*). In addition, centromeric sequences were generally found to be flanked by gene-coding sequences and other transposable elements (Fig. 3*C* and *SI Appendix*, Fig. S3*H*). A transcriptional activity of these genes is likely, because BLAST comparison of these coding sequences found high similarity between them and the pollen mother cell transcriptome.

Discussion

Origin and Genome-Wide Spreading of a Holocentromeric Satellite. How could a centromeric satellite repeat evolve along a chromosome in thousands of interspersed arrays? The chromosomes of *R. pubera* differ in their organization from all other holocentric species studied so far because no other repeat-based centromeres have been reported to date. SatDNA evolves according to the principles of concerted evolution. Within a genome, mutations are homogenized among repeats by the mechanisms of nonreciprocal sequence transfer, such as unequal crossover, gene conversion, rolling circle replication, and transposition-related mechanisms (34). Although the centromere traditionally was treated as a region of suppressed recombination, unequal crossing-over, and gene conversion have been identified as the most widespread mechanism involved in satDNA dynamics (35–37). In addition, segmental duplication has been proposed as a mechanism for massive amplification of satDNA arrays (38, 39).

However, the origin of novel satellite repeats remains elusive. Tandem repeats with homology to parts of retrotransposons have been identified in several plants, e.g., potato (40). Here, we found that the centromeric retrotransposon CRRh is very frequently (>40%) integrated into Tyba satellite arrays, although so far there is no evidence for the presence of Tyba inside CRRh. Thus, CRRh most likely did not contribute to the origin and spreading of Tyba.

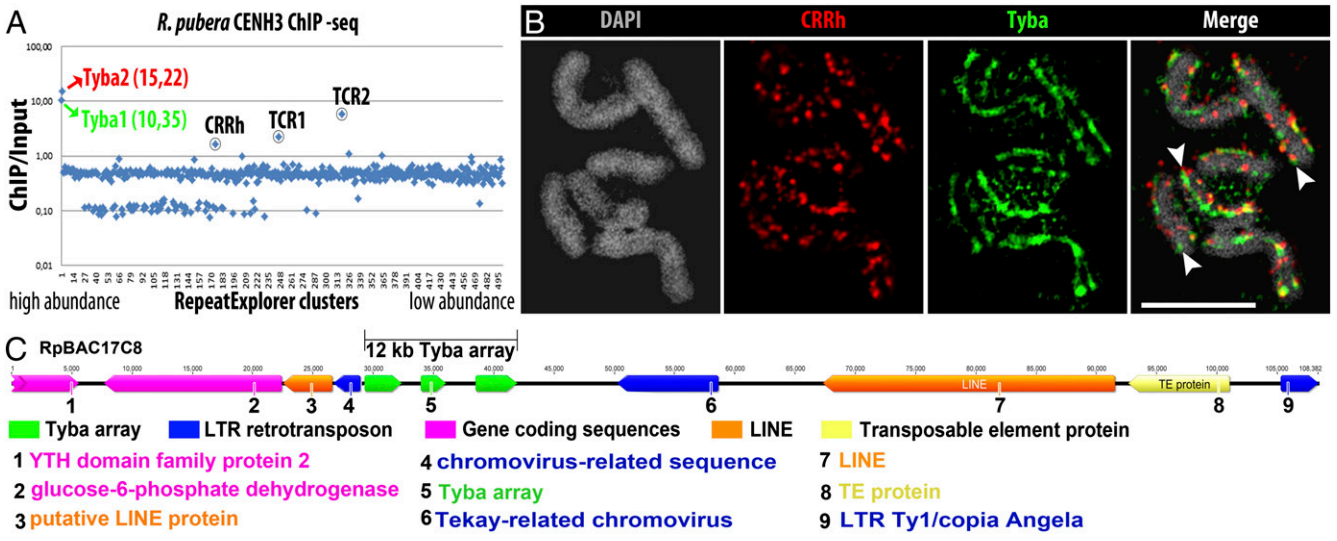

Fig. 3. Characterization of CENH3-interacting sequences. (*A*) CENH3 ChIP-seq reads mapped against the main RepeatExplorer clusters of the *R. pubera* genome. Colored circles and names indicate the main centromeric sequences in *R. pubera* CENH3 ChIP-seq. (*B*) SIM image showing FISH with CRRh (CL175) and Tyba1+2 on metaphase chromosomes. Arrowheads indicate the longitudinal centromere grooves. (Scale bar: 5 μm.) (*C*) Annotation of an *R. pubera* BAC (RpBAC17C8) containing a centromere unit showing a Tyba array of ∼12 kb divided into three subarrays inserted in the protein domains region of a chromovirus-related sequence. Additional transposable elements and single-copy coding sequences were found in close neighborhood.

Further, because CRRh integrates into Tyba at different positions, the targeting is most likely sequence independent. Furthermore, the finding that Tyba is a constituent of the repetitive unit in the transposable element TCR1 might explain the origin and spreading of Tyba throughout the genome. Additionally, a preferential insertion/stabilization of Tyba sequences into centromeric chromatin followed by positive selection might have been facilitated by CENH3 itself, thereby contributing to Tyba accumulation along the centromere groove in *Rhynchospora*. Alternatively, Tyba at a certain level might define the preferential sites for CENH3 accumulation.

A Cell-Cycle–Dependent Dynamic Shuffling of Multiple Centromeric Units Results in the Formation of Holocentromeres During Metaphase. Mitotic chromosomes of *R. pubera* exhibit a line-like centromere organization comprising a high number of centromeric units composed of consecutive CENH3 nucleosomes and enriched in centromeric tandem repeats and retroelements. In contrast to monocentric chromosomes, the prerequisite for this holokinetic centromere organization is the intermingling of coding and noncoding regions and the genome-wide interspersion of euchromatic and heterochromatic domains at large scale. Indeed, no distinguishable large-scale patterns of euchromatin- and heterochromatin-typical epigenetic marks were found along mitotic chromosomes of *R. pubera*. Furthermore, analysis of *R. pubera* BACs revealed a close proximity of the centromeric Tyba satDNA with gene-coding sequences and different classes of repetitive DNA, such as class I (*Maximus*/*SIRE* clade of *copia*-like and *Ogre*/*Tat*, and *Athila* clades of *gypsy*-like) and II (h*AT*-like, MITE-like, and *MuDR*-like) transposable elements. Many transposable elements are randomly dispersed in the genomes, but others may appear concentrated in specific chromosomal regions, such as the centromeric retrotransposon CRRh, which belongs to the chromoviral clade *CRM* (2, 41). Our finding that the CENH3-interacting Tyba satellite and CRRh are inserted into transcriptionally active gene-containing chromatin corroborates the assumption that the centromere organization type influences the organization of the genome at the global chromosomal level.

Our results show that the CENH3/repeat-containing centromeric units are the basic components of the holocentric centromere organization in *R. pubera* supporting the classical polycentric model of holocentricity (42). In support, a study of elongated polycentric chromosomes in *Pisum sativum*, representing a potential evolutionary intermediate between monocentric and holocentric chromosomes, demonstrated that all functional centromere domains are tightly associated with clusters of 13 distinct satDNA families and with one centromeric retrotransposon (CR) family (43).

To explain the observed dynamic distribution of centromeric units during the cell cycle, we propose a model in which, during interphase, holocentromeres dissociate into individual CENH3/centromere repeat-containing units. Then, in prophase and metaphase they reassociate and form the holocentromeres along the centromere groove (Fig. 4). A similar dot-like CENH3 distribution in interphase nuclei was shown for *Luzula* species (9, 10) and *C. elegans* (8), indicating that holocentromeres are composed of hundreds of individual centromeric units. Because no centromere-specific repeats were found in these species (15, 16), the dynamic cell cycle-dependent shuffling of centromeric units occurs independently of centromeric repeats. It is tempting to speculate that the dissociation of holocentromeres during interphase is required to ensure the transcription of genes located close to the centromeric units.

In parallel with the process of chromosome condensation toward metaphase, centromeric units join to form a line-like "polycentromere" within the longitudinal centromere groove to ensure faithful segregation of chromosomes. The mechanism behind this dynamic shuffling of centromeric units remains unknown. A reversible cohesive association of centromeric units might lead to the progressive shuffling of individual centromeric units, finally resulting in the formation of a line-like kinetochore composed of multiple units.

How Long Are the Centromeric Arrays of *R. pubera*? Because about 4% of the genome of this species is composed of centromeric repeats, each of the five chromosomes should harbor a sum of multiple centromeric arrays comprising about 13 Mbp of centromeric DNA, based on an estimated genome size of 1,614 Mb per 1C. In our analysis, the length of Tyba arrays varied from 3 to 16 kb, although we cannot exclude the existence of smaller and/or larger arrays. Assuming 10–15 kb as an average size and that Tyba arrays serve as preferential sites for CENH3-recruitment, each chromosome could harbor between 800 and 1,300 centromeric subunits. Considering that the *R. pubera* genome is about 16-fold larger than that of *C. elegans* (44), which was considered to harbor 707 centromeric units (16), a correlation of centromeric units per million base pairs in these genomes will give a slightly higher abundance of CENH3-hotspots in *C. elegans* (~7.2 centromeric units per million base pairs) than in *R. pubera* (2.5–4 Tyba arrays per million base pairs). Despite the small size of single centromeric

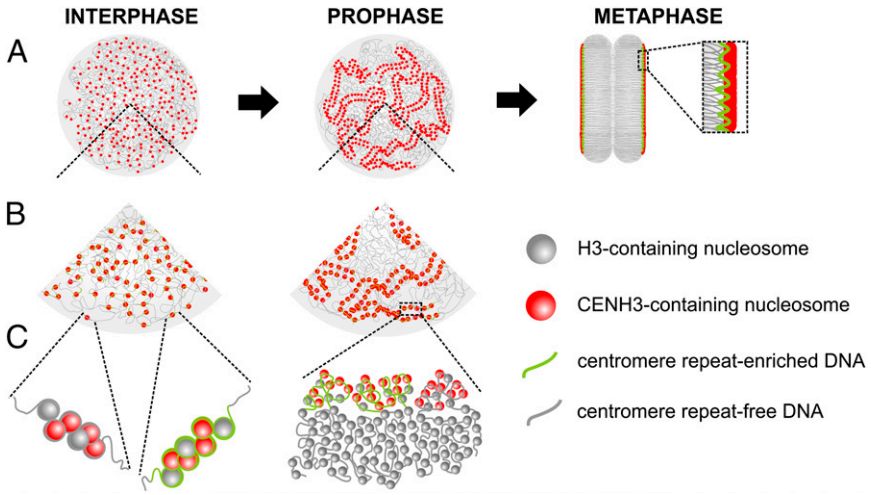

Fig. 4. Model of cell-cycle–dependent changes in the holocentromere chromatin organization of *R. pubera*. During interphase, holocentromeres dissociate into individual CENH3/centromere repeat-containing units. In prophase and metaphase they reassociate and form holocentromeres along the sister chromatids. Most of the CENH3-containing nucleosomes associate with centromere repeat-enriched sequences. Some CENH3-containing nucleosomes associate with centromere repeat-free sequences. Increasing levels of resolution are shown in *A*, *B*, and *C*.

DNA arrays in *Rhynchospora* compared to other species, the total amount of potential centromeric DNA per chromosome is among the largest reported for any species so far.

Conclusions

Although the mechanism behind the spreading of Tyba along the centromeric chromatin remains elusive, a preferential integration to CENH3-positive chromatin followed by positive selection might have occurred. On the other hand, the alternative option in which Tyba satellite repeat-rich regions may work as preferred sites for the deposition of centromeric nucleosomes and thus serve as potential kinetochore attachment sites in *R. pubera* cannot be excluded. Finally, the genome-wide distribution of centromeric repeat arrays interspersing the euchromatin observed in this species provides a previously unidentified variant of centromere organization. Thus, it is evident that different types of holocentromeres, namely centromeres with and without specific repetitive sequences and with or without CENH3/CENP-C, exist in different species. Further studies of species with holocentric chromosomes will broaden our mainly monocentric chromosome-biased knowledge about centromere organization and may help elucidate the centromere plasticity among eukaryotes.

Materials and Methods

Detailed materials and methods are described in *SI Appendix, Materials and Methods*. Briefly, high-copy repeats were identified by graph-based clustering (23) of genomic Illumina reads of *R. pubera*. A *Rhynchospora* CENH3-specific antibody was generated and used for indirect immunostaining, ChIP, ChIP-qPCR, and ChIP-seq. Centromeric repeats were characterized by FISH and sequence analysis.

ACKNOWLEDGMENTS. We thank Wayt Thomas for kindly identifying the plant material; Manuela Knauft for pulsed-field electrophoresis analysis; Karin Lipfert for art work; and Jan Vrána, Radka Tušková, and Eva Jahnová for flow sorting, BAC library construction, and filter preparation. The Brazilian Federal Agency for the Support and Evaluation of Graduate Education within the Ministry of Education of Brazil (CAPES) provided a Special Visiting Researcher Grant and project funding (to A.H.) and scholarships (to A.M. and T.R.). We thank the Fundação de Amparo à Ciência e Tecnologia do Estado de Pernambuco (FACEPE) (AMD-0025-2.00-14) for visiting research grant (to A.M.). The Brazilian National Council of Technological and Scientific Development (CNPq) provided financial support for A.P.-H. The construction of the BAC library was funded by Ministry of Education, Youth and Sports of the Czech Republic National Program of Sustainability I Grant Award LO1204. The Czech Science Foundation and the Czech Academy of Sciences provided financial support for J.M. (GBP501/12/G090 and RVO:60077344).

1. Plohl M, Meštrović N, Mravinac B (2014) Centromere identity from the DNA point of view. *Chromosoma* 123(4):313–325.
2. Neumann P, et al. (2011) Plant centromeric retrotransposons: A structural and cytogenetic perspective. *Mob DNA* 2(4):1–16.
3. Marshall OJ, Chueh AC, Wong LH, Choo KH (2008) Neocentromeres: New insights into centromere structure, disease development, and karyotype evolution. *Am J Hum Genet* 82(2):261–282.
4. Earnshaw WC, et al. (2013) Esperanto for histones: CENP-A, not CenH3, is the centromeric histone H3 variant. *Chromosome Res* 21(2):101–106.
5. Heckmann S, Houben A (2013) Holokinetic centromeres. *Plant Centromere Biology*, eds Jiang J. Birchler JA (Wiley-Blackwell, Oxford, UK), pp 83–94.
6. Guerra M, et al. (2010) Neocentrics and holokinetics (holocentrics): Chromosomes out of the centromeric rules. *Cytogenet Genome Res* 129(1-3):82–96.
7. Moore LL, Morrison M, Roth MB (1999) HCP-1, a protein involved in chromosome segregation, is localized to the centromere of mitotic chromosomes in *Caenorhabditis elegans*. *J Cell Biol* 147(3):471–480.
8. Buchwitz BJ, Ahmad K, Moore LL, Roth MB, Henikoff S (1999) A histone-H3-like protein in *C. elegans*. *Nature* 401(6753):547–548.
9. Nagaki K, Kashihara K, Murata M (2005) Visualization of diffuse centromeres with centromere-specific histone H3 in the holocentric plant *Luzula nivea*. *Plant Cell* 17(7): 1886–1893.
10. Heckmann S, et al. (2011) Holocentric chromosomes of *Luzula elegans* are characterized by a longitudinal centromere groove, chromosome bending, and a terminal nucleolus organizer region. *Cytogenet Genome Res* 134(3):220–228.
11. Wanner G, Schroeder-Reiter E, Ma W, Houben A, Schubert V (June 6, 2015) The ultrastructure of mono- and holocentric plant centromeres: An immunological investigation by structured illumination microscopy and scanning electron microscopy. *Chromosoma*, 10.1007/s00412-015-0521-1.
12. Cabral G, Marques A, Schubert V, Pedrosa-Harand A, Schlögelhofer P (2014) Chiasmatic and achiasmatic inverted meiosis of plants with holocentric chromosomes. *Nat Commun* 5:5070.
13. Chmátal L, et al. (2014) Centromere strength provides the cell biological basis for meiotic drive and karyotype evolution in mice. *Curr Biol* 24(19):2295–2300.
14. Gassmann R, et al. (2012) An inverse relationship to germline transcription defines centromeric chromatin in *C. elegans*. *Nature* 484(7395):534–537.
15. Heckmann S, et al. (2013) The holocentric species *Luzula elegans* shows interplay between centromere and large-scale genome organization. *Plant J* 73(4):555–565.
16. Steiner FA, Henikoff S (2014) Holocentromeres are dispersed point centromeres localized at transcription factor hotspots. *eLife* 3:e02025.
17. Subirana JA, Messeguer X (2013) A satellite explosion in the genome of holocentric nematodes. *PLoS One* 8(4):e62221.
18. Mello CC, Kramer JM, Stinchcomb D, Ambros V (1991) Efficient gene transfer in *C. elegans*: Extrachromosomal maintenance and integration of transforming sequences. *EMBO J* 10(12):3959–3970.
19. Riddle DL, Blumenthal T, Meyer BJ, Priess JR (1997) Introduction to *C. elegans*. *C. elegans II*, eds Riddle DL, Blumenthal T, Meyer BJ, Priess JR (Cold Spring Harbor Lab Press, Cold Spring Harborn, NY), 2nd Ed.
20. Luceno M, Vanzela ALL, Guerra M (1998) Cytotaxonomic studies in Brazilian *Rhynchospora* (Cyperaceae), a genus exhibiting holocentric chromosomes. *Canadian Journal of Botany* 76(3):440–449.
21. Vanzela ALL, Cuadrado A, Jouve N, Luceño M, Guerra M (1998) Multiple locations of the rDNA sites in holocentric chromosomes of *Rhynchospora* (Cyperaceae). *Chromosome Res* 6(5):345–349.
22. Vanzela ALL, Guerra M, Luceno M (1996) *Rhynchospora tenuis* Link (Cyperaceae), a species with the lowest number of holocentric chromosomes. *Cytobios* 88(355):219–228.
23. Novák P, Neumann P, Macas J (2010) Graph-based clustering and characterization of repetitive sequences in next-generation sequencing data. *BMC Bioinformatics* 11:378.
24. Novák P, Neumann P, Pech J, Steinhaisl J, Macas J (2013) RepeatExplorer: A Galaxy-based web server for genome-wide characterization of eukaryotic repetitive elements from next-generation sequence reads. *Bioinformatics* 29(6):792–793.
25. Plohl M, Luchetti A, Mestrović N, Mantovani B (2008) Satellite DNAs between selfishness and functionality: Structure, genomics and evolution of tandem repeats in centromeric (hetero)chromatin. *Gene* 409(1-2):72–82.
26. Melters DP, et al. (2013) Comparative analysis of tandem repeats from hundreds of species reveals unique insights into centromere evolution. *Genome Biol* 14(1):R10.
27. Kelly WG, et al. (2002) X-chromosome silencing in the germline of *C. elegans*. *Development* 129(2):479–492.
28. Nagaki K, et al. (2003) Chromatin immunoprecipitation reveals that the 180-bp satellite repeat is the key functional DNA element of *Arabidopsis thaliana* centromeres. *Genetics* 163(3):1221–1225.
29. Nagaki K, et al. (2004) Sequencing of a rice centromere uncovers active genes. *Nat Genet* 36(2):138–145.
30. Zhong CX, et al. (2002) Centromeric retroelements and satellites interact with maize kinetochore protein CENH3. *Plant Cell* 14(11):2825–2836.
31. Vafa O, Sullivan KF (1997) Chromatin containing CENP-A and alpha-satellite DNA is a major component of the inner kinetochore plate. *Curr Biol* 7(11):897–900.
32. Hall LE, Mitchell SE, O'Neill RJ (2012) Pericentric and centromeric transcription: A perfect balance required. *Chromosome Res* 20(5):535–546.
33. Iwata A, et al. (2013) Identification and characterization of functional centromeres of the common bean. *Plant J* 76(1):47–60.
34. Dover GA (1986) Molecular drive in multigene families - How biological novelties arise, spread and are assimilated. *Trends Genet* 2(6):159–165.
35. Mahtani MM, Willard HF (1998) Physical and genetic mapping of the human X chromosome centromere: Repression of recombination. *Genome Res* 8(2):100–110.
36. Smith GP (1976) Evolution of repeated DNA sequences by unequal crossover. *Science* 191(4227):528–535.
37. Talbert PB, Henikoff S (2010) Centromeres convert but don't cross. *PLoS Biol* 8(3): e1000326.
38. Horvath JE, et al. (2005) Punctuated duplication seeding events during the evolution of human chromosome 2p11. *Genome Res* 15(7):914–927.
39. Ma J, Jackson SA (2006) Retrotransposon accumulation and satellite amplification mediated by segmental duplication facilitate centromere expansion in rice. *Genome Res* 16(2):251–259.
40. Tek AL, Song J, Macas J, Jiang J (2005) Sobo, a recently amplified satellite repeat of potato, and its implications for the origin of tandemly repeated sequences. *Genetics* 170(3):1231–1238.
41. Gorinsek B, Gubensek F, Kordis D (2004) Evolutionary genomics of chromoviruses in eukaryotes. *Mol Biol Evol* 21(5):781–798.
42. Schrader F (1947) The role of the kinetochore in the chromosomal evolution of the heteroptera and homoptera. *Evolution* 1:134–142.
43. Neumann P, et al. (2012) Stretching the rules: Monocentric chromosomes with multiple centromere domains. *PLoS Genet* 8(6):e1002777.
44. *C. elegans* Sequencing Consortium (1998) Genome sequence of the nematode *C. elegans*: A platform for investigating biology. *Science* 282(5396):2012–2018.

SI Appendix

SI Materials and Methods

Plant material. Plants of *Rhynchospora pubera* (Vahl) Boeckler, *R. tenuis* Link and *R. ciliata* (Vahl) Kükenthal were cultivated at humid conditions in a greenhouse. Additionally, leaf material from other Cyperaceae species (*Carex flacca* Schreb., *Cyperus aggregatus* (Willd.) Endl., *Scleria bracteata* Cav. and *Scirpoides holoschoenus* (L.) Soják) (SI Appendix, Table S3) was collected for DNA isolation.

Somatic and meiotic meristem preparation. Chromosome preparations for in situ hybridization analysis were conducted as described by Ruban*, et al.* (1), with modifications. First, young roots (pre-treated with 8-hydroxychinolin for 24 h at 10°C) and anthers were fixed in ice-cold methanol for 30 min. After that the fixative was changed to ice-cold 3:1 (methanol:acetic acid) for 2 h. The fixed tissues were treated with an enzyme mixture (0.7% cellulase R10, 0.7% cellulase, 1.0% pectolyase, and 1.0% cytohelicase in 1× citric buffer) for 30 min at 37ºC. Material was then washed in 1× citric buffer, twice in ice-cold water and fragmented in 7 µl of 60% freshly prepared acetic acid into smaller pieces with the help of a needle on a slide. After another 7 µl of 60% acetic acid was added, and the specimen was kept for 2 min at room temperature. Next, a homogenization step was performed with an additional 7 µl 60% acetic acid and the slide was placed on a 55ºC hot plate for 2 min. The material was spread by hovering a needle over the drop without touching the hot slide. After spreading of cells, the drop was surrounded by 200 µl of ice-cold, freshly prepared 3:1 (ethanol:acetic acid) fixative. More fixative was added and the slide was briefly washed in fixative, then dipped in 60% acetic acid for 10 min and rinsed 5 times in 96% ethanol. A quality check of the air dried slides was performed by phase contrast microscopy. The slides were stored until use in 96% ethanol at 4ºC. Chromosome preparations for immunolabelling analysis were made as described by Marques*, et al.* (2).

Probe preparation and fluorescence *in situ* hybridization. FISH probes were obtained as 5′-Cy3 or 5′-FAM-labeled oligonucleotides (Eurofins MWG Operon,

http://www.eurofinsdna.com), or were PCR-amplified. All DNA probes, except oligonucleotides, were labelled with Cy3-, Texas Red- or Alexa 488-dUTP by nick translation, as described by Kato, Albert, Vega and Birchler (3). The sequences of all oligonucleotides and primers are listed in SI Appendix, Table S4. FISH was performed as described in Ma*, et al.* (4). Probes were then mixed with the hybridization mixture (50% formamide and 20% dextran sulfate in 2× SSC), dropped onto slides, covered with a cover slip and sealed. After denaturation on a heating plate at 80°C for 7 min, slides were hybridized at 37°C overnight. Post-hybridization washing was performed in 2× SSC for 20 min at 58°C. After dehydration in an ethanol series, 4′,6–diamidino-2–phenylindole (DAPI) in Vectashield (Vector Laboratories, http://www.vectorlabs.com) was applied. Microscopic images were recorded using an Olympus BX61 microscope equipped with an ORCA-ER CCD and a deconvolution system. Images were analyzed using the SIS software (Olympus).

PCR amplification of Tyba fragments. Tyba fragments for probe labelling were amplified using gDNA from *R. pubera*, *R. tenuis* and *R. ciliata* for all members using the forward primer Tyba1F: CTAAGTCATTTCATCACAATAATCTAC and the reverse primer Tyba1R: AATCCAGAAACGATTGAAATGCTC for Tyba1 and Tyba2F: GTGCAAATAATGCAATTCTGAGCATC and Tyba2R: ATATGCGTAATTACCATGTATAATCC for Tyba2. PCR reactions were performed in 25 µL reaction volume containing 100 ng of gDNA, 1 µM primers, 1× PCR buffer, 0.2 mM dNTPs, and 1 U of Taq polymerase (Qiagen). Thirty-five amplification cycles (45 s at 95°C, 45 s at 57 °C annealing temperature and 45 s at 72°C) were run.

Expression analysis of Tyba and RpCENH3 by semi-quantitative RT-PCR. Total DNase treated RNA was isolated from root, leaf and anther tissue of *R. pubera* using the SpectrumTM plant total RNA kit (Sigma) according to manufacturer's instructions. The cDNA was synthesized from 1µg of total RNA using the RevertAid First Strand cDNA Synthesis Kit (Thermo Scientific). PCR reactions were performed as described above. Primers sequences are listed in SI Appendix, Table S4, specific primers for the

constitutively expressed GAPDH gene (5), GAPDH-F CAATGATAGCTGCACCACCAACTG and GAPDH-R CTAGCTGCCCTTCCACCTCTCCA, were used as control for equal amount of gDNA and cDNA. Amplified fragments of RpCENH3 were cloned into the StrataClone PCR Cloning Vector pSC-A-amp/kan (Agilent Technologies). Consensus sequences derived from sequencing of 10 randomly selected clones revealed two minor CENH3 variants which have been deposited in GenBank under accession numbers KR029618 and KR029619.

RNAseq and *de novo* assembly for identification of CENH3 gene. Total RNA was isolated from *R. pubera* pollen mother cells using the Spectrum^{TM} plant total RNA kit (Sigma) according to manufacturer's instructions followed by cDNA library preparation. Final libraries were paired-end sequenced 2x100bp on Illumina HiSeq 2000. D*e novo* assembly was performed using Velvet assembler (6), running a total of 87 million of paired-end reads, accession number PRJEB9645 at the Sequence Read Archive (http://www.ebi.ac.uk/ena/). Assembled contigs were finally submitted to a consensus assembly using Geneious assembler, Geneious version 7.1.7 [http://www.geneious.com/, (7)] producing 75,353 contigs. The Velvet assembly was performed using the Geneious provided plugin (Geneious v. 7.1.7). The assembly summary is shown on SI Appendix, Table S5.

Generation of a CENH3 antibody. The peptide ARTKHFSVRSGKKSASRTK was used to generate a *R. pubera* CENH3-specific (RpCENH3) polyclonal antibody. Peptide synthesis, immunization of rabbits and peptide affinity purification of antisera was performed by LifeTein (http://www.lifetein.com).

Preparation of extended fibers and immuno-FISH. Extended DNA fibers were obtained by first isolating leaf nuclei according to Li, Yang, Tong, Zhao and Song (8). Briefly, nuclei were obtained by chopping leaves according to the following method: 100 mg of fresh young leaves were collected for the preparation of 5-10 slides, and leaves

were chopped with a sharp sterile scalpel in a Petri dish that contained 1 ml of ice-cold nucleus isolation buffer (0.01 M MgSO4, 0.005 M KCl, 0.0005 M HEPES, 1 mg/ml dithiothreitol, and 0.25% Triton X-100) (9, 10). The materials obtained by chopping were filtered through 33-µm nylon mesh, filtrates were centrifuged at high speed (16,000g) for 40 s, and the supernatant was discarded. The sediment was resuspended in 10 µl of nucleus isolation buffer. DNA fibers were obtained by dropping 2 µl of the suspension on one end of a coated slide and air dried for 5 to 10 min at room temperature. Thirty microliters of nucleus lysis buffer (0.5% sodium dodecylsulfate, 5 mM ethylenediaminetetraacetic acid, 100 mMTris, pH7.0) was added to the nuclei and incubated at room temperature for 9 min. DNA fibers were dragged and extended with a clean coverslip followed by fixation in 4% paraformaldehyde for immuno-FISH.

Immuno-FISH on extended fibers and somatic cells was performed as described in Ishii, Sunamura, Matsumoto, Eltayeb and Tsujimoto (11). Finally, preparations were stained with DAPI/Vectashield (Vector Laboratories, Burlingame, CA, USA).

Flow-sorting of nuclei for immuno-FISH signal overlapping quantification. Young leave tissue of *R. pubera* was fixed for 20 min under vacuum in 4% formaldehyde in Tris.Cl buffer (100 mM TRIS-HCl, pH 7, 5 mM $MgCl_2$, 85 mM NaCl, 0.1% Triton X100), washed twice for 10 min in TRIS buffer and chopped with a sharp razor blade in about 1 ml of ice-cold nuclei isolation buffer LB01 (12). Resulting suspension was filtered through a 35µm mesh and nuclei were stained with 4′,6-diamidino-2-phenylindole (DAPI) (1 µg/ml) and flow-sorted using a FACSAria (BD Biosciences). 12 µl of sorted nuclei were mixed with equal amounts of sucrose buffer (100mM Tris, 50mM KCl, 2mM MgCl, 0.05% Tween-20, 5% sucrose) on slides. The slides were dried at room temperature and either used immediately or stored at -20°C until use.

Super-resolution microscopy. To analyze the structures and spatial arrangement of immunosignals and chromatin at a lateral optical resolution of ~120 nm (super-resolution, achieved with a 488 nm laser), 3D structured illumination microscopy (3D-SIM) was applied using a C-Apo 63×/1.2W Korr objective of an Elyra PS.1 microscope

system and the software ZEN (Zeiss, Germany). Image stacks were captured separately for each fluorochrome using the 561, 488, and 405 nm laser lines for excitation and appropriate emission filters, and then merged using the ZEN software. The degree of co-localization between Tyba and CENH3 was measured in a single representative slice of each image stack and calculated by the ZEN software.

Southern blot hybridization. The Southern hybridization procedure was performed according to Sambrook, Fritsch and Maniatis (13) with modifications. Total genomic DNA was isolated from leaf tissue of *R. pubera*, *R. ciliata*, *R. tenuis*, *Carex flacca, Cyperus aggregatus*, *Scleria bracteata* and *Scirpoides holoschoenus,* using the DNeasy plant maxi kit (Qiagen) according to manufactures' instructions. The genomic DNAs of all species were further digested with the enzyme *Dra*I, which recognize only one restriction site within the Tyba monomer, size-fractionated by 1.8% agarose gel electrophoresis and transferred to Hybond N+ nylon membranes (Amersham). Probes for Tyba 1 and Tyba 2 were prepared after PCR amplification from genomic DNA of *R. pubera* or *R. tenuis* and labelling by random primer with α-^{32}P-dATP (Thermo Scientific). Hybridization was done overnight at 65 °C in Church and Gilbert hybridization buffer and post-hybridization washes carried out at 65 °C in 2× SSC, 0.5% SDS for 20 min followed by 1× SSC, 0.5% SDS at 65 °C for 20 min and 0.5× SSC, 0.5% SDS at 65 °C for 20 min for high stringency and 2× SSC, 0.5% SDS at 65 °C for 20 min followed by 1× SSC, 0.5% SDS at 65 °C for 20 min for low stringency, respectively.

BAC library construction and screening. Cell nuclei of *R. pubera* were isolated from young leaves following the protocol of Doležel, Číhalíková and Lucretti (14). Briefly, the leaves were fixed for 20 min in 2% (v/v) formaldehyde and immediately afterwards chopped by a razor blade in ice-cold isolation buffer (15). The suspension of released nuclei was stained by DAPI (2 µg/ml). The nuclei were purified by flow cytometry and used to prepare high-molecular-weight (HMW) DNA as described in Šimková, Číhalíková, Vrána, Lysák and Doležel (15). HMW DNA of 1.2 million nuclei of *R. pubera* (~4.2 µg DNA) were used to construct a large insert library. *Hin*dIII digested HMW DNA

was cloned in pIndigoBAC-5 vector (Epicentre, Madison, WI, USA) as described in Šimková*, et al.* (16). The *R. pubera* BAC library is composed of 3,840 clones of 120 kb insert size, which cover 0.25x of *R. pubera* genome (2C = 3.3 pg).

Screening of BACs containing Tyba was carried out by hybridization with PCR-amplified Tyba probes using the procedure described in Ming*, et al.* (17). BACs showing a wide range of hybridization intensity were chosen for sequencing.

Illumina HiSeq sequencing of genomic DNA and BACs. Library preparation was carried out by using ~1 µg of genomic DNA or BAC-DNA. Following random shearing by ultra-sonication (Covaris S220; Covaris Inc.) fragmented DNA was end-repaired, adapter-ligated, barcoded and amplified as previously described by Meyer and Kircher (18). Adapter-ligated DNA was size-selected in a range of 400 – 500 bp for sequencing 2x100 bp on Illumina HiSeq2000. The original Illumina sequencing data for the genomic DNA and BACs are available under study accession number PRJEB9643 and PRJEB9649 at the Sequence Read Archive (http://www.ebi.ac.uk/ena/), respectively.

Repeat identification and ChIP-seq analysis. Identification and characterization of moderately to highly repeated genomic sequences was achieved by graph-based clustering (19) of genomic Illumina reads using RepeatExplorer pipeline (20). A total of 8 million reads (SI Appendix, Table S1), representing 3.6× genome coverage, were used for the clustering and 369 largest clusters with genome proportions of at least 0.01% were examined in detail. Clusters containing satellite repeats were identified based on the presence of tandem sub-repeats within their read or assembled contig sequences. These satellite repeats were characterized using oligomer frequency analysis of the reads within their clusters as described previously (21). To identify repeats associated with CENH3-containing chromatin, reads from the ChIP-seq experiment obtained by sequencing DNA from isolated chromatin prior to (the input control sample) and after immunoprecipitation with the CENH3 antibody (the ChIP sample) were separately mapped to the repeat clusters. The mapping was based on read similarities to contigs representing individual clusters, using BLASTn (22) with parameters "-m 8 -b 1 -e 1e-20

-W 9 -r 2 -q -3 -G 5 -E 2 -F F" and custom Perl scripts for parsing the results. Each read was mapped to a maximum of one cluster, based on its best similarity detected among the contigs. Ratio of ChIP/input reads assigned to individual clusters was then used to identify repeats enriched in the ChIP sample as compared to the input.

CENH3-ChIP, ChIP-qPCR and ChIPseq. Immunoprecipitation experiments were done as described in Kuhlmann and Mette (23). First, young leaves and buds were collected and cross-linked with formaldehyde 1% for 30 min on ice. Leaves and buds were then ground in liquid nitrogen and sonicated using a Diagenode Sonicator. Sonicated chromatin-DNA ranging from ~400-800 bp was immunoprecipitated using anti-RpCENH3. To verify the quality of our IP-DNA we have performed real-time quantitative PCR using Tyba primers as putative positive markers and the 26S ribosomal primers (SI Appendix, Table S4) as negative control in three different samples: input chromatin isolated DNA, immunoprecipitated DNA and no antibody control (noAB).

Immunoprecipitated DNA and input samples (3-7ng for each sample) were used for library preparation following manufacturer's recommendations (Illumina TruSeq ChIP Sample Preparation Kit #IP-202-1012). Subsequently, prepared libraries were paired-end sequenced 2x100bp on Illumina HiSeq 2000. The original ChIPseq sample data are available under study accession number PRJEB9647 at the Sequence Read Archive (http://www.ebi.ac.uk/ena/).

BAC assembly and annotation. Seven positive clones from the *R. pubera* library were sequenced, producing millions of HiSeq paired-end reads (100bp, with >500× coverage). Next, reads were assembled using MIRA (24) and Velvet (6) assemblers. Contigs obtained from both assemblers were then submitted to several rounds of assembly using the Geneious assembler (Geneious v. 7.1.7) and manually edited. Contigs best-matching the estimated BAC length as measured by pulse-field-gel-electrophoresis (PFGE) were then used for annotation. For quantification and annotation of repetitive sequences we performed clustering analysis on RepeatExplorer on each batch of BAC paired-end reads. This approach helped mainly in the correct

quantification and annotation of transposable elements and Tyba arrays. In parallel, Phobos, a tandem repeat search tool (Phobos 3.3.11, 2006-2010, http://www.rub.de/spezzoo/cm/cm_phobos.htm), was used for correct localization and annotation of Tyba arrays. Phobos was also used for the identification of Tyba high order repeat structures. Coding sequences were identified using the gene prediction tools Augustus and Glimmer and manually annotated by BLAST searches. All the analyses were performed inside Geneious v. 7.1.7 with the provided plugins, except for the clustering analyses. BAC annotation is described in SI Appendix, Table S2. To infer whether coding sequences presents in the BACs are transcriptionally active we isolated and blasted each individual predicted coding sequence against our PMC transcriptome database. Assembled BAC sequences are available through iPlant Data Store and can be accessed via iPlant Discovery Environment or at http://de.iplantcollaborative.org/dl/d/8258A143-C5F5-4DF1-84F2-88C94BE8EA8F/R_pubera_holocentromeres_data.rar).

Phylogenetic analysis. Reference IDs for all CENH3 sequences used in this study are available in SI Appendix, Table S6. Multiple alignment of protein sequences encoding the entire CENH3 sequences was generated using MUSCLE (25) and refined manually. Evolutionary analyses were conducted with IQ-TREE (26) using ultrafast bootstrap (27). Phylogenetic history was inferred using the Maximum Likelihood method. The analysis involved 113 protein sequences. All positions containing gaps and missing data were eliminated. There were a total of 101 positions in the final dataset.

Phylogenetic analysis of CRRh was done as previously and using the same alignment matrix from Neumann*, et al.* (28).

Supplementary Figures

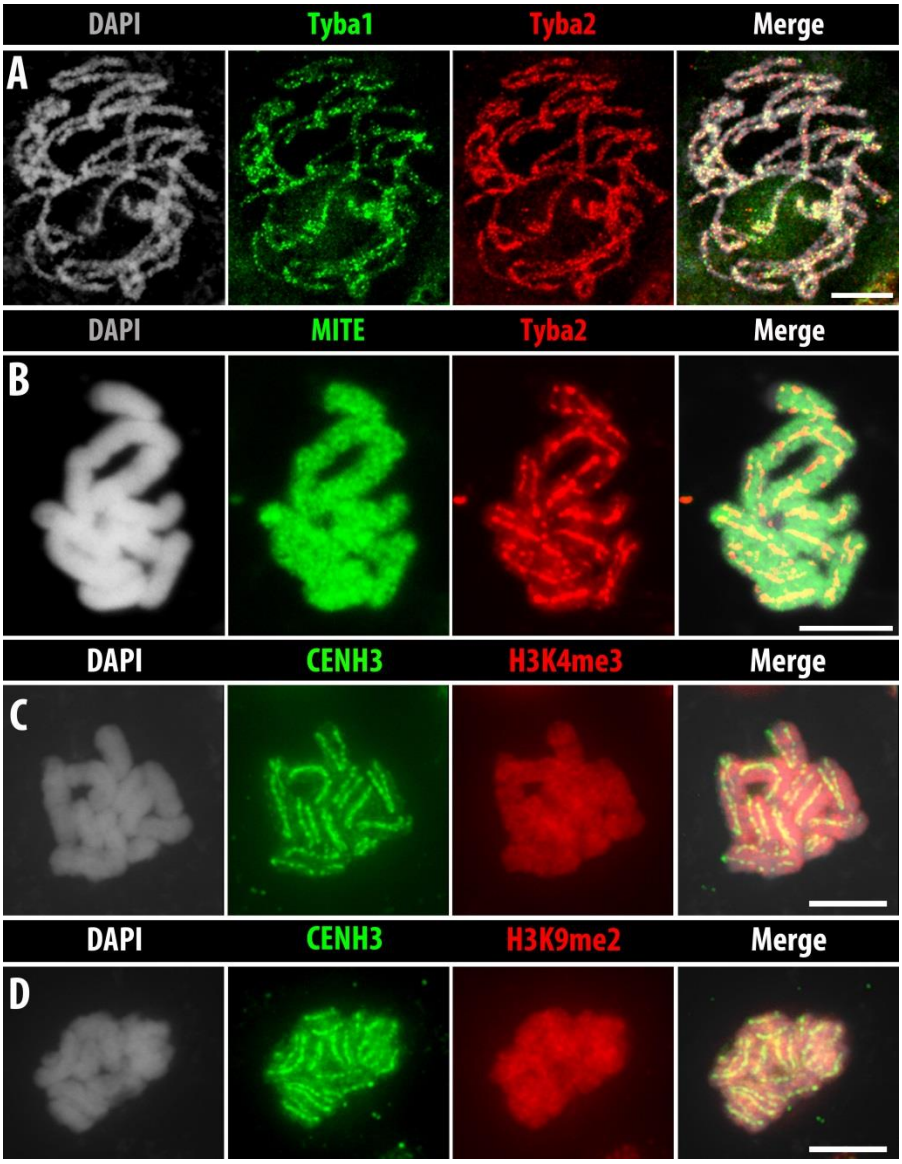

Fig. S1. Overall chromosomal chromatin organization in *R. pubera*. (**A-B**) FISH localization of Tyba and MITE repeats in *R. pubera* chromosomes. (**A**) Hybridization signals of both Tyba members in prophase chromosomes showing a line-like labeling on the poleward surface of each chromatid. (**B**) MITE signals are dispersed while Tyba2 displays a holocentromere-like pattern in metaphase chromosomes. (**C-D**) Metaphase chromosomes of *R. pubera* immunostained with antibodies recognizing H3K4me3 (**C**) and H3K9me2 (**D**) histone modifications in combination with anti-CENH3. Note, the disperse distribution of both H3 modifications. Scale bars: 5 µm.

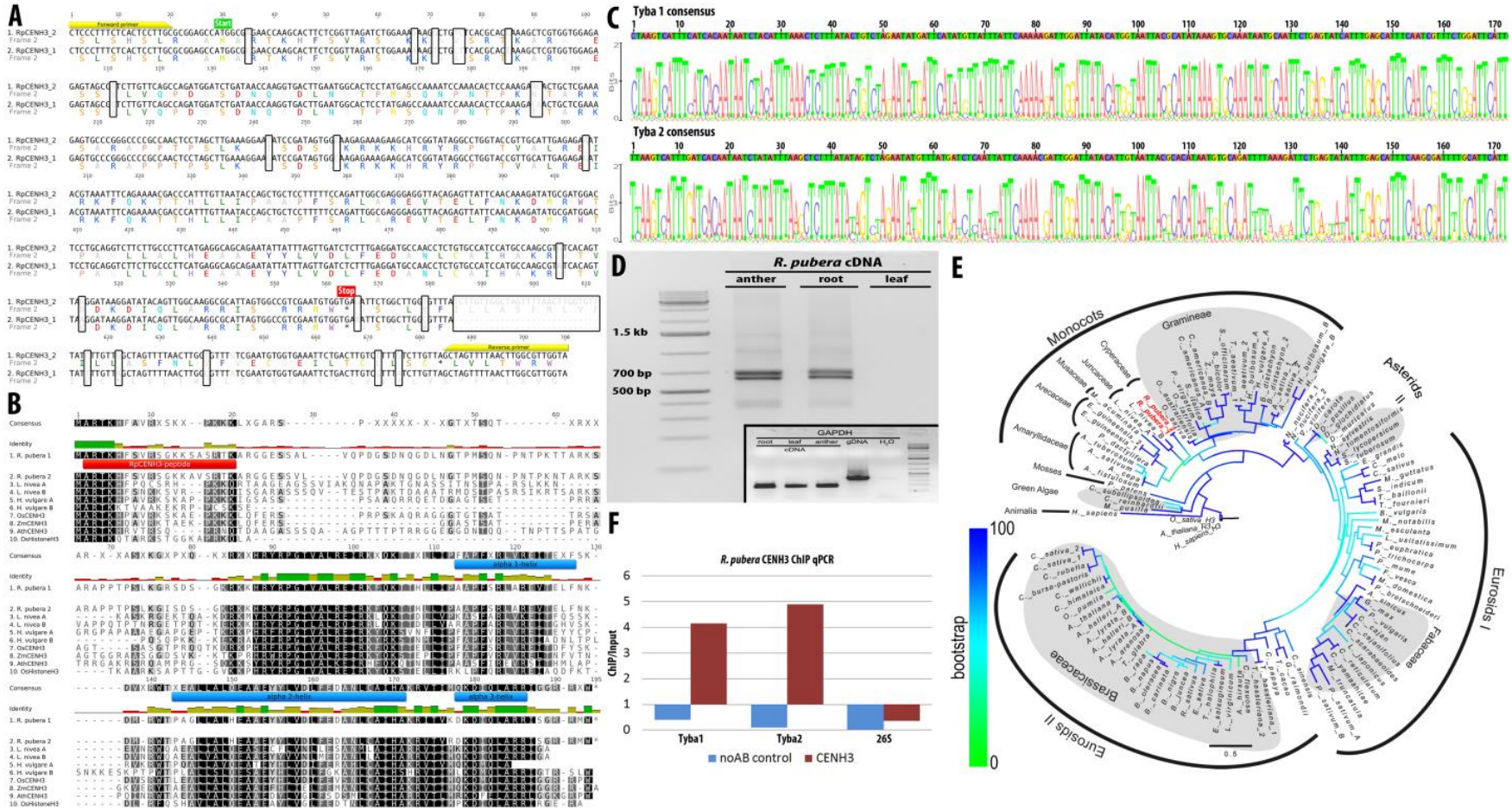

Fig. S2. CENH3 sequence characterization, Tyba monomer reconstruction and CENH3-ChIP analysis. (**A**) DNA and amino acid alignment of *R. pubera* CENH3 variants. Yellow boxes indicate the primer-binding sites used to amplify the fragments; green and red boxes indicate start and stop codons, respectively. Nucleotide disagreements between the variants are high-lightened by black-lined boxes. (**B**) Amino acid alignment of *R. pubera* CENH3 variants and other plant CENH3 sequences. Red box and blue boxes indicate the amino acid residues used for generation of anti-RpCENH3 and

histone alpha helixes fold domains, respectively. (**C**) Monomer reconstruction of Tyba1and Tyba2 using base frequency logo representation. (**D**) RT-PCR analysis of RpCENH3s in different tissues. (**E**) Analysis of evolutionary divergence in plant CENH3 sequences. The evolutionary history was inferred by using the Maximum Likelihood method based on the LG matrix-based model (79). The tree with the highest log likelihood (-5988.401) is shown. The tree is drawn to scale, with branch lengths measured in the number of substitutions per site. (**F**) Quantitative real-time PCR of *R. pubera* CENH3-ChIP using Tyba1 and 2 specific primers. As negative control we used a set of primers to specifically amplify a short region of the 26S ribosomal RNA gene. No antibody control (noAB) was used as a negative control for amplification.

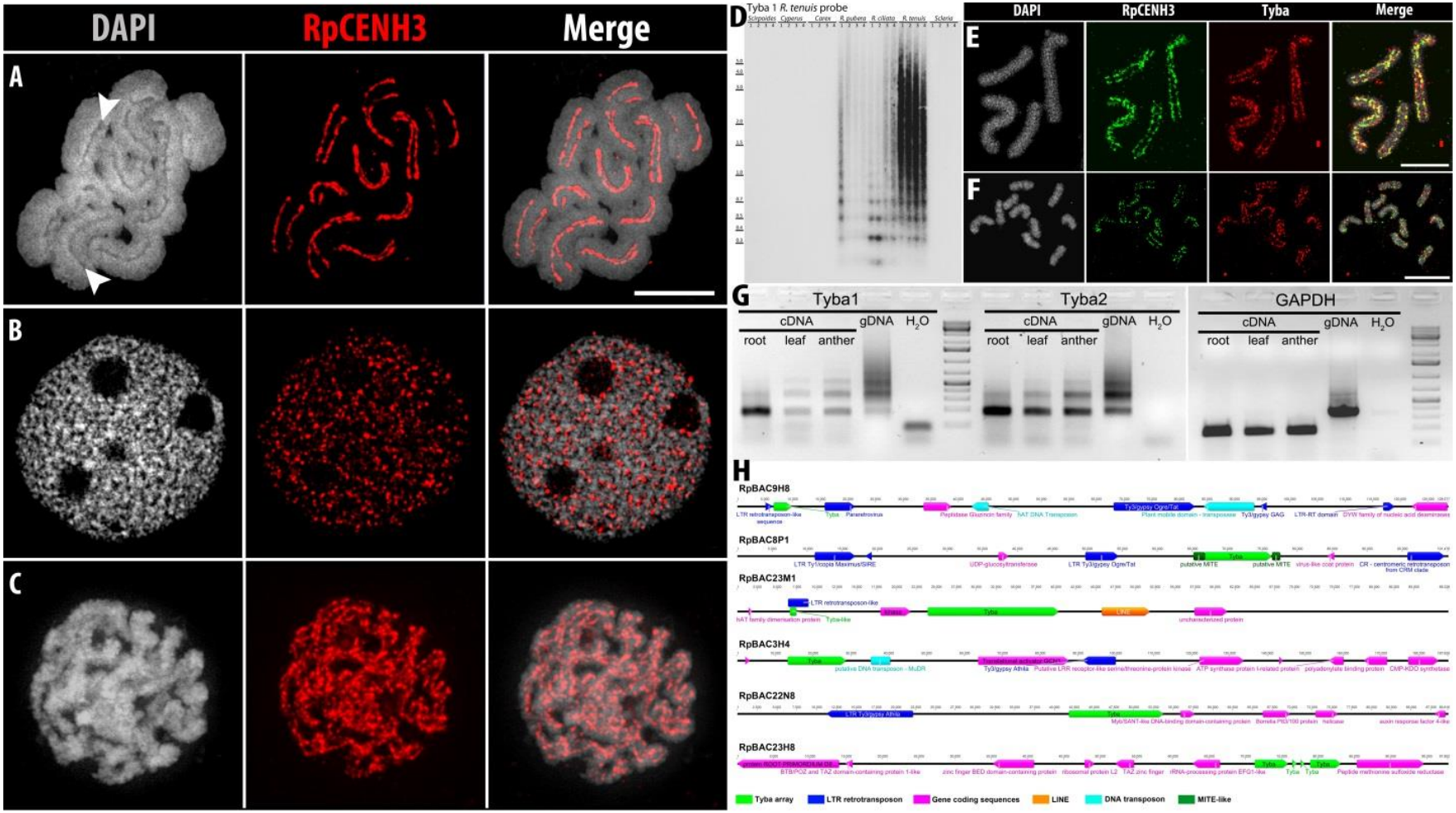

Fig. S3. Localization of anti-RpCENH3 during the cell cycle of *R. pubera*, characterization of the satellite features of Tyba, its presence in the Cyperaceae family, and analysis of Tyba-containing BACs. (**A-C**) CENH3 immunostaining in *R. pubera*, (**A**) metaphase, (**B**) interphase and (**C**) prophase. In metaphase CENH3 is only present densely within the centromere groove (arrowheads). (**A-B**) SIM images. Scale bar: 5µm. (**D**) Southern blot hybridization of different *Rhynchospora* species (*R. ciliata*, *R. pubera* and *R. tenuis*) and other genera of Cyperaceae (*Cyperus aggregatus*, *Scleria bracteata*,

Scirpoides holoschoenus and *Carex flacca*) with Tyba1 repeat amplified from *R. tenuis*. Numbers 1-4 on top represent different enzyme concentrations (0.3 U, 0.6 U, 1U and 5U of *Dra*I, respectevely). (**E-F**) Immuno-FISH colocalization of both CENH3 and Tyba in metaphase chromosomes of *Rhynchospora* species, SIM images of *R. tenuis* (2n = 4) (**E**) and of *R. ciliata* (2n = 10) (**F**) (scale bar: 5 µm). (**G**) Semi-quantitative RT-PCR reveals the transcriptional activity of Tyba1 and 2 in all tissues analyzed. GAPDH was used as control. (**H**) Annotation of *R. pubera* BACs containing centromeric repeats. RpBAC9H8 shows a ~3 kb Tyba array very close to the protein domain region of a Pararetrovirus, as well as a hAT DNA transposon, a Ty3/gypsy LTR retrotransposon of Ogre/Tat clade, other TE related proteins and single copy coding sequences. RpBAC8P1 shows a ~10 kb Tyba array flanked on both sides by MITE-like sequences with a centromeric retrotransposon on the neighborhood, a Ty1/copia LTR retrotransposon of Maximus/SIRE clade, a Ty3/gypsy LTR retrotransposon of Ogre/Tat clade, and other single copy coding sequences. RpBAC23M1 shows a ~17 kb Tyba array, a putative LTR-related region with a Tyba-like insertion and other single copy coding sequences. RpBAC3H4 shows a ~16 kb Tyba array, a MuDR-like DNA transposon, a Ty3/gypsy LTR retrotransposon of Athila clade and additional single copy coding sequences. RpBAC22N8 shows a ~12 kb Tyba array, a Ty3/gypsy LTR retrotransposon of Athila clade and additional single copy coding sequences. RpBAC23H8 shows a ~12 kb Tyba array with an apparently degenerated region and additional single copy coding sequences.


A
CRRh-1 (5263bp)
gag
prot
rt
rnaseH
int
CL175Contig152 4993bp/55.8
CRRh-2 (5034 bp)
gag
prot
rt
rnaseH
int
CL175Contig56 1174bp/37.7
CL175Contig21 3408bp/32.8
noaCRRh-1 (2264 bp)
ORF 1200 bp
CL175Contig105 157bp/18.6
CL175Contig117 397bp/49.8
CL175Contig107 1397bp/75.9
CL175Contig112 191bp/20.7
noaCRRh-2 (4264 bp)
ORF 1542 bp
CL175Contig105 157bp/18.6
CL175Contig117 397bp/49.8
CL175Contig79 1758bp/38.1
CL175Contig53 1480bp/30.9
CL175Contig85 729bp/108.6
noaCRRh-3 (1475 bp)
ORF 614 bp
CL175Contig129 443bp/9.0
CL175Contig66 432bp/18.0

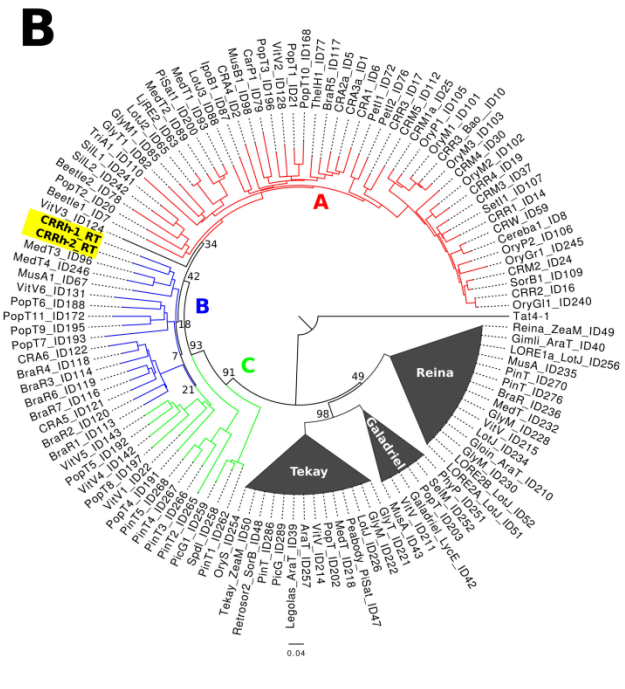
B
A
B
C
CRRh-1_RT
CRRh-2_RT
Reina
Galadriel
Tekay
0.04

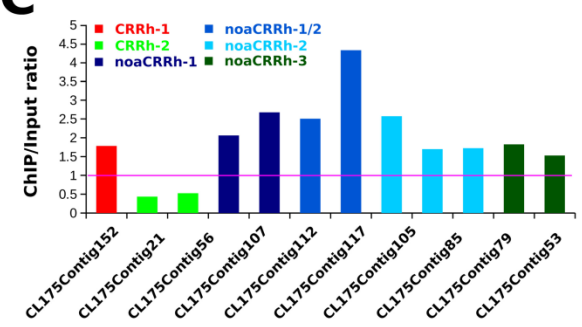
C
CRRh-1
CRRh-2
noaCRRh-1
noaCRRh-1/2
noaCRRh-2
noaCRRh-3
ChIP/Input ratio
CL175Contig152
CL175Contig21
CL175Contig56
CL175Contig107
CL175Contig112
CL175Contig117
CL175Contig105
CL175Contig85
CL175Contig79
CL175Contig53

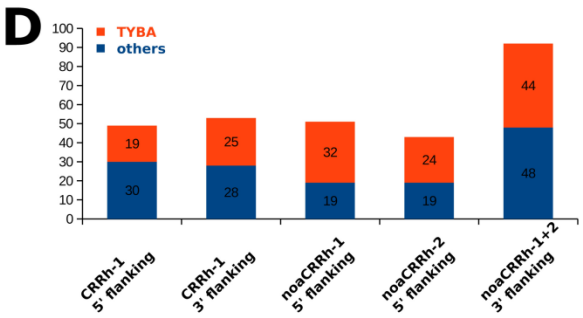
D
TYBA
others
CRRh-1 5' flanking
CRRh-1 3' flanking
noaCRRh-1 5' flanking
noaCRRh-2 5' flanking
noaCRRh-1+2 3' flanking

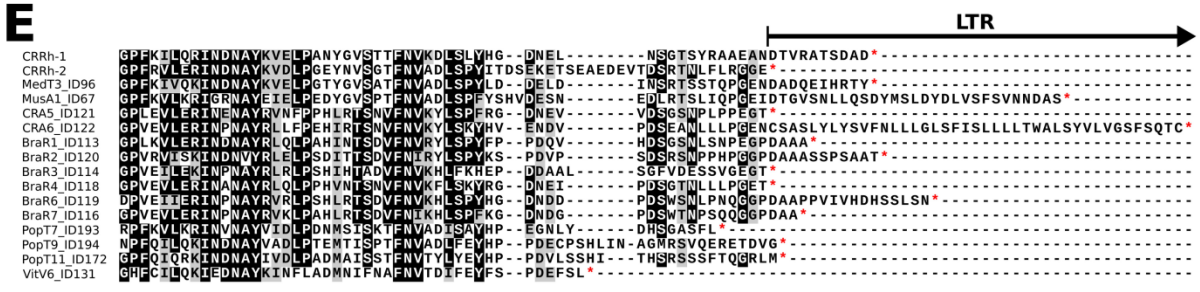
E
LTR
CRRh-1
CRRh-2
MedT3_ID96
MusA1_ID67
CRA5_ID121
CRA6_ID122
BraR1_ID113
BraR2_ID120
BraR3_ID114
BraR4_ID118
BraR6_ID119
BraR7_ID116
PopT7_ID193
PopT9_ID194
PopT11_ID172
VitV6_ID131

Fig. S4. Features of CRRh elements of *R. pubera*. (**A**) Schematics of CRRh elements. LTRs are shown in black, internal fragments in gray and ORF in white. Lines below the schemes show positions of the most representative contigs that were used to reconstruct sequences of full length elements. (**B**) Neighbor-joining tree inferred from a comparison of RT domain sequences. It demonstrates that CRRh-1 and CRRh-2 elements belong to CRM clade of chromoviruses, being most similar to those that form the group B. Classification of CRM into groups A, B, and C is based on differences at the C-terminus of integrase (3). The non-chromovirus element Tat4-1 was used as an outgroup, while members of the Tekay, Reina, and Galadriel clades were included as representatives of non-CRM clade chromoviruses. (**C**) A chart showing ChIP-enrichment calculated for contigs representing fragments of different CRRh elements. (**D**) Analysis of insertion sites sequences of CRRh elements revealed that CRRh-1, noaCRRh-1 and noaCRRh-2 integrates frequently into Tyba. Sequences at insertion sites of CRRh-2 and noaCRRh-3 could not be analyzed because LTR sequences were variable and shared similarity with other repeats. (**E**) Alignment of sequences at the C-terminus of integrase. Only sequences from CRM group B elements are included (3). Characteristic feature of this group of CRM elements is the absence of PTD domain at integrase C-terminus and termination of the coding region around the start of 3' LTR (3). This is in contrast to CRM group A elements having the coding region extended deeply into 3’ LTR and encoding for PTD domain (3). Stop codons at the end of each open reading frame are indicated by red asterisks. Beginning of 3’ LTR is depicted as an arrow above the alignment. Arrow shows a part of integrase which is encoded by sequence in the 3’ LTR. RT-domain sequences used for the phylogenetic analysis were obtained from the study of (3).

Supplementary Tables

Table S1. Repetitive DNA composition of the *R. pubera* genome

			Analyzed reads:	8,032,451
Repeat class	Subclass	Family	Genome [%]	(group sum)
LTR retrotransposons				17.13
	Ty1/copia	Angela	5.79	8.68
		Maximus	1.17	
		AleII	0.91	
		Tork	0.21	
		TAR	0.20	
		Bianca	0.19	
		Ivana	0.19	
		AleI	0.01	
	Ty3/gypsy	Athila	2.54	5.14
		Tat/Ogre	1.86	
		chromovirus	0.74	
	unclassified		3.32	
Non-LTR retrotransposons	LINE		0.55	0.72
	SINE		0.17	
Pararetrovirus			0.51	
DNA transposons	MITE		5.10	8.81
	hAT		0.84	
	unclassified		2.87	
Helitron			0.59	
TEs unclassified			2.69	
Others				
Satellite DNA			3.60	
rDNA			0.70	
Classified repeats			34.75	
Total repeats >= 0.01%			41.16	

Table S2. BAC annotation

RpBAC3H4				
Name	Type	Start base	End base	Length
not annotated	gene	2,138	3,256	1,119
Translational activator GCN1	gene	63,575	87,529	23,955
Putative LRR receptor-like serine/threonine-protein kinase	gene	122,120	133,775	11,656
not annotated	gene	143,214	144,067	854
ATP synthase protein I-related protein	gene	156,388	160,107	3,720
polyadenylate binding protein	gene	165,600	171,622	6,023
CMP-KDO synthetase	gene	177,295	185,236	7,942
Ty3/gypsy Athila	LTR retrotransposon	91,290	99,919	8,630
putative DNA transposon - MuDR	transposable element protein	35,290	40,298	5,009
Tyba	Tyba_array	13,333	28,723	15,391
862-nucleotide Repeat (Tyba HOR pentamer)	Tyba_array	14,456	16,813	2,358
844-nucleotide Repeat (Tyba HOR pentamer)	Tyba_array	19,976	22,426	2,451
862-nucleotide Repeat (Tyba HOR pentamer)	Tyba_array	23,488	25,286	1,799
863-nucleotide Repeat (Tyba HOR pentamer)	Tyba_array	26,126	28,113	1,988

Total length (kb) obtained in the assembly				187
Total length (kb) obtained by PFGE				140
RpBAC8P1				
Name	Type	Start base	End base	Length
UDP-glucosyltransferase	gene	37,320	38,735	1,416
virus-like coat protein	gene	84,288	85,301	1,014
LTR Ty1/copia Maximus/SIRE	LTR retrotransposon	11,053	16,873	5,821
LTR	LTR retrotransposon	18,270	19,178	909
LTR Ty3/gypsy Ogre/Tat	LTR retrotransposon	49,742	54,452	4,711
CR - chromovirus from CRM clade	LTR retrotransposon	95,761	101,062	5,302
putative MITE	MITE	65,171	66,805	1,635
putative MITE	MITE	76,391	77,519	1,129
Tyba	Tyba_array	66,822	76,329	9,508
334-nucleotide Repeat (Tyba HOR dimer)	Tyba_array	67,857	69,106	1,250
837-nucleotide Repeat (Tyba HOR pentamer)	Tyba_array	70,311	72,011	1,701
843-nucleotide Repeat (Tyba HOR pentamer)	Tyba_array	72,000	75,112	3,113
Total length (kb) obtained in the assembly				101
Total length (kb) obtained by PFGE				110
RpBAC9H8				
Name	Type	Start base	End base	Length

Peptidase Gluzincin family	gene	33,747	38,766	5,020
DYW family of nucleic acid deaminases	gene	122,112	128,542	6,431
LTR	LTR retrotransposon	5,126	6,494	1,369
Ty3/gypsy Ogre/Tat	LTR retrotransposon	68,135	82,856	14,722
Ty3/gypsy GAG	LTR retrotransposon	94,476	95,861	1,386
RT domain	LTR retrotransposon	116,924	118,979	2,056
Pararetrovirus	Pararetrovirus	15,855	21,257	5,403
hAT DNA Transposon	transposable element protein	42,447	45,458	3,012
Plant mobile domain - transposase	transposable element protein	84,413	93,547	9,135
Tyba	Tyba_array	6,473	9,853	3,381
851-nucleotide Repeat (Tyba HOR pentamer)	Tyba_array	6,473	9,853	3,381
Total length (kb) obtained in the assembly				128
Total length (kb) obtained by PFGE				140

RpBAC17C8

Name	Type	Start base	End base	Length
YTH domain family protein 2	gene	<1	5,601	>5601
glucose-6-phosphate dehydrogenase	gene	7,692	22,403	14,712
putative LINE protein	LINE	22,544	26,598	4,055
LINE	LINE	67,335	101,028	33,694

retrotransposon sequence	LTR retrotransposon	26,738	28,937	2,200
Tekay-chromovirus-related	LTR retrotransposon	50,272	58,624	8,353
LTR Ty1/copia Angela	LTR retrotransposon	105,313	108,382	3,070
TE protein - endoribonuclease	transposable element protein	67,335	82,808	15,474
RT domain	transposable element protein	85,380	89,144	3,765
GAG domain	transposable element protein	89,519	91,219	1,701
TE protein	transposable element protein	92,671	101,028	8,358
Tyba	Tyba_array	29,272	32,400	3,129
Tyba	Tyba_array	33,983	36,060	2,078
Tyba	Tyba_array	38,483	41,922	3,440
862-nucleotide Repeat (Tyba HOR pentamer)	Tyba_array	29,281	32,353	3,073
870-nucleotide Repeat (Tyba HOR pentamer)	Tyba_array	34,002	35,967	1,966
837-nucleotide Repeat (Tyba HOR pentamer)	Tyba_array	38,511	41,887	3,377
Total length (kb) obtained in the assembly				108
Total length (kb) obtained by PFGE				120

RpBAC22N8

Name	Type	Start base	End base	Length

Myb/SANT-like DNA-binding domain-containing protein	gene	55,932	57,708	1,777
Borrelia P83/100 protein	gene	66,313	69,706	3,394
helicase	gene	72,958	75,765	2,808
auxin response factor 4-like	gene	88,036	89,341	1,306
LTR Ty3/gypsy Athila	LTR retrotransposon	11,254	22,129	10,876
Tyba	Tyba_array	41,857	53,749	11,893
860-nucleotide Repeat (Tyba HOR pentamer)	Tyba_array	41,977	53,539	11,563
Total length (kb) obtained in the assembly				89
Total length (kb) obtained by PFGE				90

RpBAC23H8

Name	Type	Start base	End base	Length
protein ROOT PRIMORDIUM DEFECTIVE 1 isoform X2	gene	1	13,987	13,987
BTB/POZ and TAZ domain-containing protein 1-like	gene	14,836	15,883	1,048
zinc finger BED domain-containing protein	gene	35,222	40,847	5,626
ribosomal protein L2	gene	47,828	49,201	1,374
TAZ zinc finger	gene	52,087	54,622	2,536
rRNA-processing protein EFG1-like	gene	62,711	66,483	3,773
Peptide methionine sulfoxide reductase	gene	85,345	94,589	9,245
Tyba	Tyba_array	71,297	75,867	4,571
Tyba	Tyba_array	76,479	77,066	588

Tyba	Tyba_array	77,622	78,096	475
Tyba	Tyba_array	78,945	83,144	4,200
858-nucleotide Repeat (Tyba HOR pentamer)	Tyba_array	71,313	75,859	4,547
172-nucleotide Repeat (Tyba monomer)	Tyba_array	76,483	77,060	578
170-nucleotide Repeat (Tyba monomer)	Tyba_array	77,631	78,084	454
860-nucleotide Repeat (Tyba HOR pentamer)	Tyba_array	78,971	83,055	4,085
Total length (kb) obtained in the assembly				97
Total length (kb) obtained by PFGE				110

RpBAC23M1

Name	Type	Start base	End base	Length
hAT family dimerisation protein	gene	1,423	1,854	432
kinase	gene	17,963	21,750	3,788
uncharacterized protein	gene	57,436	61,561	4,126
LINE	LINE	45,783	51,849	6,067
LTR retrotransposon-like	LTR	6,368	8,900	2,533
367-nucleotide Repeat (Tyba-like dimer)	repeat_region	6,632	7,370	739
Tyba	Tyba_array	23,918	40,387	16,470
362-nucleotide Repeat (Tyba HOR dimer)	Tyba_array	24,009	25,718	1,710
869-nucleotide Repeat (Tyba HOR pentamer)	Tyba_array	26,047	28,660	2,614
364-nucleotide Repeat (Tyba HOR dimer)	Tyba_array	28,809	29,822	1,014
836-nucleotide Repeat (Tyba HOR pentamer)	Tyba_array	29,964	33,250	3,287

361-nucleotide Repeat (Tyba HOR dimer)	Tyba_array	33,701	38,275	4,575
827-nucleotide Repeat (Tyba HOR pentamer)	Tyba_array	38,716	40,380	1,665
Total length (kb) obtained in the assembly				89
Total length (kb) obtained by PFGE				120

Table S3. Species name and collecting places

Species name	Collected places
Rhynchospora pubera (Vahl) Boeckler	Curado, Recife, Brazil
Rhynchospora tenuis Willd. ex Link	Curado, Recife, Brazil
Rhynchospora ciliata (Vahl) Kükenthal	Curado, Recife, Brazil
Carex flacca Schreb.	Gatersleben, Germany
Cyperus aggregatus (Willd.) Endl.	Curado, Recife, Brazil
Scleria bracteata Cav.	Dois Irmãos, Recife, Brazil
Scirpoides holoschoenus (L.) Soják	Gatersleben, Germany

Table S4. List of oligonucleotide probes and primer sequences used

Target	oligo/primer name	oligo/primer sequence	fluorescence
Tyba1	Tyba1 oligo probe	ATTGGATTATACATGGTAATTACGCATATAAAGTGCAAATAATGCAATTC	FAM
Tyba2	Tyba2 oligo probe	ACAGATTCTGAGTATATTTGAGCATTTCAAGCGATTTTGCATT	Cy3
MITE	MITE oligo probe	AATTTATTATAAACAATCCAAACTCTTCACAAAGTTACACACTTCCCAAT	FAM
Tyba primer1	Tyba1F	CTAAGTCATTTCATCACAATAATCTAC	none
	Tyba1R	AATCCAGAAACGATTGAAATGCTC	none
Tyba primer2	Tyba2F	GTGCAAATAATGCAATTCTGAGCATC	none
	Tyba2R	ATATGCGTAATTACCATGTATAATCC	none
RpCENH3	RpCENH3F	CTCCCTTTCTCACTCCTTGC	none
	RpCENH3R	CGATCAAAATTGAACCGCAACCAT	none
CRRh-1	CRRh-1F	GACTAATCATCCCAGCCATGT	none
	CRRh-1R	GTGGCTCGAACGGTGTC	none
CRRh-2	CRRh-2F	TATTTTACTTTTGTGCACGGTAGAC	none
	CRRh-2R	GTTAAAGCCCATGTTATGTTCG	none
		control primers	
GAPDH	GAPDH-F	CAATGATAGCTGCACCACCAACTG	none
	GAPDH-R	CTAGCTGCCCTTCCACCTCTCCA	none
26S ribosomal RNA	26S-F	CCTCCGAAGTTTCCCTCAG	none
	26s-R	GCCTCTAATCATTGGCTTTACCT	none

Table S5. Summary of Velvet assembly from the cDNA library of the pollen mother cell transcriptome of *R. pubera*

Statistics	**All Contigs**	**Contigs >=100 bp**	**Contigs >=1000 bp**
Number of contigs	75.353	74.120	20.290
Min Length (bp)	62	100	1.000
Median Length (bp)	491	502	1.594
Mean Length (bp)	794	806	1.847
Max Length (bp)	15.473	15.473	15.473
N50 Length (bp)	1.341	1.344	1.908
Number of contigs >= N50	13.783	13.747	6.770
Length Sum (bp)	59.848.133	59.751.873	37.478.675

Table S6. List of sequence identifiers and description of plant CENH3 sequences used

Sequence identifier	Database	Description
KR029618	Genbank	>Rhynchospora pubera CENH3_1
KR029619	Genbank	>Rhynchospora pubera CENH3_2
AF465801	Genbank	>gi|19338703|gb|AF465801.1| Arabidopsis arenosa centromeric histone H3 HTR12 (HTR11) gene, complete cds
AB081501	Genbank	>gi|33146135|dbj|AB081501.1| Arabidopsis halleri subsp. gemmifera gene for histone H3 like protein, complete cds, histone H2 like-a
AB081503	Genbank	>gi|33146139|dbj|AB081503.1| Arabidopsis halleri subsp. gemmifera gene for histone H3 like protein, complete cds, histone H2 like-b
DQ450587	Genbank	>gi|91179111|gb|DQ450587.1| Arabidopsis lyrata subsp. petraea strain Mt. Esja11 histone H3 (HTR11A) gene, complete cds
DQ450557	Genbank	>gi|91178276|gb|DQ450557.1| Arabidopsis lyrata subsp. petraea strain Mt. Esja11 histone H3 (HTR11B) gene, complete cds
AB081500	Genbank	>gi|33146133|dbj|AB081500.1| Arabidopsis thaliana mRNA for histone H2 like protein, complete cds
AB299169	Genbank	>gi|134152506|dbj|AB299169.1| Arabis hirsuta cenp-A gene for putative centromeric histone H3-like protein_0, complete cds
GU166738	Genbank	>gi|268376515|gb|GU166738.1| Brassica nigra isolate BrCENH3-2 centromere-specific H3 variant protein (CENH2) mRNA, complete cds
GU166739	Genbank	>gi|268376517|gb|GU166739.1| Brassica oleracea isolate BrCENH3-3 centromere-specific H3 variant protein (CENH2) mRNA, complete cds
GU166737	Genbank	>gi|268376513|gb|GU166737.1| Brassica rapa isolate BrCENH3-1 centromere-specific H3 variant protein (CENH2) mRNA, complete cds
AB299175	Genbank	>gi|134152518|dbj|AB299175.1| Capsella bursa-pastoris cenp-A gene for centromeric histone H3-like protein-0, complete cds
XM_00630418	Genbank	>gi|565493209|ref|XM_006304182.1| Capsella rubella hypothetical protein (CARUB_v10010435mg) mRNA,

2		complete cds
AB299171	Genbank	>gi|134152510|dbj|AB299171.1| Cardamine flexuosa cenp-A gene for centromeric histone H3-like protein-0, complete cds
AY612790	Genbank	>gi|51103316|gb|AY612790.1| Crucihimalaya himalaica centromeric histone (HTR11) gene, complete cds
AB299177	Genbank	>gi|134152522|dbj|AB299177.1| Crucihimalaya wallichii cenp-A gene for centromeric histone H2-like protein, complete cds
AB299180	Genbank	>gi|134152528|dbj|AB299180.1| Eruca sativa cenp-A gene for centromeric histone H3-like protein-0, complete cds
AB299181	Genbank	>gi|134152530|dbj|AB299181.1| Lepidium virginicum cenp-A gene for centromeric histone H3-like protein_0, complete cds
AB299167	Genbank	>gi|134152502|dbj|AB299167.1| Olimarabidopsis pumila cenp-A gene for putative centromeric histone H3-like protein_0, complete cds
AB299183	Genbank	>gi|134152534|dbj|AB299183.1| Raphanus sativus cenp-A gene for centromeric histone H3-like protein_0, complete cds
Thhalv10008889m	Phytozome	>Thhalv10008888m
AB081505	Genbank	>gi|33146143|dbj|AB081505.1| Turritis glabra gene for histone H2 like protein, complete cds
AB649144	Genbank	>gi|365799494|dbj|AB649144.1| Astragalus sinicus AsCENH3 mRNA for centromere specific histone H2 variant, complete cds
EX259948	Genbank	>gi|186738465|gb|EX259948.1|EX259948 1440421_5_E19_076 PY05 Carica papaya cDNA, mRNA sequence
XM_006491184	Genbank	>gi|568876356|ref|XM_006491184.1| PREDICTED: Citrus sinensis histone H3-like centromeric protein HTR12-like (LOC102614120), transcript variant X1, mRNA
XM_004139613	Genbank	>gi|449443791|ref|XM_004139613.1| PREDICTED: Cucumis sativus histone H3-like centromeric protein HTR12-like (LOC101210010), mRNA
Eucgr.D00189.1	Phytozome	>Eucgr.D00189.0
XM_004306639	Genbank	>gi|470141951|ref|XM_004306639.1| PREDICTED: Fragaria vesca subsp. vesca histone H3-like centromeric protein HTR12-like (LOC101294589), mRNA

XM_003528751	Genbank	>gi|571465058|ref|XM_003528751.2| PREDICTED: Glycine max histone H3-like centromeric protein HTR12-like (LOC100811871), mRNA
Gorai.001G155600.1	Phytozome	>Gorai.001G155600.0
Lus10008119	Phytozome	>Lus10008118
BT137822	Genbank	>gi|388499101|gb|BT137822.1| Lotus japonicus clone JCVI-FLLj-13P8 unknown mRNA
XP_008361919.1	Genbank	>gi|657953278|ref|XP_008361919.1| PREDICTED: histone H3-like centromeric protein cnp0 [Malus domestica]
FF379687	Genbank	>gi|182383948|gb|FF379687.1|FF379687 CASL069TF CASL Manihot esculenta cDNA 4', mRNA sequence
XM_003637685	Genbank	>gi|358347374|ref|XM_003637685.1| Medicago truncatula Histone H3 (MTR_100s0022) mRNA, complete cds
KC491791	Genbank	>gi|523371675|gb|KC491791.1| Phaseolus vulgaris centromere specific histone H3 variant (CENH2) mRNA, complete cds
JF739989	Genbank	>gi|371486399|gb|JF739989.1| Pisum sativum centromere-specific variant of histone H3 type 0 gene, complete cds
JF739990	Genbank	>gi|371486401|gb|JF739990.1| Pisum sativum centromere-specific variant of histone H3 type 1 gene, complete cds
XM_002320818	Genbank	>gi|224130507|ref|XM_002320818.1| Populus trichocarpa centromeric histone H3 HTR12 family protein (POPTR_0014s09209g) mRNA, complete cds
XM_007051531	Genbank	>gi|590721367|ref|XM_007051531.1| Theobroma cacao Histone superfamily protein, putative isoform 1 (TCM_005175) mRNA, complete cds
XM_002281037	Genbank	>gi|731421864|ref|XM_002281037.2| PREDICTED: Vitis vinifera histone H3-like centromeric protein HTR12 (LOC100260234), transcript variant X1, mRNA
GR117778	Genbank	>gi|238366551|gb|GR117778.1|GR117778 CCBG8245.g1 CCBG Mimulus guttatus IM62 floral buds (H+L) Erythranthe guttata cDNA clone CCBG8245 2', mRNA sequence
AB467328	Genbank	>gi|218744595|dbj|AB467328.1| Nicotiana sylvestris NsCENH3 mRNA for centromere specific histone H2 variant, complete cds
AB467329	Genbank	>gi|218744597|dbj|AB467329.1| Nicotiana tomentosiformis NtoCENH3 mRNA for centromere specific histone H2

		variant, complete cds
BG127218	Genbank	>gi|12627406|gb|BG127218.1|BG127218 EST472864 tomato shoot/meristem Solanum lycopersicum cDNA clone cTOF14D12 4' sequence, mRNA sequence
XM_006339625	Genbank	>gi|565345203|ref|XM_006339625.1| PREDICTED: Solanum tuberosum histone H3-like centromeric protein HTR12-like (LOC102603326), mRNA
AB600275	Genbank	>gi|371940020|dbj|AB600275.1| Allium cepa AceCENH3 mRNA for centromere specific histone H2 variant, complete cds
AB571555	Genbank	>gi|371940014|dbj|AB571555.1| Allium fistulosum AfiCENH3 mRNA for centromere specific histone H2 variant, complete cds
AB571556	Genbank	>gi|371940016|dbj|AB571556.1| Allium sativum AsaCENH3 mRNA for centromere specific histone H2 variant, complete cds
AB571557	Genbank	>gi|371940018|dbj|AB571557.1| Allium tuberosum AtuCENH3 mRNA for centromere specific histone H2 variant, complete cds
XM_003566059	Genbank	>gi|357128898|ref|XM_003566059.1| PREDICTED: Brachypodium distachyon uncharacterized LOC100830307 (LOC100830306), mRNA
GU245882	Genbank	>gi|282895619|gb|GU245882.1| Hordeum bulbosum centromeric histone H3 (CENH2) mRNA, partial cds
JF419330	Genbank	>gi|339836913|gb|JF419330.1| Hordeum bulbosum beta centromeric histone H3 (CENH2) mRNA, complete cds
JF419328	Genbank	>gi|339836909|gb|JF419328.1| Hordeum vulgare subsp. vulgare alpha centromeric histone H3 (CENH2) mRNA, partial cds
JF419329	Genbank	>gi|339836911|gb|JF419329.1| Hordeum vulgare subsp. vulgare beta centromeric histone H3 (CENH2) mRNA, complete cds
AB201356	Genbank	>gi|90652790|dbj|AB201356.2| Luzula nivea LnCENH3 mRNA for centromere specific histone H2 variant, complete cds
HM988988	Genbank	>gi|304277059|gb|HM988988.1| Luzula nivea centromeric histone H3 isoform B (CENH2-B) mRNA, complete cds
AY438639	Genbank	>gi|40365139|gb|AY438639.1| Oryza sativa (japonica cultivar-group) centromeric histone 3 (CenH2) mRNA, complete cds
FL730019	Genbank	>gi|197988596|gb|FL730019.1|FL730019 CCGB10819.g1 CCGB Panicum virgatum apex + stem (L) Panicum

		virgatum cDNA clone CCGB10819 2', mRNA sequence
CA127217	Genbank	>gi|35006880|gb|CA127217.1|CA127217 SCCCLR2004A05.g LR2 Saccharum hybrid cultivar SP80-3280 cDNA clone SCCCLR2004A05 4', mRNA sequence
XM_004961625	Genbank	>gi|514748700|ref|XM_004961625.1| PREDICTED: Setaria italica histone H3-like centromeric protein HTR12-like (LOC101784681), transcript variant X1, mRNA
XM_002441245	Genbank	>gi|242090914|ref|XM_002441245.0| Sorghum bicolor hypothetical protein, mRNA
NM_001112050	Genbank	>gi|162460347|ref|NM_001112050.1| Zea mays centromeric histone H3 (cenH2), mRNA
AEH95350.1	Genbank	>gi|336041546|gb|AEH95350.1| centromeric histone 3 [Triticum aestivum]
AEH95351.1	Genbank	>gi|336041548|gb|AEH95351.1| centromeric histone 3 [Triticum aestivum]
ACZ04985.1	Genbank	>gi|268376530|gb|ACZ04985.1| centromere-specific H3 variant protein [Brassica napus]
ACZ04980.1	Genbank	>gi|268376520|gb|ACZ04980.1| centromere-specific H3 variant protein [Brassica juncea]
ACZ04982.1	Genbank	>gi|268376524|gb|ACZ04982.1| centromere-specific H3 variant protein [Brassica carinata]
KJ201906.1	Genbank	>gi|656991661|gb|KJ201906.1| Daucus glochidiatus centromeric histone H3 (CENH3) mRNA, partial cds
AHW98233.1	Genbank	>gi|612176255|gb|AHW98233.1| centromeric histone 3, partial [Cicer reticulatum]
XM_009346944.1	Genbank	>gi|694436201|ref|XM_009346944.1| PREDICTED: Pyrus x bretschneideri histone H3-like centromeric protein cnp1 (LOC103937036), transcript variant X2, mRNA
XM_008234980.1	Genbank	>gi|645254791|ref|XM_008234980.1| PREDICTED: Prunus mume histone H3-like centromeric protein HTR12 (LOC103332255), mRNA
XM_010482040.1	Genbank	>gi|727429465|ref|XM_010482040.1| PREDICTED: Camelina sativa histone H3-like centromeric protein HTR12 (LOC104759068), transcript variant X1, mRNA
XM_010482047.1	Genbank	>gi|727429467|ref|XM_010482047.1| PREDICTED: Camelina sativa histone H3-like centromeric protein HTR12 (LOC104759068), transcript variant X2, mRNA
KJ507236.1	Genbank	>gi|612176248|gb|KJ507236.1| Cajanus scarabaeoides isolate Pigeonpea_ICP 15731 centromeric histone 3 (CenH3) mRNA, partial cds
XM_01055829	Genbank	>gi|729412033|ref|XM_010558290.1| PREDICTED: Tarenaya hassleriana histone H3-like centromeric protein

0.1		HTR12 (LOC104825875), transcript variant X2, mRNA
XM_010558289.1	Genbank	>gi|729412030|ref|XM_010558289.1| PREDICTED: Tarenaya hassleriana histone H3-like centromeric protein HTR12 (LOC104825875), transcript variant X1, mRNA
KJ507233.1	Genbank	>gi|612176242|gb|KJ507233.1| Cajanus cajan isolate Pigeonpea_ICPL 87119_Asha centromeric histone 3 (CenH3) mRNA, complete cds
KJ507235.1	Genbank	>gi|612176246|gb|KJ507235.1| Cajanus cajanifolius isolate Pigeonpea_ICP 15631 centromeric histone 3 (CenH3) mRNA, complete cds
XM_006418354.1	Genbank	>gi|567156644|ref|XM_006418354.1| Eutrema salsugineum hypothetical protein (EUTSA_v10008889mg) mRNA, complete cds
XM_011039624.1	Genbank	>gi|743790056|ref|XM_011039624.1| PREDICTED: Populus euphratica histone H3-like centromeric protein HTR12 (LOC105134977), mRNA
AB793503.1	Genbank	>gi|586941098|dbj|AB793503.1| Torenia fournieri TfCENH3 mRNA for centromere specific histone H3, complete cds
AB793504.1	Genbank	>gi|586941100|dbj|AB793504.1| Torenia baillonii TbCENH3 mRNA for centromere specific histone H3, complete cds
XM_011094744.1	Genbank	>gi|747090693|ref|XM_011094744.1| PREDICTED: Sesamum indicum histone H3-like centromeric protein HTR12 (LOC105173094), mRNA
XM_010263215.1	Genbank	>gi|720017605|ref|XM_010263215.1| PREDICTED: Nelumbo nucifera histone H3-like centromeric protein HTR12 (LOC104600331), transcript variant X2, mRNA
XM_010268168.1	Genbank	>gi|720033563|ref|XM_010268168.1| PREDICTED: Nelumbo nucifera histone H3-like centromeric protein HTR12 (LOC104603975), transcript variant X1, mRNA
KJ201904.1	Genbank	>gi|656991657|gb|KJ201904.1| Daucus muricatus centromeric histone H3 (CENH3) mRNA, partial cds
KJ201903.1	Genbank	>gi|656991655|gb|KJ201903.1| Daucus carota centromeric histone H3 (CENH3) mRNA, partial cds
KJ201905.1	Genbank	>gi|656991659|gb|KJ201905.1| Daucus pusillus centromeric histone H3 (CENH3) mRNA, partial cds
XM_010696392.1	Genbank	>gi|731365747|ref|XM_010696392.1| PREDICTED: Beta vulgaris subsp. vulgaris histone H3 (LOC104907459), mRNA
KJ507243.1	Genbank	>gi|612176262|gb|KJ507243.1| Cicer yamashitae isolate Chickpea_ICC 17117 centromeric histone 3 (CenH3)

		mRNA, complete cds
XM_008794232.1	Genbank	>gi|672137449|ref|XM_008794232.1| PREDICTED: Phoenix dactylifera histone H3-like (LOC103709056), mRNA
HQ123579.1	Genbank	>gi|313104721|gb|HQ123579.1| Oryza latifolia isolate DD centromeric histone 3 (CenH3) mRNA, complete cds
XM_009413514.1	Genbank	>gi|260072772|gb|GQ849341.1| Oryza australiensis isolate EE CENH3 (CenH3) mRNA, complete cds
AB649144.1	Genbank	>gi|695047791|ref|XM_009413514.1| PREDICTED: Musa acuminata subsp. malaccensis histone H3-like centromeric protein cnp1 (LOC103993441), mRNA
XM_010933196.1	Genbank	>gi|743819355|ref|XM_010933196.1| PREDICTED: Elaeis guineensis histone H3.3 type c-like (LOC105052399), transcript variant X1, mRNA
XM_010933197.1	Genbank	gi|743819358|ref|XM_010933197.1| PREDICTED: Elaeis guineensis histone H3.3 type c-like (LOC105052399), transcript variant X2, mRNA
AB770163.1	Genbank	>gi|670453236|dbj|AB770163.1| Cenchrus americanus CENH3 mRNA for centromeric histone H3 isoform a, complete cds
AB770164.1	Genbank	>gi|670453238|dbj|AB770164.1| Cenchrus americanus CENH3 mRNA for centromeric histone H3 isoform b, complete cds
AB981585.1	Genbank	>gi|745991781|dbj|AB981585.1| Avena sativa AsCENH3-2 mRNA for centromere specific histone H3, partial cds
AB981584.1	Genbank	>gi|745991779|dbj|AB981584.1| Avena sativa AsCENH3-1 mRNA for centromere specific histone H3, partial cds
XM_008463887.1	Genbank	>gi|659124344|ref|XM_008463887.1| PREDICTED: Cucumis melo histone H3-like centromeric protein HTR12 (LOC103500538), partial mRNA
XM_010101295.1	Genbank	>gi|703110467|ref|XM_010101295.1| Morus notabilis Histone H3-like centromeric protein partial mRNA
XM_010232934.1	Genbank	>gi|721637023|ref|XM_010232934.1| PREDICTED: Brachypodium distachyon histone H3-like (LOC100830307), mRNA
XM_001785914	Genbank	>gi|168068179|ref|XM_001785914.1| Physcomitrella patens subsp. patens histone H3 (HTR1515) mRNA, complete cds
XM_00169781	Genbank	>gi|159479581|ref|XM_001697817.1| Chlamydomonas reinhardtii strain CC-503 cw91 mt+

7		
XM_005647320	Genbank	>gi|545364669|ref|XM_005647320.1| Coccomyxa subellipsoidea C-169 histone-fold-containing protein (COCSUDRAFT_24063) mRNA, complete cds
XM_003056465	Genbank	>gi|303274379|ref|XM_003056465.1| Micromonas pusilla CCMP1545 histone H2, mRNA
NM_001809.3	Genbank	>gi|109637780|ref|NM_001809.3| Homo sapiens centromere protein A (CENPA), transcript variant 0, mRNA
AF093633.1	Genbank	>gi|3885889|gb|AF093633.1| Oryza sativa histone H2 mRNA, complete cds
NM_125934.2	Genbank	>gi|30698117|ref|NM_125934.2| Arabidopsis thaliana histone H3.0 mRNA, complete cds
X57128.1	Genbank	>gi|31981|emb|X57128.1| H.sapiens H3.1 gene for H2 histone

SI References

1. Ruban A*, et al.* (2014) B chromosomes of *Aegilops speltoides* are enriched in organelle genome-derived sequences. *PloS one* 9(2):e90214.
2. Marques A*, et al.* (2011) Characterization of eu- and heterochromatin of *Citrus* with a focus on the condensation behavior of 45S rDNA chromatin. *Cytogenetic and genome research* 134(1):72-82.
3. Kato A, Albert PS, Vega JM, & Birchler JA (2006) Sensitive fluorescence *in situ* hybridization signal detection in maize using directly labeled probes produced by high concentration DNA polymerase nick translation. *Biotechnic & histochemistry : official publication of the Biological Stain Commission* 81(2-3):71-78.
4. Ma L*, et al.* (2010) Synteny between *Brachypodium distachyon* and *Hordeum vulgare* as revealed by FISH. *Chromosome Research* 18(7):841-850.
5. Banaei-Moghaddam AM, Meier K, Karimi-Ashtiyani R, & Houben A (2013) Formation and expression of pseudogenes on the B chromosome of rye. *The Plant cell* 25(7):2536-2544.
6. Zerbino DR & Birney E (2008) Velvet: algorithms for de novo short read assembly using de Bruijn graphs. *Genome research* 18(5):821-829.
7. Kearse M*, et al.* (2012) Geneious Basic: an integrated and extendable desktop software platform for the organization and analysis of sequence data. *Bioinformatics* 28(12):1647-1649.
8. Li L, Yang J, Tong Q, Zhao L, & Song Y (2005) A novel approach to prepare extended DNA fibers in plants. *Cytometry. Part A : the journal of the International Society for Analytical Cytology* 63(2):114-117.
9. Galbraith DW*, et al.* (1983) Rapid flow cytometric analysis of the cell cycle in intact plant tissues. *Science* 220(4601):1049-1051.
10. Arumuganathan K, Slattery JP, Tanksley SD, & Earle ED (1991) Preparation and flow cytometric analysis of metaphase chromosomes of tomato. *Theoretical and Applied Genetics* 82(1):101-111.
11. Ishii T, Sunamura N, Matsumoto A, Eltayeb AE, & Tsujimoto H (2015) Preferential recruitment of the maternal centromere-specific histone H3 (CENH3) in oat (*Avena sativa* L.) x pearl millet (*Pennisetum glaucum* L.) hybrid embryos. *Chromosome Research*.
12. Doležel J, Binarova P, & Lucretti S (1989) Analysis of nuclear DNA content in plant cells by flow-cytometry. *Biologia Plantarum* 31(2):113-120.
13. Sambrook J, Fritsch EF, & Maniatis T (1989) Analysis of genomic DNA by southern hybridization and northern hybridization. *Molecular Cloning: A Laboratory Manual*, (Cold Spring Harbor Press: Cold Spring Harbor, NY, USA), 2nd Ed, pp E21–E25.
14. Doležel J, Číhalíková J, & Lucretti S (1992) A high-yield procedure for isolation of metaphase chromosomes from root tips of *Vicia faba* L. *Planta* 188(1):93-98.
15. Šimková H, Číhalíková J, Vrána J, Lysák MA, & Doležel J (2003) Preparation of HMW DNA from plant nuclei and chromosomes isolated from root tips. *Biologia Plantarum* 46(3):369-373.
16. Šimková H*, et al.* (2011) BAC libraries from wheat chromosome 7D: efficient tool for positional cloning of aphid resistance genes. *Journal of biomedicine & biotechnology* 2011:302543.
17. Ming R*, et al.* (2001) Construction and characterization of a papaya BAC library as a foundation for molecular dissection of a tree-fruit genome. *Theoretical and Applied Genetics* 102:892-899.
18. Meyer M & Kircher M (2010) Illumina sequencing library preparation for highly multiplexed target capture and sequencing. *Cold Spring Harbor protocols* 2010(6):pdb prot5448.
19. Novak P, Neumann P, & Macas J (2010) Graph-based clustering and characterization of repetitive sequences in next-generation sequencing data. *BMC bioinformatics* 11:378.
20. Novak P, Neumann P, Pech J, Steinhaisl J, & Macas J (2013) RepeatExplorer: a Galaxy-based web server for genome-wide characterization of eukaryotic repetitive elements from next-generation sequence reads. *Bioinformatics* 29(6):792-793.

21. Macas J, Neumann P, Novak P, & Jiang J (2010) Global sequence characterization of rice centromeric satellite based on oligomer frequency analysis in large-scale sequencing data. *Bioinformatics* 26(17):2101-2108.
22. Altschul SF*, et al.* (1997) Gapped BLAST and PSI-BLAST: a new generation of protein database search programs. *Nucleic acids research* 25(17):3389-3402.
23. Kuhlmann M & Mette MF (2012) Developmentally non-redundant SET domain proteins SUVH2 and SUVH9 are required for transcriptional gene silencing in Arabidopsis thaliana. *Plant Mol Biol* 79(6):623-633.
24. Chevreux B, Wetter T, & Suhai S (1999) Genome sequence assembly using trace signals and additional sequence information. *Computer Science and Biology: Proceedings of the German Conference on Bioinformatics* 99:45-56.
25. Edgar RC (2004) MUSCLE: a multiple sequence alignment method with reduced time and space complexity. *BMC bioinformatics* 5:113.
26. Nguyen LT, Schmidt HA, von Haeseler A, & Minh BQ (2015) IQ-TREE: a fast and effective stochastic algorithm for estimating maximum-likelihood phylogenies. *Molecular biology and evolution* 32(1):268-274.
27. Minh BQ, Nguyen MA, & von Haeseler A (2013) Ultrafast approximation for phylogenetic bootstrap. *Molecular biology and evolution* 30(5):1188-1195.
28. Neumann P*, et al.* (2011) Plant centromeric retrotransposons: a structural and cytogenetic perspective. *Mobile DNA* 2(1):4.

Capítulo 3: Loss of the line-like holocentromere structure during inverted meiosis in a holocentric plant

Artigo a submetido ao periódico *eLIFE*

Loss of the line-like holocentromere structure during inverted meiosis in a holocentric plant

André Marques[a], Veit Schubert[b], Andreas Houben[b,1], Andrea Pedrosa-Harand[a,1]

[a]Laboratory of Plant Cytogenetics and Evolution, Department of Botany, Federal University of Pernambuco, 50670-420 Recife, Pernambuco, Brazil; [b]Leibniz Institute of Plant Genetics and Crop Plant Research (IPK) Gatersleben, 06466 Stadt Seeland, Germany,
[1]email: houben@ipk-gatersleben.de, andrea.pedrosaharand@pesquisador.cnpq.br

Abstract:
The centromeres are responsible for the correct segregation of chromosomes during mitosis and meiosis. Holocentric chromosomes, which are characterized by multiple centromere units along each chromatid, have particular adaptations to ensure regular disjunction during meiosis. Here we show that holocentromeres undergo differential organization between mitosis and inverted meiosis in *Rhynchospora pubera* by tracing CENH3, CENP-C and tubulin, and detecting centromeric repeats. Contrasting to the mitotic line-like holocentromere organization in this species, meiotic centromeres show resilient reorganization. During meiosis I several clusters of centromere units (cluster-holocentromeres) in interaction with spindle fibers accumulate along the poleward surface of perpendicularly spindle-oriented bivalents. During meiosis II cluster-holocentromeres are visualized mostly as a single cluster in the mid-region of each chromatid. In contrast to meiosis I, chromatid pairs are associated by their telomeres showing parallel orientation to spindle poles at metaphase II. A line-like holocentromere organization is restored after meiosis at first pollen mitosis. Our findings demonstrate an extreme case of centromere plasticity and provide a newly identified dynamic centromere organization during meiosis among holocentric organisms.
Key words: holocentric chromosomes, meiosis, holocentromeres, CENP-C, centromere structure/organization, centromere units

Introduction

The centromere is the chromosome site responsible for spindle fiber attachment and faithful chromosome segregation during mitosis and meiosis. In general, every eukaryotic chromosome has a centromere on which the kinetochore complex assembles (***Burrack and Berman, 2012; Cleveland et al., 2003***). In most eukaryotes, centromeric nucleosomes contain CENH3 (also known as CENP-A, a histone H3 variant that replaces canonical H3 at the centromere), and usually spans several hundred kilobase-pairs (kb) often in association with centromere-specific repeats (***Steiner and Henikoff, 2015***).

The centromere organization and dynamics vary between mitosis and meiosis (***Duro and Marston, 2015; Ohkura, 2015***). During mitosis, sister-chromatids are hold together by centromere cohesion until metaphase. Simultaneous with the loss of cohesion, sister-chromatids are pulled to opposite poles during anaphase. In contrast, during meiosis cohesion of sister centromeres is ensured until metaphase II (***Ishiguro and Watanabe, 2007***). The stepwise regulation of cohesion release during meiosis I and II is well-studied in organisms with one primary constriction per chromosome (monocentric), ensuring the segregation of homologs at meiosis I followed by the segregation of sister chromatids at meiosis II (***Duro and Marston, 2015***).

Contrary to monocentrics, centromeres of holocentric chromosomes are distributed almost over the entire chromosome length and cohesion occurs along the entire associated sister chromatids (***Maddox et al., 2004***). Although this does not imply much difference during mitotic divisions, the presence of a holokinetic centromere (holocentromere) imposes obstacles to the dynamics of chromosome segregation in meiosis. Due to their alternative chromosome organization, species with holocentric chromosomes cannot perform the two-step cohesion loss during meiosis typical for monocentric species that requires the distinction between chromosome arms and sister centromeres. In addition, the extension of an individual holocentric kinetochore increases the risk of a stable attachment to microtubules from both poles of the mitotic spindle (merotelic attachment), and hence an aberrant segregation of chromosomes may occur. As adaptation, species with holocentric chromosomes

have evolved different solutions during meiosis, such as a localized kinetochore activity, ensuring canonical meiosis order, and “inverted meiosis”, where a reverse order of meiotic events occur [reviewed in ***Viera et al. (2009)***; (***Cuacos et al., 2015***)].

In the nematode *C. elegans*, the chromosomes form a single chiasma per bivalent and either end of the chromosomes has the capacity of forming crossovers (COs); crossover location determines which chromosome end orientates polewards (***Albertson et al., 1997***). This process triggers the redistribution of proteins along the bivalent axis, creating subdomains that define the region of cohesin removal and protection during meiosis I (***Albertson et al., 1997; Martinez-Perez et al., 2008***). Kinetochore components uniformly coat each half bivalent but are excluded from the so-called mid-bivalent region (bivalent center). During female meiosis, the bivalents are then surrounded by microtubule bundles running along their sides, whereas microtubule density is extremely low at chromosome ends despite a high concentration of kinetochore proteins at those regions (***Wignall and Villeneuve, 2009***). Then, during anaphase I microtubules are formed between the segregating chromosomes from the mid-bivalent regions towards the poles in a kinetochore-independent mechanism (***Dumont et al., 2010***). Since only a few microtubules attach to the ends of the bivalents, the orientation of the bivalents on the spindle is largely driven by kinetochores interactions along the long arms with the lateral microtubule bundles (***Dumont et al., 2010; Wignall and Villeneuve, 2009***). However, in male meiosis, microtubule bundles are enriched at the bivalent ends facing polewards, indicative of a ‘telokinetic-like’ behavior (***Shakes et al., 2009; Wignall and Villeneuve, 2009***). In both cases, this allows one pair of sister chromatids to face one spindle pole and the other pair of them belonging to the second homolog to face the opposite pole. Finally, the sister chromatids remain attached via one chromosome end and become separated during the second meiotic division (***Albertson and Thomson, 1993; Dumont et al., 2010; Martinez-Perez et al., 2008***).

Meiotic adaptations are also observed in other holocentric organisms as in *Heteroptera* (***Hughes-Schrader and Schrader, 1961; Perez et al., 2000; Viera et al., 2009***) and *Parascaris* species (***Pimpinelli and Goday, 1989***), where spindle fibers attach to a restricted kinetochore region at a single chromosome end of each

homologue during meiosis I (telokinetic meiosis). Thus, this type of meiosis acts functionally as in monocentric species, since the homologs segregate to opposite poles already during meiosis I. Remarkably, during meiosis II the same telokinetic behavior is observed, although which ends acquire kinetic activity in both divisions seems to be random (***Melters et al., 2012***). These findings support a high plasticity for centromere/kinetochore structure during meiotic divisions in holocentric organisms.

In contrast, holocentric plant species of the genera *Rhynchospora* and *Luzula* evolved an alternative strategy to deal with meiosis. They display individual chromatids at prophase II, indicating the complete loss of sister chromatid cohesion during meiosis I. Accordingly, sister chromatids segregate to opposite poles at anaphase I followed by the separation of homologous non-sister chromatids in anaphase II (***Cabral et al., 2014; Heckmann et al., 2014***). In contrast to a monopolar sister centromere orientation of monocentric chromosomes and the restriction of kinetochore activity found in other holocentrics, *Luzula elegans* show maintenance of the holocentromeres throughout meiosis and sister centromeres are not fused. They interact individually and bi-orientated with the meiotic spindles. This results in the separation of sister chromatids already during meiosis I. To ensure a faithful haploidization, the homologous non-sister chromatids remain linked at their termini by chromatin threads after metaphase I until metaphase II, separating at anaphase II. Thus, an inverted sequence of meiotic sister chromatid separation occurs (***Heckmann et al., 2014***).

Similarly, in the Cyperaceae *Rhynchospora pubera* an amphitelic attachment of multiple spindle fibers at the sister chromatids appear during meiosis I (***Cabral et al., 2014; Guerra et al., 2010***). In contrast to mitotic chromosomes, disperse labelling of meiotic chromosomes was found with antibodies recognizing the (peri)centromere-marker histone H2AThr120ph, suggesting a different centromere organization between mitosis and meiosis in *R. pubera* (***Cabral et al., 2014***). Indeed, multiple patches of CENH3 labelling enhanced at the poleward chromosome surface was reported for highly condensed metaphase I bivalents (***Cabral et al., 2014***). However, the lack of simultaneous CENH3 and tubulin localization in other stages of meiosis

and the limited microscopic resolution hampered a comprehensive characterization of the kinetic activity and centromere organization throughout the meiosis of this species.

In mitosis, the chromosomes of *R. pubera* exhibit a line-like holocentromere organization comprising CENH3-containing centromere units enriched in centromeric tandem repeats (named Tyba) and centromeric retroelements. In interphase, the holocentromeres dissociate and form multiple individual centromere units. During chromosome condensation towards mitotic metaphase, the centromeric units rejoin and form a line-like distinct longitudinal centromere within a groove, to ensure faithful chromosome segregation (***Marques et al., 2015***).

Because of the differential labeling patterns between mitotic and meiotic chromosomes with H2AThr120ph observed by ***Cabral et al. (2014)***, we asked whether a different centromeric organization was associated with the progression of its inverted meiosis, what would possibly imply in a different adaptation to holocentricity when compared to *Luzula*. Thus, we performed a comprehensive analysis with specific antibodies against the centromeric components CENH3 and CENP-C, α-tubulin, as well as the centromeric repeat Tyba and applied super-resolution microscopy to characterize the organization and dynamics of *R. pubera* holocentromeres throughout meiosis. We report here that the holocentromere organization of *R. pubera* differs significantly between mitosis and meiosis, providing the identification of a not yet reported meiotic centromere organization among eukaryotes.

Results

During *R. pubera* meiosis a chromosome-wide random distribution of CENH3 signals is present during early prophase I until diakinesis (***Figure 1A-B***). At metaphase I multiple clustered CENH3 signals appear (***Figure 1C***). 3D surface rendering confirmed the absence of a centromere groove at meiosis (***Figure 1B; Movie S1***). These results strongly contrast to the line-like holocentromeres of *R. pubera*, which

colocalize within a distinct longitudinal centromere groove (***Marques et al., 2015***) (***Figure 1D, Movie S2***).

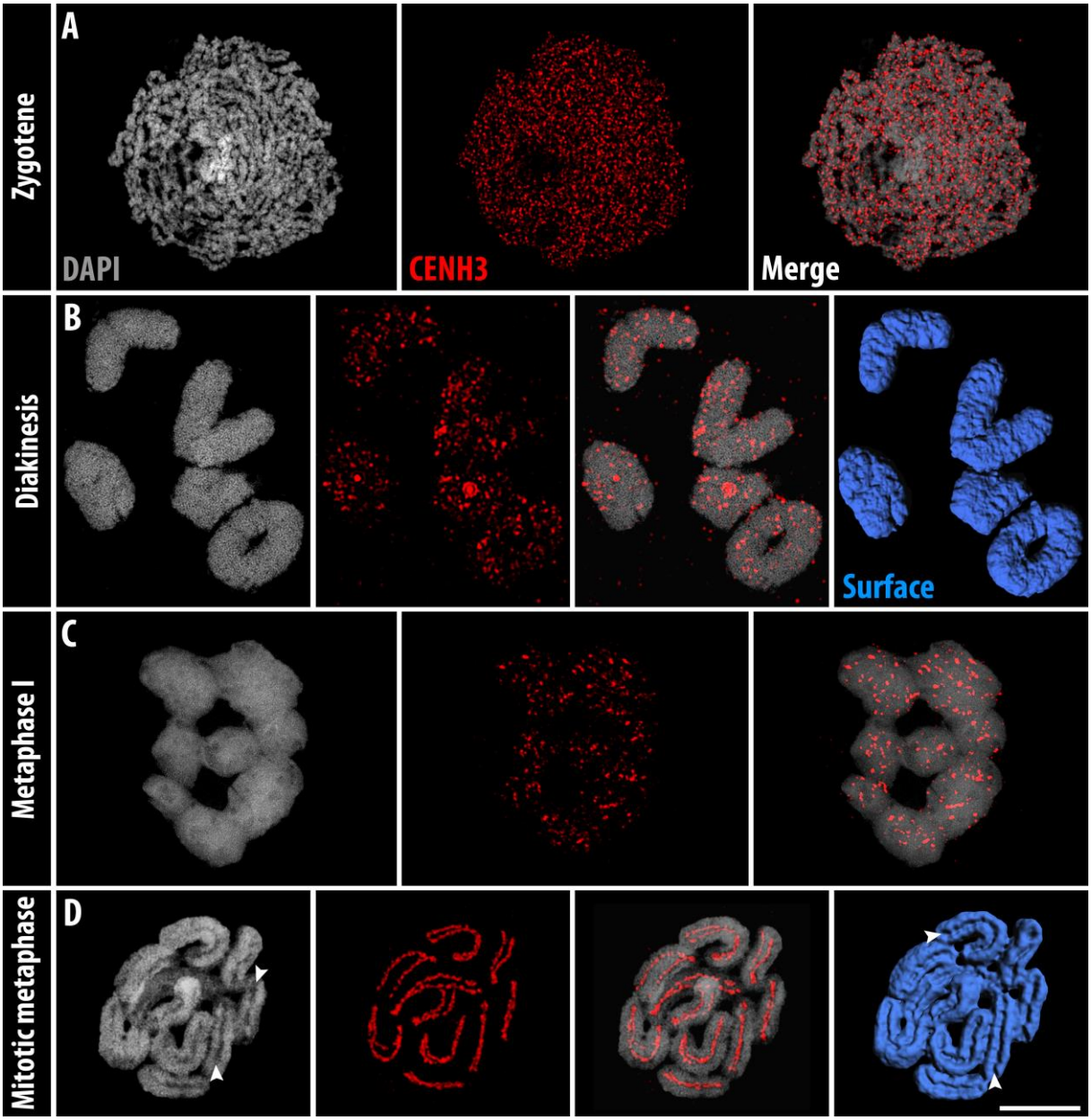

Figure 1. Contrasting holocentromere formation between meiosis and mitosis of *R. pubera*. CENH3 labeling of meiotic chromosomes at (**A**) zygotene, (**B**) diakinesis, (**C**) metaphase I and (**D**) mitotic metaphase. Bar = 5 µm.

To confirm the observed contrasting centromere organization we used the inner kinetochore protein CENP-C (*Rp*CENP-C) as an additional centromere-marker. CENP-C is a key component of most eukaryotic centromeres and links between the

inner and outer (microtubule-binding) components of the kinetochore (***Earnshaw, 2015***). It has been shown that CENP-C colocalizes to CENH3, thus defining active centromere chromatin (***Carroll et al., 2010; Falk et al., 2015; Kato et al., 2013***).

In silico analysis of the pollen mother cell transcriptome of *R. pubera* identified a single *CENP-C* candidate. The alignment of a RT-PCR generated 713 bp partial transcript with the *CENP-C* sequences of other species supported the correct identification (***Figure S1A***). Phylogenetic analysis grouped *Rp*CENP-C as a sister branch of Juncaceae, and both as sister to the Poaceae clade (***Figure S1B***). Thus, an *Rp*CENP-C antibody was generated.

During mitosis CENP-C specific centromeric signals were observed along the mitotic groove in all chromosomes, well colocalized with CENH3 (***Figure S2A; Movie S3***). In interphase nuclei, a disperse distribution of both centromeric marks was found (***Figure S2B***), while only a weak colocalization was seen (***Figure S2C***). Prophase and pro-metaphase chromosomes displayed interrupted line-like CENH3/CENP-C signals showing increased level of colocalization (***Figure S2D***). Additionally, a progressive cell-cycle-dependent colocalization of both proteins was observed.

To validate the contrasting centromere organization observed on meiotic chromosomes we performed co-immunostaining with CENH3 and CENP-C. From early prophase I until diakinesis, CENH3 and CENP-C signals were observed as dispersed dot-like signals all over the chromosomes partially colocalized (***Figure 2A-B; Movie S4***). At metaphase I onset, bivalents were ordered at the equatorial plate and CENH3/CENP-C signals were seen as clustered signals well abundant along the poleward surface of chromatids (***Figure 2C and 2E; Movie S5***). At metaphase II, CENH3 and CENP-C signals were highly clustered mostly occupying the mid-region of each chromatid (***Figure 2D***). Hence, in contrast to the line-like holocentromere organization observed during mitosis, a different assembly of centromere units occurs during meiosis, forming the so-called cluster-holocentromeres.

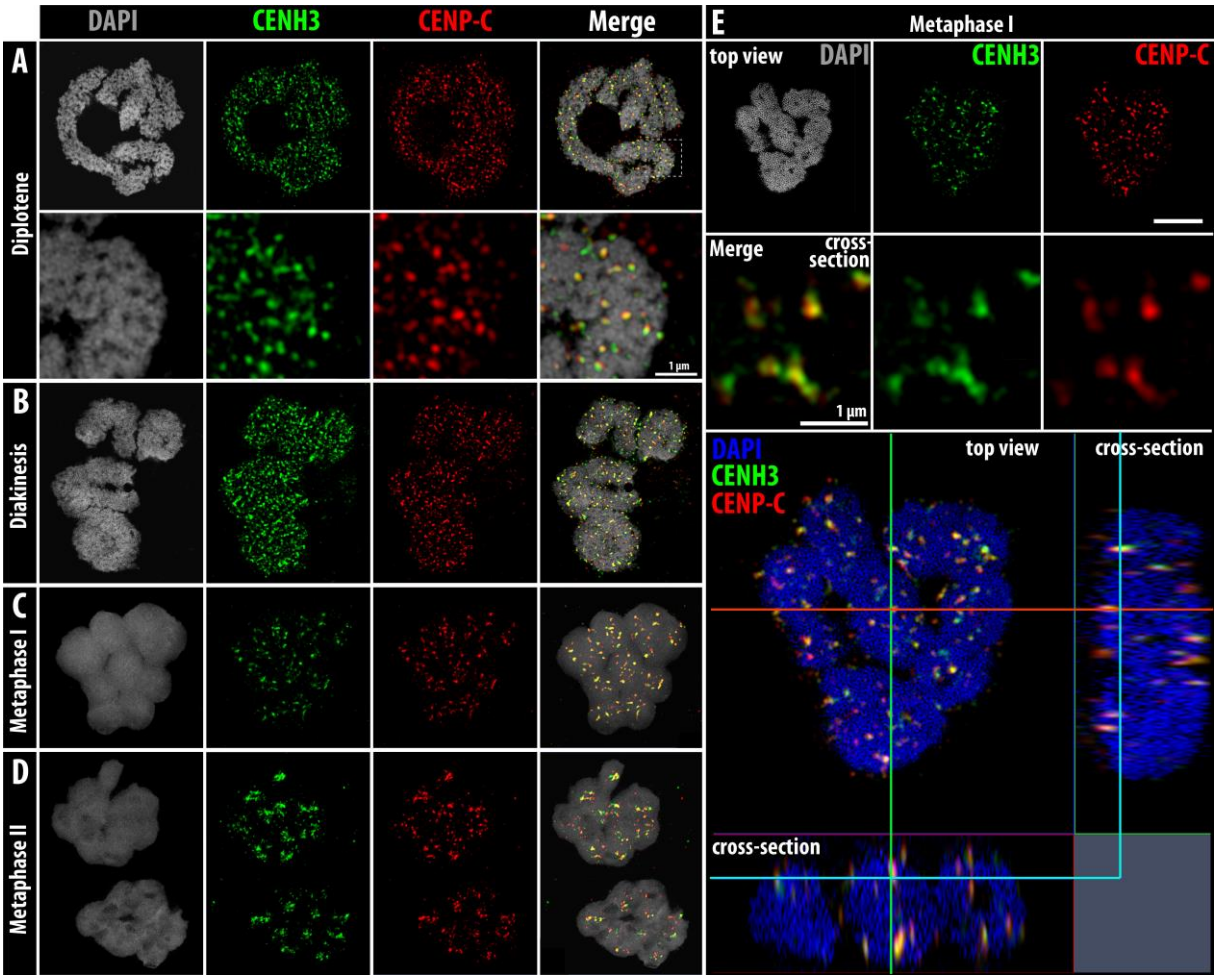

Figure 2. Co-immunostaining of *Rp*CENH3 and *Rp*CENP-C during different meiotic stages. (**A**) Diplotene, (**B**) diakinesis, (**C**) metaphase I and (**D**) II. (**E**) Interactive view of a metaphase I plate showing specific colocalization of CENH3 and CENP-C in cluster-holocentromeres. Overlapping signals are seen as yellow signals in merged images. Bar in **E** is equivalent to 5 µm for all images, except when indicated.

The mitotic holocentromeres of *R. pubera* associate with the centromeric tandem repeat Tyba (cenDNA) (Marques et al., 2015). Because of the odd meiotic centromere organization found in *R. pubera*, we asked whether the same interplay exists for meiotic chromosomes. Indeed, specific overlapping CENH3 and cenDNA signals were found throughout meiosis I and II (***Figure S3A-C***), whereas cenDNA signals were always stronger and well defined compared to CENH3/CENP-C signals. Thus, despite a different centromere organization, the DNA composition of centromere units does not differ between meiosis and mitosis and Tyba repeats can be used as additional maker for tracking the centromere organization during meiosis.

To check how and when the spindle fibers attach to centromere units, the distribution of α-tubulin and CENH3/cenDNA were analyzed throughout meiosis. From early prophase I until diakinesis no interaction was found between spindle fibers and centromeres, which were scattered distributed overall the chromosomes (***Figure 3A; Figure 4A-B; Movie S5***). At diakinesis, bivalents are seen as typical rod- and ring-bivalents, corresponding to one and two chiasmata, respectively (***Figure 3A***). At early metaphase I bivalents were equatorially oriented and clustered CENH3/cenDNA signals were observed mostly enriched along the poleward surface of bivalents, which showed bipolar orientation of sister chromatids (***Figure 3B; Figure 4C I, inserts***). At late metaphase I, sister cluster-holocentromeres showing interaction with spindle fibers from opposite poles (amphitelic attachment) was first observed and centromeres units were more dispersed (***Figure 3C; Movie S6***). Univalents are often (3.5%) found in *R. pubera* (***Cabral et al., 2014***) and they always show the same amphitelic attachment (***Figure 4D, inserts***). At anaphase I, sister cluster-holocentromeres were pulled by spindle fibers from opposite poles, resulting in separation of sister chromatids (***Figure 3D; Figure 4E***). At this stage spindle fibers were seen interacting with centromere units best, which were more dispersed (***Figure 3E; Movie S7***), most likely due to differential tension applied by spindle fibers. Chromatids occasionally migrate as single chromatids in both univalents and bivalents (***Figure 4E, inserts***), supporting early loss of sister chromatid cohesion and chiasmata resolution. At telophase I, cluster-holocentromeres were more accumulated in the mid-region of each chromatid showing little interaction to spindle fibers (***Figure 3F***). Thus, regardless of the different centromere organization during meiosis I of *R. pubera*, centromere units interact with spindle fibers after diakinesis.

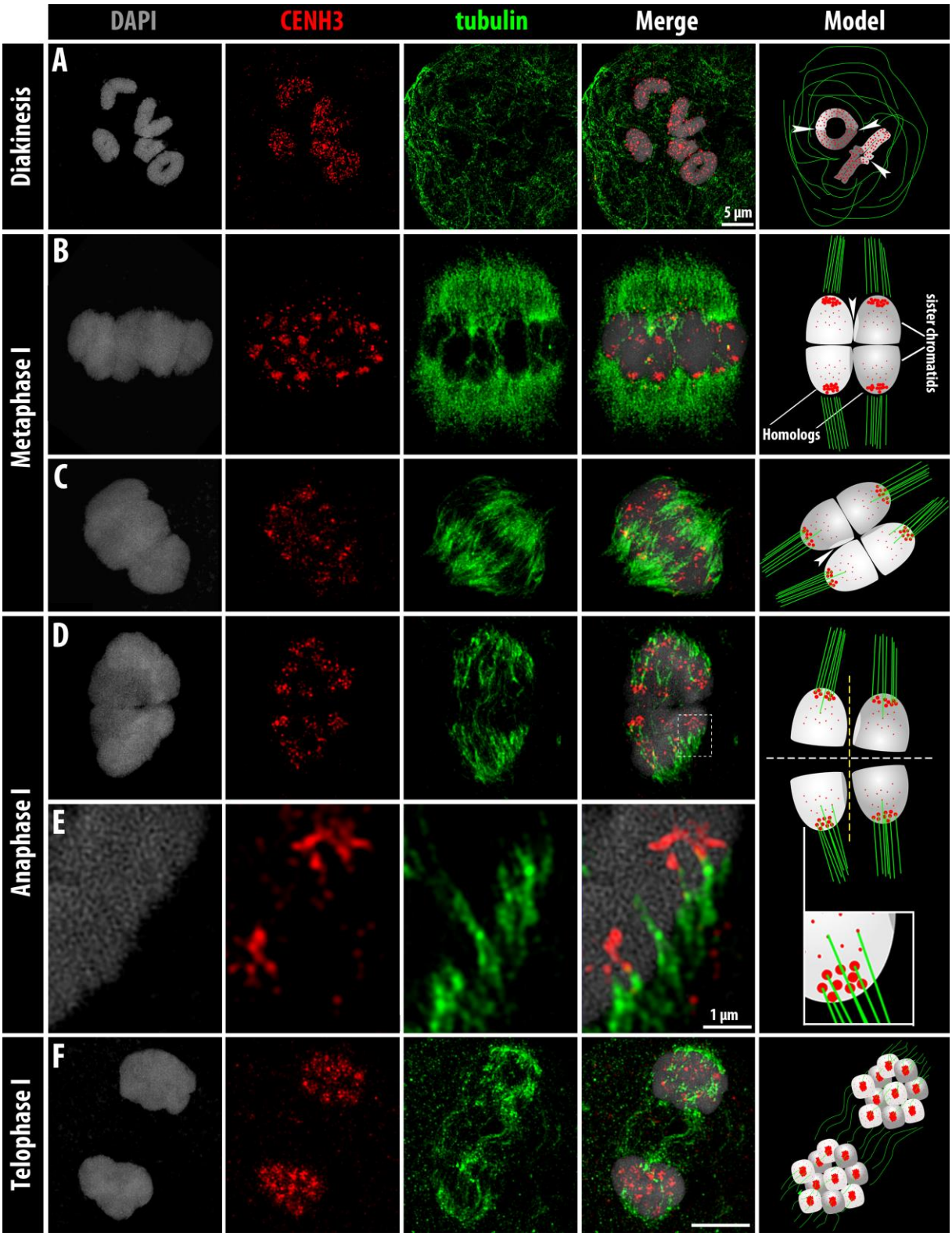

Figure 3. Co-immunostaining of CENH3 and α-tubulin during meiosis I of *R. pubera*. (**A**) Diakinesis, (**B**) early and (**C**) late metaphase I, (**D**) anaphase I, (**E**) enlargement of **D** (squared) and (**F**) telophase I. Interpretation models are illustrated at the last right column; sister chromatids are indicated by equal grayscale, while dark and light

gray indicate homologs. CO positions are indicated by exchanged light and dark gray chromatin (arrowheads); note in **A** that while rod-bivalents have one chiasmata ring-bivalents have two. Dashed white and yellow lines indicate early sister chromatid cohesion loss and chiasmata resolution, respectively. Bar in **F** is equivalent to 5 µm for all images, except when indicated.

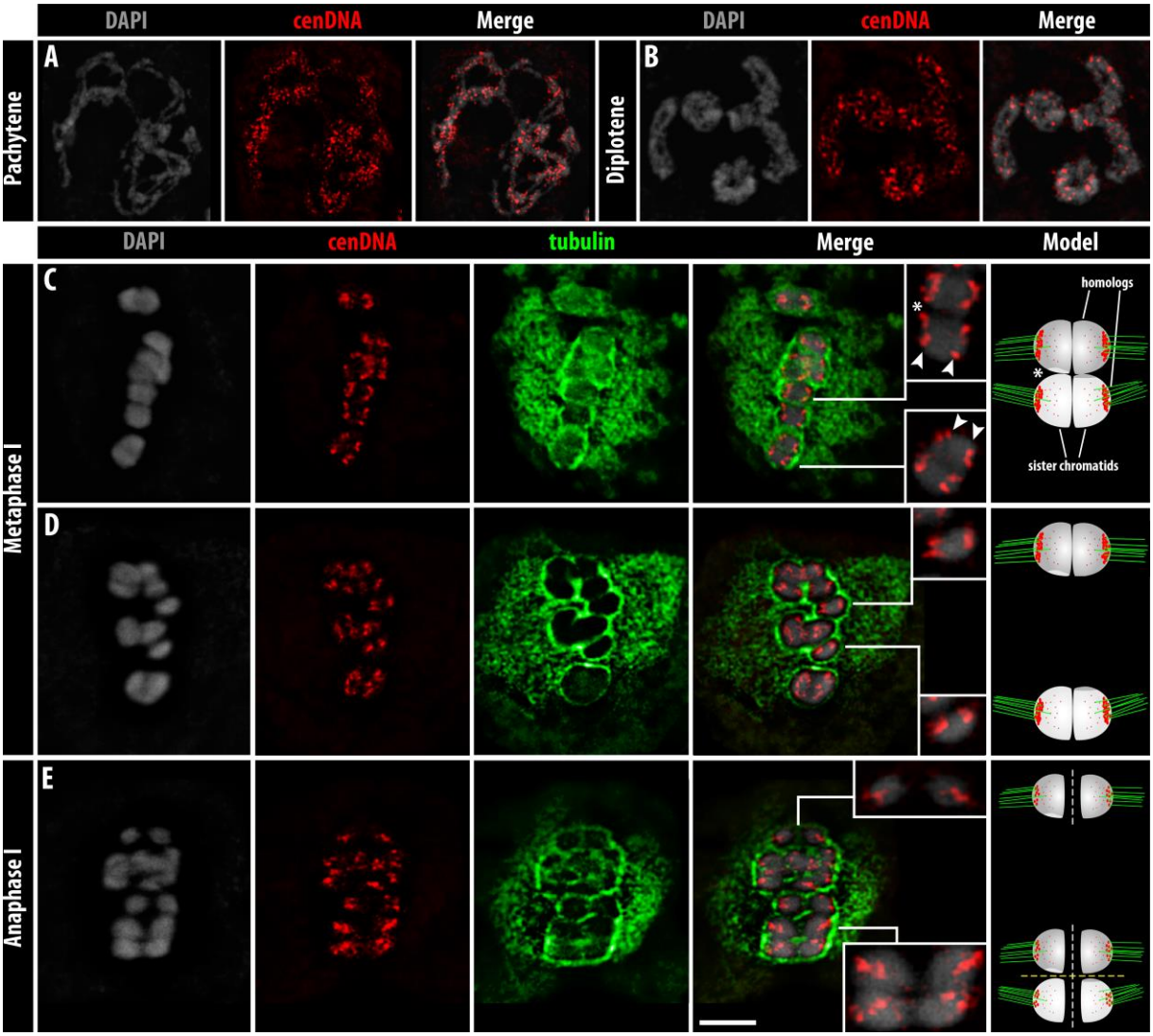

Figure 4. Detection of cenDNA Tyba and α-tubulin staining during meiosis I of *R. pubera*. (**A-B**) Detection of cenDNA during prophase I. (**C-E**) Immuno-FISH with cenDNA and α-tubulin on (**C-D**) Metaphase I and (**E**) anaphase I. Inserts in **C** show bi-orientation of sister centromeres (arrowheads) at metaphase I. Inserts in **D** show bi-orientation of sister centromeres of univalents. Upper and bottom inserts in **E** show chromatids migrating as single of a univalent and a bivalent, respectively. Interpretation models are illustrated at the last right column; sister chromatids are

indicated by equal grayscale, while dark and light gray indicate homologs. CO position is indicated by exchanged light and dark gray chromatin (asterisk). Dashed white and yellow lines indicate early sister chromatid cohesion loss and chiasmata resolution, respectively. Bar = 5 µm.

During early meiosis II, at prophase II, a diploid number (10) of individualized chromatids in each cell was observed as round-like structures displaying a dispersed distribution of centromeric signals (***Figure 5A***). As homologous non-sister chromatids associate in pairs towards metaphase II, centromeric signals were seen as few cluster signals in the mid-region of each chromatid (***Figure 5B***). At metaphase II onset, pairs of homologous non-sister chromatids mostly showed a single cluster-holocentromere in the mid-region of each chromatid, which were stretched by spindle fibers from opposite poles (***Figure 5C, E-F inserts***). Chromatids were of drop-like shape likely due to the tension applied by the spindle fiber forces (***Figure F insert***). 3D surface rendering of metaphase II cells confirmed cluster-holocentromeres mostly organized as a single cluster in the mid-region in each chromatid occupying external and internal domains (***Figure 5I; Movie S8, S9***). During anaphase II stretched homologous non-sister chromatids were then pulled to opposite poles (***Figure 5D, G***). Finally, at telophase II, tetrads showed four haploid nuclei with five chromatids each, showing five clustered centromeric signals (***Figure 5F***). Thus, in contrast to the several cluster-holocentromeres observed in metaphase I, at metaphase II mostly a single cluster-holocentromere is observed occupying a specific domain extending from the internal to external mid-region of each chromatid.

Because of the odd arrangement of homologous non-sister chromatids at metaphase II, we asked whether orientation of chromatids occur by their telomeres (axial orientation) or not. Since the 45S rDNA clusters are located terminally on three chromosome pairs of *R. pubera* (***Sousa et al., 2011***), we performed FISH with 45S rDNA probe. FISH signals were always observed facing the pole sides (***Figure 5J***), supporting preferential association of homologous non-sister chromatids by non-rDNA telomeres as previously indicated (***Cabral et al., 2014***). These results indicate that homologous non-sister chromatids during metaphase II are axially oriented contrasting to the equatorial orientation of bivalents at metaphase I.

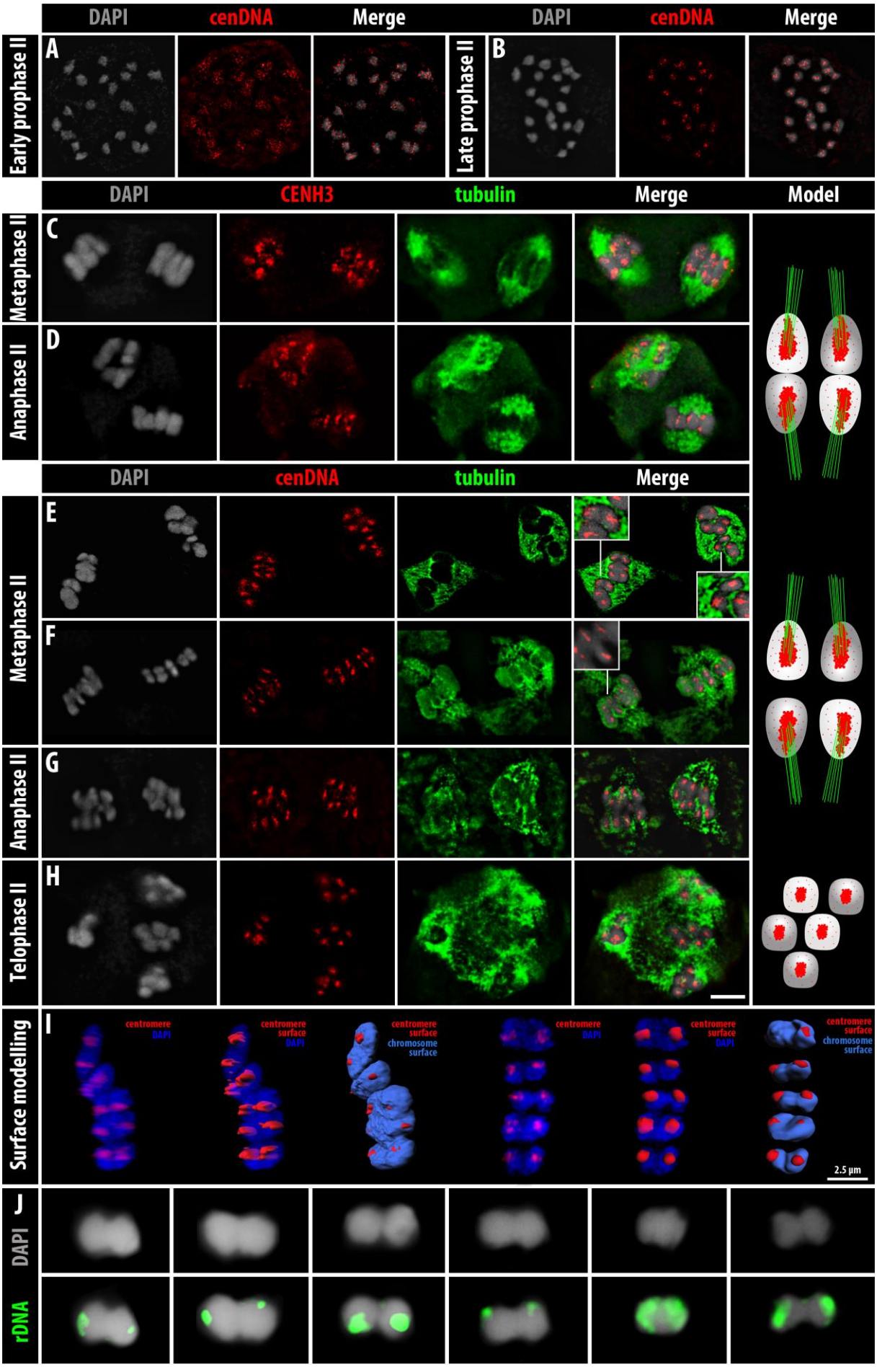
DAPI
cenDNA
Merge
Early prophase II
A
Late prophase II
B
DAPI
CENH3
tubulin
Merge
Model
Metaphase II
C
Anaphase II
D
DAPI
cenDNA
tubulin
Merge
Metaphase II
E
F
Anaphase II
G
Telophase II
H
Surface modelling
I
centromere
DAPI
centromere
surface
DAPI
centromere
surface
chromosome
surface
2.5 µm
J
DAPI
rDNA

Figure 5. Cluster-holocentromere organization and homologous non-sister chromatids orientation during meiosis II of *R. pubera*. (**A-B**) Detection of cenDNA Tyba during early meiosis II. (**C-D**) Immunostaining of CENH3 and tubulin of (**C**) metaphase II and (**D**) anaphase II chromosomes. (**E-H**) Immuno-FISH of α-tubulin and cenDNA Tyba during (**E-F**) metaphase II, (**G**) anaphase II and (**H**) telophase II. (**I**) 3D surface rendering of metaphase II chromosomes showing centromere structure. (**J**) FISH with 45S rDNA probe on pairs of homologous non-sister chromatids. Bar = 5 µm, except when indicated.

To test whether a line-like centromere structure is reestablished after meiosis, the subsequent pollen mitosis was analyzed. In most plants at the end of male meiosis tetrads fall apart and each one of the four haploid products produces a single pollen. In contrast in *R. pubera*, tetrads do not fall apart and a selective microspore abortion occurs, leading to pollen dispersal as pseudomonads (***San Martin et al., 2013***). Thus, at the end of male meiosis three out of four haploid spores degenerate and a single one remain functional to develop the mature pollen. At late tetrad stage the four haploid nuclei decondense and cluster-holocentromeres dissociate in small centromere units (***Figure 6A***). Finally, a line-like holocentromere organization is found at first pollen mitosis in all four cells of the pseudomonad after FISH with cenDNA (***Figure 6B***), whereas no groove-like structure has been found at this stage (***Movie S10***). Remarkably, only the functional cell replicates, as indicated by double lines of cenDNA signals, while the degenerative cells possess non-replicated chromatids (***Figure 6B***). Surprisingly, CENH3 line-like signals were observed only in the three degenerative nuclei, while the functional cell showed weak indistinct CENH3 signals (***Figure 6C***).

In summary, the arrangement of centromere units differs between mitosis and meiosis in *R. pubera.* A transition occurs from the mitotic line- to the cluster-holocentromeres at meiosis as summarized in ***Figure 7***. Finally, a line-like holocentromere organization is reestablished at first pollen mitosis (***Figure 7B***).

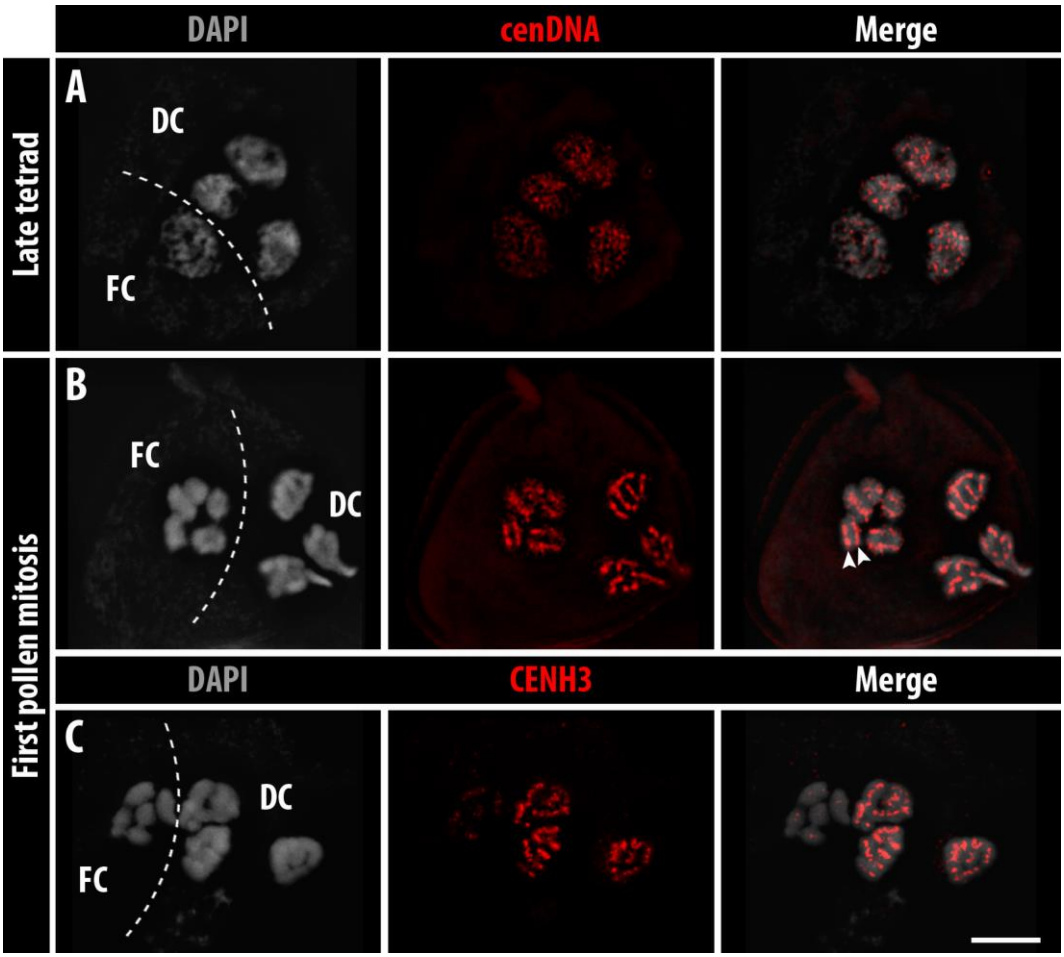

Figure 6. Reestablishment of a line-like holocentromere organization in the chromosomes of *R. pubera* during pseudomonad development. (**A-B**) Centromeric DNA Tyba and (**C**) CENH3 labeling. FC = functional cell, DC = degenerative cells. Bar = 5 µm.

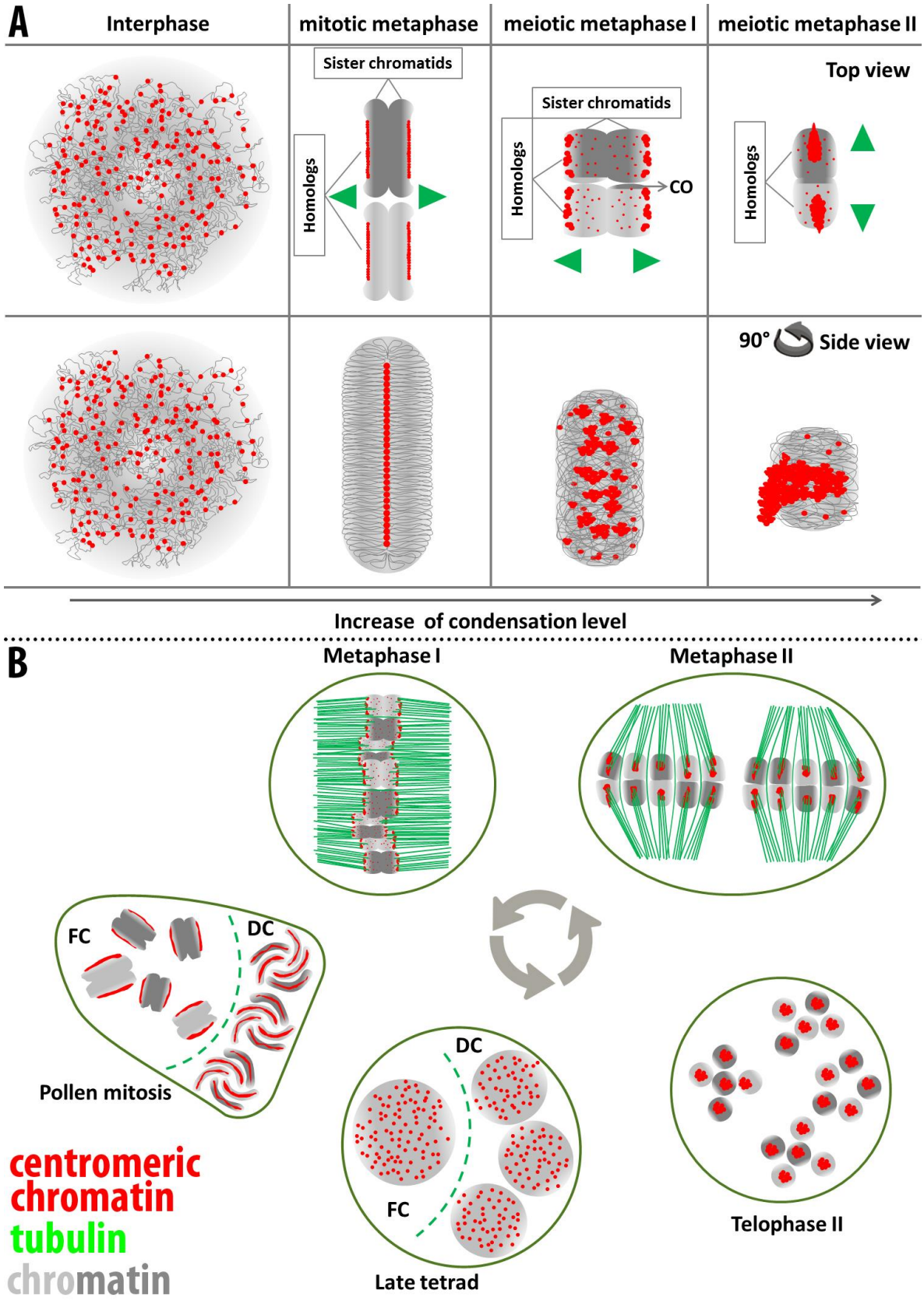

Figure 7. Model of differential holocentromere organization in the holocentric plant *R. pubera*. (**A**) Top and side (90^{o} left turn) views of centromere organization during

mitosis and meiosis. During interphase centromere units are dispersed genome-wide in both somatic and meiotic cells. While the process of chromosome condensation occurs, striking differences are seen between mitotic and meiotic chromosomes, i.e. in mitotic ones a line-like holocentromeres is formed within the groove, whereas both meiosis I and II chromosomes show a cluster-holocentromere organization and no groove are seen. (**B**) Cell cycle dynamics of cluster-holocentromere organization and spindle fibers. During meiosis I cluster-holocentromeres are oriented along the poleward surface of equatorially oriented bivalents; sister chromatids interact with spindle fibers from opposite poles (amphitelic attachment) causing their separation in anaphase I (equational meiosis). During meiosis II cluster-holocentromeres are localized in the mid-region of each chromatid. At this stage pairs of homologous non-sisters chromatids are axially orientated and adopt a drop-like shape most likely due to the tension applied by the spindle forces at anaphase II, causing the segregation of homologous chromatids (reductional meiosis). At telophase II each chromatid assumes a round-like shape with a strong cluster-holocentromere in the mid-region. During decondensation at late tetrads, centromere units dissociate and reassociate later on during the first pollen mitosis, where a line-like holocentromere is reestablished. At this last stage only the functional cell shows double centromeric signals, whereas CENH3 signals are reduced in this cell.

Discussion

The holocentromeres of *R. pubera* display reorganization across mitosis and meiosis

Although *R. pubera* and *L. elegans* belong to the same order *Poales*, the structure of meiotic centromeres of both holokinetic chromosome species shows striking differences. While both species possess a line-like holocentromere organization during mitotic metaphase, only *L. elegans* exhibits the same centromere structure during meiosis (***Heckmann et al., 2014***). In contrast, in *R. pubera* the centromere units cluster during meiosis and no distinct line-like holocentromere within a groove is formed. Restoration of the line-like holocentromere organization occurs after meiosis, during first pollen mitosis, although no groove is formed.

Why does the centromere organization differ between mitotic and meiotic chromosomes in *Rhynchospora*? The distinct meiotic centromere organization found in *R. pubera* could be caused by an alternative association of centromeric units likely due to a stronger degree of chromosome condensation and/or the absence of factors required for the line-like organization of the holocentromere. Differences in the composition and dynamics of cohesion and condesin proteins might explain the striking divergences between mitosis and meiosis (***Zamariola et al., 2014***). Indeed, a differential cohesion/condensation dynamics might explain the odd arrangement observed in *R. pubera*, since meiotic chromatids lose their elongated and groove structure to become highly condensed frequently assuming a round-like shape. In contrast, a similar chromatid and groove structure are found during mitosis and meiosis in *L. elegans* (***Heckmann et al., 2014***). Less likely a differential CENH3 loading dynamics during meiosis may acts as adaptation to deal with holocentricity during meiosis. Indeed, meiotic CENH3 loading dynamics differs from mitosis among plants (***Ravi et al., 2011; Schubert et al., 2014***).

A deviating centromere structure during meiosis has been reported for a number of holocentric species. In *C. elegans*, kinetochore activity involves a mechanism independent of CENH3 and CENP-C during meiosis I and II (***Monen et al., 2005***) and chromosomes are ensheathed by bundles of microtubules that run laterally along their sides during female meiosis (***Schvarzstein et al., 2010; Wignall and Villeneuve, 2009***). However, in male meiosis, microtubule bundles are enriched at the bivalent ends facing polewards indicative of a 'telokinetic-like' activity (***Wignall and Villeneuve, 2009***). The holocentric worm *P. univalens* undergo restriction of kinetic activity to the heterochromatic terminal regions during male meiosis. These regions lack long kinetochore structures and interact directly with spindle microtubules (***Goday and Pimpinelli, 1989; Pimpinelli and Goday, 1989***). In holocentric Heteroptera, a localized kinetic activity during meiosis I and II was also reported (***Papeschi et al., 2003; Perez et al., 2000***). Moreover, in most cases telokinetic meiosis seems to involve a mechanism where either end of chromatids can acquire kinetic activity, demonstrating a special case of kinetochore plasticity.

In the hemiptera *Oncopehus*, the presence of a holokinetic kinetochore plate during mitosis, but its absence during meiosis, was concluded based on electron microscopic studies. Multiple microtubule attachment sites were observed in meiotic chromosomes (***Comings and Okada, 1972***). Similar findings were reported for other holocentric organisms, i.e. the nematode *Ascaris lumbricoides* (***Goldstein, 1977***), the hemipteras *Rhodnius prolixus* (***Buck, 1967***) and *Graphosoma italicum* (***Rufas and Gimenez-Martin, 1986***) and the lepdoptera *Bombyx mori* (***Friedlander and Wahrman, 1970***). Moreover, in the holocentric scorpion *Tityus bahiensis*, a kinetochore plate throughout meiosis was found, while in the spiders *Dysdera crocata* and *Segestria florentina* kinetochore plates were observed only during meiosis II (***Benavente, 1982***). Thus, the absence of a kinetochore plate during the meiosis seems to occur rather frequently among holocentric organisms and was postulated to be related to the restriction of kinetic activity and terminalization of chiasmata in those organisms (***Comings and Okada, 1972; Pimpinelli and Goday, 1989***). Yet it is interesting to notice that all holocentric insects lacking kinetochore plates during meiosis also lack the CENH3 and CENP-C genes and occasionally some other inner kinetochore proteins, whereas most of the outer kinetochore genes were found still (***Drinnenberg et al., 2014***). Whether the lack of CENH3 and CENP-C is causing a misassembly of kinetochore plates during meiosis in these organisms is still unknown.

A line-like holocentromere organization is not required for the reversion chromatid segregation during meiosis

We confirmed the previously reported inverted meiosis in *R. pubera* (***Cabral et al., 2014***) by showing a bipolar orientation of sister centromeres and their attachment to microtubules from opposite spindle poles in meiosis I (amphitelic attachment), segregation of sister chromatids to opposite poles in anaphase I (equational division), and alignment and segregation of homologous non-sister chromatids during the second meiotic division. Remarkably, a differential orientation of cluster-holocentromeres was observed from meiosis I and II. While during meiosis I cluster-holocentromeres were observed mostly accumulated along the poleward surface of bivalents, in meiosis II cluster-holocentromeres were mostly seen as a single cluster in the mid-region occupying an internal and external domain of each chromatid.

Notably, homologous non-sister chromatids seem to be preferentially associated by their non-rDNA termini at metaphase II in *R. pubera* (***present study; Cabral et al., 2014***). These results together indicate a distinct orientation and interaction of spindle fibers with the cluster-holocentromeres between meiosis I and II. While during metaphase I bivalents orient perpendicular to the spindle poles, during metaphase II pairs of homologous non-sister chromatids orient with their longer axis parallel to the spindle poles.

Moreover, our results show that a line-like holocentromere organization as found in *L. elegans* is not required for reversion in the segregation of sister/homologous chromatids during meiosis. Actually, considering an end-to-end interaction of homologous non-sister chromatids in metaphase II, this line-like structure is only compatible with a proper segregation of chromatids to opposite poles because *Luzula* chromosomes maintain a U-shape conformation in meiosis II. In fact, the highly clustered holocentromere found at metaphase II/anaphase II in *R. pubera* seems to less-effective solve this problem by reducing the risk of merotelic attachment of microtubules. However, while no mis-segregation is found during meiosis I in *R. pubera*, it is reported that 19.5% of all meiosis II products had incorrect numbers of chromosomes (***Cabral et al., 2014***). In the nematode *C. elegans*, the chromokinesin KLP-19 counteracts persistent merotelic attachments (***Powers et al., 2004***). Whether in *R. pubera* a similar correction mechanism exists is unknown. Although merotelic attachments might be a cause of missegregation during meiosis II of *R. pubera*, ***Cabral et al. (2014)*** supported a model where pairs of homologous non-sister chromatids have failed to connect to each other, thus missegregating in meiosis II.

During first pollen mitosis, CENH3 signals were much stronger in the degenerative cells, while the functional cell showed a weak and indistinct labeling. These differences might be explained by the absence of *de novo* incorporation of CENH3 molecules after exit of meiosis. Thus, preexisting CENH3 could be partitioned equally between duplicated sister centromeres as a result of cell replication, which occurs only in the functional cell (evidenced by double lines of cenDNA signals). Thereby, halving a fixed number of CENH3 molecules in the generative and vegetative nucleus

(***Ishii et al., 2016***). Alternatively, active CENH3 removal in the functional haploid cell only after exit of meiosis could cause the reduction of CENH3 molecules (***Merai et al., 2014; Schoft et al., 2009***). Furthermore, the weak CENH3 signals observed in the functional cell suggests that a reduced amount of CENH3 is still sufficient for proper chromosome segregation (***Ishii et al., 2016; Lermontova et al., 2011; Liu et al., 2006***).

The meiotic holocentromeres in *R. pubera* are unique as it is the only holocentric species so far to show differential centromere organization from mitosis and meiosis, while having spindle fibers attaching to its centromere units composed of CENH3 and CENP-C. As discussed above, most organisms showing differential centromere organization either lack CENH3 and CENP-C (***Drinnenberg et al., 2014***) or these proteins do not play a role in chromosomes segregation during meiosis (i.e. *C. elegans*). In contrast, a similar organization of mitotic and meiotic holocentromeres is found in *L. elegans*, although no CENP-C antibody has been generated for this species (***Heckmann et al., 2014***).

What does the odd meiotic centromere arrangement of *R. pubera* implicate?

Inappropriate occurrence of COs in the proximity of centromeres negatively effects meiotic chromosome segregation by affecting pericentric cohesion and CO formation close to centromeres is infrequent (***Talbert and Henikoff, 2010; Vincenten et al., 2015***). Indeed, it is reported for holocentric organisms the occurrence of very few COs, generally one or two per rod- and ring-bivalent, respectively, mostly located at non-centromeric terminal regions (***Cuacos et al., 2015***). This is also true for *R. pubera* and its odd centromere arrangement of meiotic chromosomes could certainly cause a high risk of misorientation and/or failure on meiotic recombination during meiosis I. Remarkably, no chromosome fragmentation or anaphase bridges have been observed during meiosis of *R. pubera*. However, the weird centromere organization might cause the frequent (3.5%) occurrence of univalents by failure on incidence of crossover recombination. In fact, this could also explain the only occurrence of univalents in the achiasmatic meiosis of *Rhynchospora tenuis* (***Cabral et al., 2014***), since univalents in *Rhynchospora* always show sister chromatids segregation to opposite poles at anaphase I (***present study; Cabral et al., 2014***).

Thus, inverted meiosis in *Rhynchospora* could also work as an adaptation to solve potential meiotic errors due to the odd centromere arrangement.

It was recently evidenced that in yeast the Cf19 complex (also known as the Constitutive Centromere-Associated Network – CCAN – in other organisms) prevents meiotic DNA break formation, the initiating event of recombination, proximal to the centromeres (***Vincenten et al., 2015***). Nonetheless, it is interesting that meiotic DSBs are normally formed and processed in early prophase I of *Rhynchospora*, as evidenced by the presence of multiple RAD51 foci, indicating that recombination events might be normally occurring (***Cabral et al., 2014***). Moreover, in *R. pubera* meiosis axis formation is apparently normally formed since the axial element protein ASY1 is detected showing the typical monocentric-like pattern (***Cabral et al., 2014***). Therefore, it is surprisingly that the odd meiotic centromere arrangement found in *R. pubera* does not disturb normal development of axis architecture and synaptonemal complex. It is known that meiotic DSBs, despite being more suppressed at centromeric regions, may occur with certain frequency at only a few kilobases far-off of centromeres in yeast (***Buhler et al., 2007; Pan et al., 2011***). Thus, to deal with its centromere architecture during meiosis a very accurate regulation of meiotic recombination is likely to exist in *R. pubera*.

In conclusion holocentromeres of *R. pubera* are unique in respect to their differential organization during mitosis and meiosis. Our results reinforce the idea of centromere plasticity among holocentric organisms and offer a novel model for understanding centromere evolution and function among eukaryotes.

Material and Methods

Plant material. *Rhynchospora pubera* (Vahl) Boeckler plants were cultivated under humid conditions at the Experimental Garden of the Laboratory of Plant Cytogenetics and Evolution (Recife, Brazil) and in a greenhouse at the Leibniz Institute of Plant Genetics and Crop Plant Research (Gatersleben, Germany).

Identification and validation of the CENP-C gene and generation of a CENP-C antibody. The *CENP-C* gene was *in silico* identified by BLAST search from the

transcriptome data of *R. pubera* (accession number PRJEB9645, http://www.ebi.ac.uk/ena/). For the validation of expression, semi-quantitative RT-PCR was performed with DNase treated total RNA isolated from root, leaf and anther tissue of *R. pubera* using the SpectrumTM plant total RNA kit (Sigma). The cDNA was synthesized from 1 µg of total RNA using the RevertAid First Strand cDNA Synthesis Kit (Thermo Scientific). PCR reactions were performed with the primer sequences: forward 5´-AATGACTTCACCCTCACCCG-3´ and reverse 5´-CCTTCTTGCAGGTCTAGTGC-3´. Primers for the constitutively expressed GAPDH gene (Banaei-Moghaddam et al. 2013), GAPDH-F CAATGATAGCTGCACCACCAACTG and GAPDH-R CTAGCTGCCCTTCCACCTCTCCA, were used as control for applying equal amounts of gDNA and cDNA. The amplified fragments were cloned into the StrataClone PCR Cloning Vector pSC-A-amp/kan (Agilent Technologies). Sequences of 10 randomly selected clones revealed only one *CENP-C* variant (GenBank, accession number KU516997).

The peptide **VRVKSFMSDEHADLIAKLAK** was used to generate a *R. pubera* CENP-C-specific (*Rp*CENP-C) polyclonal antibody. Peptide synthesis, immunization of rabbits and peptide affinity purification of antisera was performed by LifeTein (http://www.lifetein.com).

Phylogenetic analysis of plant CENP-C sequences.

Reference IDs for all CENP-C sequences used in this study are available in Table S1. Multiple alignment of protein sequences encoding the entire CENP-C sequences was generated using MAFFT (***Katoh and Standley, 2013***) and refined manually. Evolutionary analyses were conducted with IQ-TREE (***Nguyen et al., 2015***) using ultrafast bootstrap (***Minh et al., 2013***). Phylogenetic history was inferred using the Maximum Likelihood method using the Best-fit model: JTT+I+G4 acquired automatically with IQ-TREE. The analysis involved 30 protein sequences. Alignments and trees are available through the iPlant Data Store and can be accessed via iPlant Discovery Environment or at http://de.iplantcollaborative.org/dl/d/C34A1998-A409-4E52-A732-2FCD8C906E53/RpCENPC.rar.

Immunostaining of somatic and meiotic cells. Immunostaining for CENH3 and CENP-C was performed as described in ***Cabral et al. (2014)*** with some modifications. Anthers were fixed in ice-cold 4% paraformaldehyde in 1×PBS buffer pH 7.5 (1.3M NaCl, 70mM Na_2HPO_4, 30mM NaH_2PO_4) for 1 h 30 min and squashed in a drop of the same buffer. Tapetum cells of young anthers were used for the preparation of mitotic cells. Then, slides were washed in 1×PBS and blocked with 3% BSA for 30 min at 37 °C. The antibodies used were rabbit anti-RpCENH3 (***Marques et al., 2015***) directly labeled with FITC, and rabbit anti-RpCENP-C, both diluted 1:500 in 1% BSA in 1×PBS. The detection of anti-RpCENP-C was done with goat anti-rabbit-Cy3 (Sigma, #F9887), diluted 1:200 in 1×PBS containing 1% BSA. The slides were counterstained with 2 µg/ml 4'6-diamidino-2-phenylindole (DAPI) in Vectashield H-1000.

For the simultaneous detection of CENH3 and tubulin, the anthers were fixed in methanol:acetic acid (3:1) for 2 to 24 h. Then, the anthers were rinsed three times in 1×PBS for 5 min, and the pollen mother cells were squeezed out from the anthers and squashed in a drop of 1×PBS. The coverslips were removed after freezing in liquid nitrogen. Then, the material was washed in 1×PBS and immersed in 1× citric buffer for 1 min in a microwave at 800 W. Afterwards, the slides were immediately washed in 1×PBS. The immunostaining procedure was conducted as described above. The CENH3 antibodies were detected by Cy3 or Alexa488 goat anti-rabbit antibodies. Mouse anti-α-tubulin antibodies (Sigma, #T5168) were diluted 1:50 in 1×PBS containing 1% BSA and detected with Alexa488 or Cy5 goat anti-mouse antibodies (ThermoFisher, #A-11001) diluted 1:100 in the same buffer.

Fluorescence *in situ* hybridization (FISH). The centromere-specific repeat Tyba was detected with directly labelled 5′-Cy3 oligonucleotides (Tyba1: ATTGGATTATACATGGTAATTACGCATATAAAGTGCAAATAATGCAATTC; Tyba2: ACAGATTCTGAGTATATTTGAGCATTTCAAGCGATTTTGCATT) (Eurofins MWG Operon, http://www.eurofinsdna.com). FISH after immunostaining was performed as described by ***Ishii et al. (2015)***.

Widefield and super-resolution fluorescence microscopy. Widefield fluorescence images were recorded using a Leica DM5500B microscope equipped with a Leica DFC FX camera and a deconvolution system. To analyze the substructures and spatial arrangement of immunosignals and chromatin beyond the classical Abbe/Raleigh limit (super-resolution), spatial Structured Illumination Microscopy (3D-SIM) was applied using a Plan-Apochromat 63×/1.4 oil objective of an Elyra PS.1 microscope system and the software ZEN (Carl Zeiss GmbH). Images were captured using 405, 488, 561 and 642 nm laser lines for excitation and the appropriate emission filters, and merged using the ZEN software (***Weisshart et al., 2016***). The degree of co-localization between the centromeric Tyba repeats and CENH3 was measured in image stacks using the Imaris 8.0 (Bitplane) software. SIM image stacks were used to produce 3D movies by the Imaris 8.0 (Bitplane) software.

Acknowledgement

We thank the Brazilian Agency CAPES for the Special Visiting Researcher grant and project funding for A.H., and fellowship for A.M., CNPq for financial support for A.P.-H and the IPK for support. We thank Dr. Stefan Heckmann for insightful comments and discussion on the MS.

Competing interests

The authors declare no conflict of interests.

Supplementary Figures

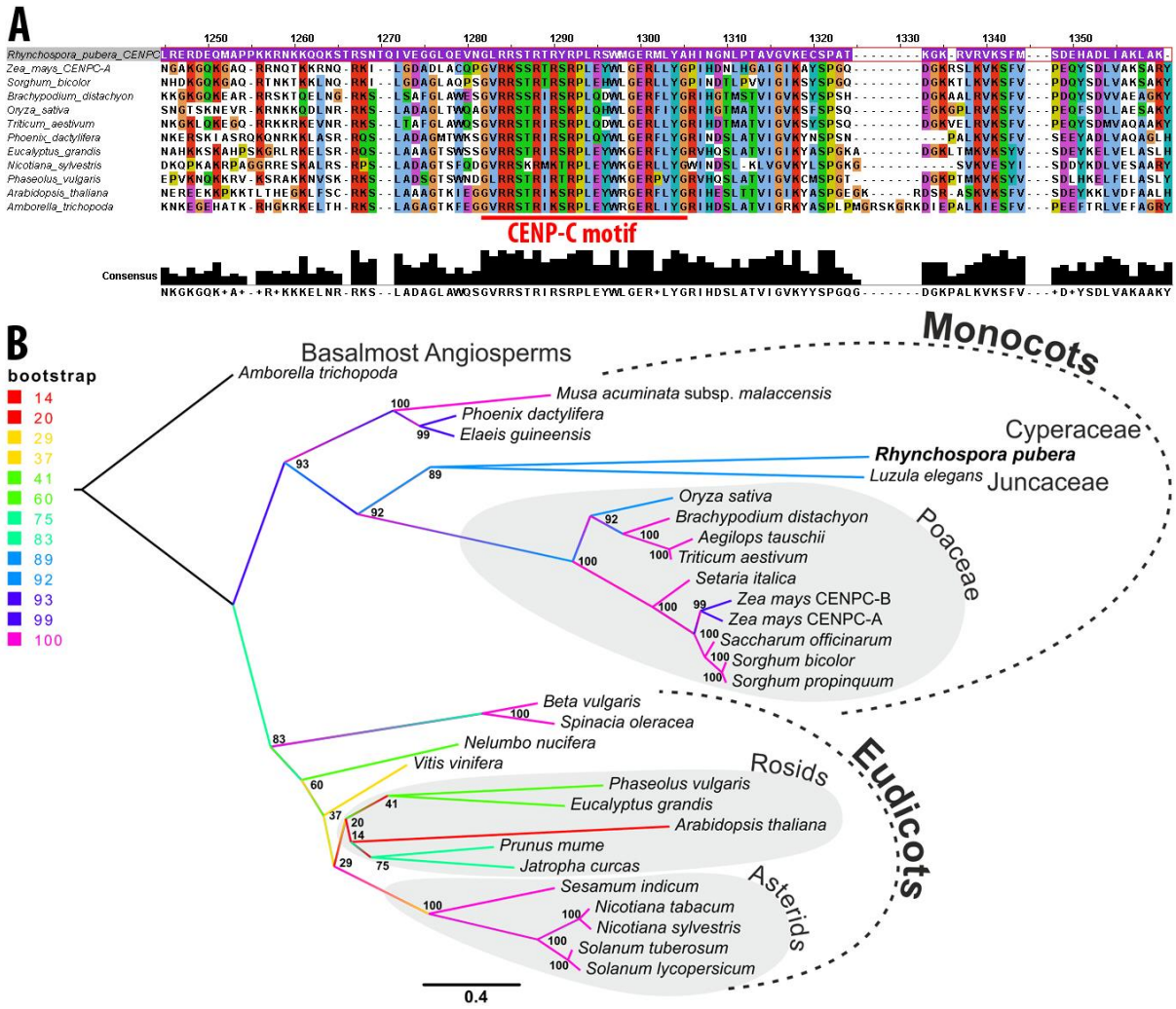

Figure S1. Characterization of *Rp*CENP-C. (**A**) Sequence alignment of the C-terminal tail of RpCENP-C and further plant homologs. (**B**) Maximum likelihood phylogenetic analysis of complete plant CENP-C amino acid sequences.

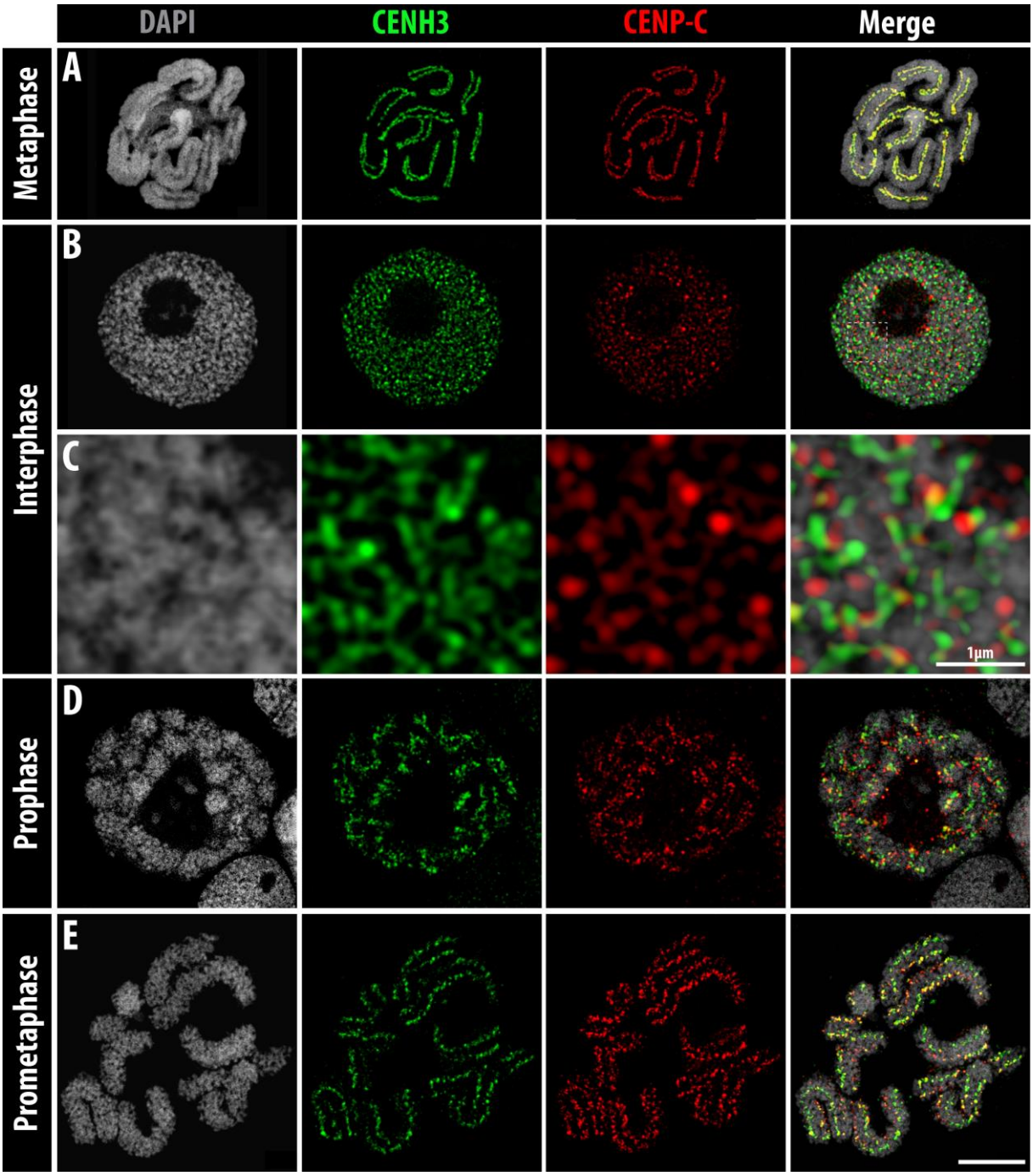

Figure S2. Co-immunolabeling of CENH3 and CENP-C during the mitotic cell cycle of *R. pubera*, obtained from tapetum cells. (**A**) Metaphase, (**B-C**) interphase, (**C**) enlargement of **B** (squared), (**D**) prophase and (**E**) prometaphase. Colocalized CENH3 and CENP-C signals are seen as yellow in merge images. Bar = 5 µm, except when indicate.

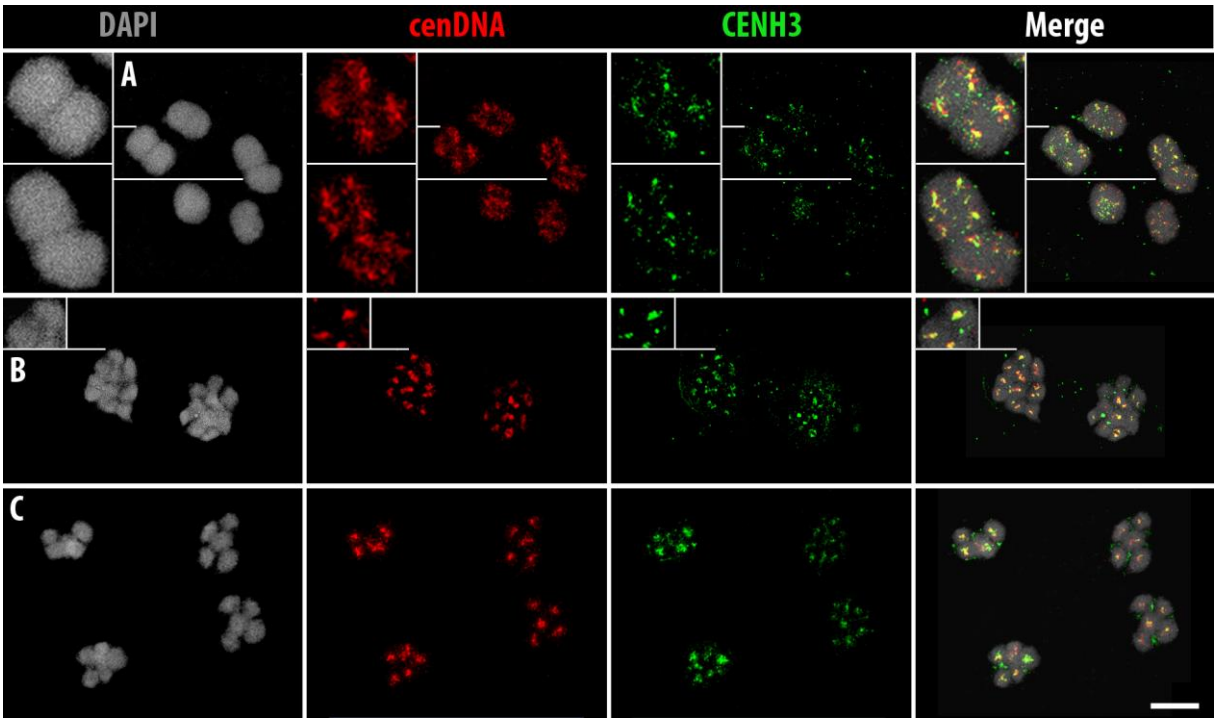

Figure S3. Immunolabeling of CENH3 followed by FISH with centromeric DNA Tyba during meiosis of *R. pubera*. (**A**) Metaphase I, (**B**) Metaphase II and (**C**) telophase II. Colocalized signals are seen as yellow in merged images. Bar = 5 µm.

Table S1. CENP-C plant sequences retrieved for phylogenetic analysis.

Genbank accession number	Taxa	Sequence Name	High taxonomic affiliation
ERN06072.1	*Amborella trichopoda*	*Amborella trichopoda* CENP-C	Basalmost Angiosperms
XP_009407449.1	*Musa acuminata* subsp. *malaccensis*	*Musa acuminata* subsp. *malaccensis* CENP-C	Monocots
KU516997	***Rhynchospora pubera***	***Rhynchospora pubera* CENP-C**	**Monocots/Commelinids**
EMT11913.1	*Aegilops tauschii*	*Aegilops tauschii* CENP-C	Monocots/Commelinids
XP_010232028.1	*Brachypodium distachyon*	*Brachypodium distachyon* CENP-C	Monocots/Commelinids
XP_010925103.1	*Elaeis guineensis*	*Elaeis guineensis* CENP-C	Monocots/Commelinids
A. Houben (personal communication)	*Luzula elegans*	*Luzula elegans* CENP-C	Monocots/Commelinids
AAU04616.1	*Oryza sativa*	*Oryza sativa* CENP-C	Monocots/Commelinids
XP_008792976.1	*Phoenix dactylifera*	*Phoenix dactylifera* CENP-C	Monocots/Commelinids
AAU04626.1	*Saccharum officinarum*	*Saccharum officinarum* CENP-C	Monocots/Commelinids
XP_004969174.1	*Setaria italica*	*Setaria italica* CENP-C	Monocots/Commelinids
AAU04623.1	*Sorghum bicolor*	*Sorghum bicolor* CENP-C	Monocots/Commelinids
AAU04624.1	*Sorghum propinquum*	*Sorghum propinquum* CENP-C	Monocots/Commelinids
CDM83393.1	*Triticum aestivum*	*Triticum aestivum* CENP-C	Monocots/Commelinids
AAD39435.1	*Zea mays*	*Zea mays* CENPC-B	Monocots/Commelinids
NP_001104933.1	*Zea mays*	*Zea mays* CENPC-A	Monocots/Commelinids
XP_010249869.1	*Nelumbo nucifera*	*Nelumbo nucifera* CENP-C	Basal eudicots
AAU04614.1	*Beta vulgaris*	*Beta vulgaris* CENP-C	Core Eudicots
KNA21045.1	*Spinacia oleracea*	*Spinacia oleracea* CENP-C	Core eudicots
NP_001289528.1	*Nicotiana sylvestris*	*Nicotiana sylvestris* CENP-C	Core Eudicots/Asterids
BAI48084.1	*Nicotiana tabacum*	*Nicotiana tabacum* CENP-C	Core Eudicots/Asterids
XP_011072288.1	*Sesamum indicum*	*Sesamum indicum* CENP-C	Core Eudicots/Asterids
XP_010318558.1	*Solanum lycopersicum*	*Solanum lycopersicum* CENP-C	Core Eudicots/Asterids
XP_006343106.1	*Solanum tuberosum*	*Solanum tuberosum* CENP-C	Core Eudicots/Asterids
NP_173018.2	*Arabidopsis thaliana*	*Arabidopsis thaliana* CENP-C	Core Eudicots/Rosids
XP_010062443.1	*Eucalyptus grandis*	*Eucalyptus grandis* CENP-C	Core Eudicots/Rosids
XP_012073303.1	*Jatropha curcas*	*Jatropha curcas* CENP-C	Core Eudicots/Rosids
XP_007160179.1	*Phaseolus vulgaris*	*Phaseolus vulgaris* CENP-C	Core Eudicots/Rosids
XP_008228592.1	*Prunus mume*	*Prunus mume* CENP-C	Core Eudicots/Rosids
CBI36186.3	*Vitis vinifera*	*Vitis vinifera* CENP-C	Core eudicots/Rosids

References

Albertson DG, Rose AM, and Villeneuve AM. 1997. Chromosome organization, mitosis, and meiosis. In: DL Riddle, T Blumenthal, BJ Meyer, and JR Priess, editors. *C elegans II*. (Cold Spring Harbor, NY: Cold Spring Harbor Laboratory Press). pp. 47–48.

Albertson DG, and Thomson JN. 1993. Segregation of holocentric chromosomes at meiosis in the nematode, *Caenorhabditis elegans*. *Chromosome Research* **1**:15-26.

Benavente R. 1982. Holocentric chromosomes of arachnids: Presence of kinetochore plates during meiotic divisions. *Genetica* **59**:23-27. Doi 10.1007/Bf00130811.

Buck RC. 1967. Mitosis and meiosis in *Rhodnius prolixus*: the fine structure of the spindle and diffuse kinetochore. *Journal of Ultrastructural Research* **18**:489-501.

Buhler C, Borde V, and Lichten M. 2007. Mapping meiotic single-strand DNA reveals a new landscape of DNA double-strand breaks in *Saccharomyces cerevisiae*. *PLoS Biol* **5**:e324. 10.1371/journal.pbio.0050324.

Burrack LS, and Berman J. 2012. Flexibility of centromere and kinetochore structures. *Trends in Genetics* **28**:204-212. 10.1016/j.tig.2012.02.003.

Cabral G, Marques A, Schubert V, Pedrosa-Harand A, and Schlogelhofer P. 2014. Chiasmatic and achiasmatic inverted meiosis of plants with holocentric chromosomes. *Nat Commun* **5**:5070. 10.1038/ncomms6070.

Carroll CW, Milks KJ, and Straight AF. 2010. Dual recognition of CENP-A nucleosomes is required for centromere assembly. *Journal of Cell Biology* **189**:1143-1155. 10.1083/jcb.201001013.

Cleveland DW, Mao Y, and Sullivan KF. 2003. Centromeres and kinetochores: from epigenetics to mitotic checkpoint signaling. *Cell* **112**:407-421.

Comings DE, and Okada TA. 1972. Holocentric chromosomes in *Oncopeltus*: kinetochore plates are present in mitosis but absent in meiosis. *Chromosoma* **37**:177-192.

Cuacos M, Franklin FCH, and Heckmann S. 2015. Atypical centromeres in plants - what they can tell us. *Front Plant Sci* **6**:913. 10.3389/fpls.2015.00913.

Drinnenberg IA, deYoung D, Henikoff S, and Malik HS. 2014. Recurrent loss of CenH3 is associated with independent transitions to holocentricity in insects. *Elife* **3**:e03676. 10.7554/eLife.03676.

Dumont J, Oegema K, and Desai A. 2010. A kinetochore-independent mechanism drives anaphase chromosome separation during acentrosomal meiosis. *Nat Cell Biol* **12**:894-901. 10.1038/ncb2093.

Duro E, and Marston AL. 2015. From equator to pole: splitting chromosomes in mitosis and meiosis. *Genes and Development* **29**:109-122. 10.1101/gad.255554.114.

Earnshaw WC. 2015. Discovering centromere proteins: from cold white hands to the A, B, C of CENPs. *Nature Reviews Molecular Cell Biology* **16**:443-449. 10.1038/nrm4001.

Falk SJ, Guo LY, Sekulic N, Smoak EM, Mani T, Logsdon GA, Gupta K, Jansen LET, Van Duyne GD, Vinogradov SA, Lampson MA, and Black BE. 2015. CENP-C reshapes and stabilizes CENP-A nucleosomes at the centromere. *Science* **348**:699-703. 10.1126/science.1259308.

Friedlander M, and Wahrman J. 1970. The spindle as a basal body distributor. A study in the meiosis of the male silkworm moth, *Bombyx mori*. *Journal of Cell Science* **7**:65-89.

Goday C, and Pimpinelli S. 1989. Centromere organization in meiotic chromosomes of *Parascaris univalens*. *Chromosoma* **98**:160-166.

Goldstein P. 1977. Spermatogenesis and spermiogenesis in *Ascaris lumbricoides* Var. suum. *Journal of Morphology* **154**:317-337. 10.1002/jmor.1051540302.

Guerra M, Cabral G, Cuacos M, Gonzalez-Garcia M, Gonzalez-Sanchez M, Vega J, and Puertas MJ. 2010. Neocentrics and holokinetics (holocentrics): chromosomes out of the centromeric rules. *Cytogenet Genome Res* **129**:82-96. 10.1159/000314289.

Heckmann S, Jankowska M, Schubert V, Kumke K, Ma W, and Houben A. 2014. Alternative meiotic chromatid segregation in the holocentric plant *Luzula elegans*. *Nat Commun* **5**:4979. 10.1038/ncomms5979.

Hughes-Schrader S, and Schrader F. 1961. The kinetochore of the Hemiptera. *Chromosoma* **12**:327-350.

Ishiguro K, and Watanabe Y. 2007. Chromosome cohesion in mitosis and meiosis. *Journal of Cell Science* **120**:367-369. 10.1242/jcs.03324.

Ishii T, Karimi-Ashtiyani R, and Houben A. 2016. Haploidization via chromosome elimination: means and mechanisms. *Annual Review of Plant Biology* **67**:10.11–10.18. 10.1146/annurev-arplant-043014-114714.

Ishii T, Sunamura N, Matsumoto A, Eltayeb AE, and Tsujimoto H. 2015. Preferential recruitment of the maternal centromere-specific histone H3 (CENH3) in oat (*Avena sativa* L.) x pearl millet (*Pennisetum glaucum* L.) hybrid embryos. *Chromosome Research*. 10.1007/s10577-015-9477-5.

Kato H, Jiang J, Zhou BR, Rozendaal M, Feng H, Ghirlando R, Xiao TS, Straight AF, and Bai Y. 2013. A conserved mechanism for centromeric nucleosome recognition by centromere protein CENP-C. *Science* **340**:1110-1113. 10.1126/science.1235532.

Katoh K, and Standley DM. 2013. MAFFT multiple sequence alignment software version 7: improvements in performance and usability. *Mol Biol Evol* **30**:772-780. 10.1093/molbev/mst010.

Lermontova I, Koroleva O, Rutten T, Fuchs J, Schubert V, Moraes I, Koszegi D, and Schubert I. 2011. Knockdown of CENH3 in Arabidopsis reduces mitotic divisions and causes sterility by disturbed meiotic chromosome segregation. *Plant J* **68**:40-50. 10.1111/j.1365-313X.2011.04664.x.

Liu ST, Rattner JB, Jablonski SA, and Yen TJ. 2006. Mapping the assembly pathways that specify formation of the trilaminar kinetochore plates in human cells. *Journal of Cell Biology* **175**:41-53. 10.1083/jcb.200606020.

Maddox PS, Oegema K, Desai A, and Cheeseman IM. 2004. "Holo"er than thou: chromosome segregation and kinetochore function in *C. elegans*. *Chromosome Research* **12**:641-653. 10.1023/B:CHRO.0000036588.42225.2f.

Marques A, Ribeiro T, Neumann P, Macas J, Novak P, Schubert V, Pellino M, Fuchs J, Ma W, Kuhlmann M, Brandt R, Vanzela AL, Beseda T, Simkova H, Pedrosa-Harand A, and Houben A. 2015. Holocentromeres in *Rhynchospora* are associated

with genome-wide centromere-specific repeat arrays interspersed among euchromatin. *Proc Natl Acad Sci U S A* **112**:13633-13638. 10.1073/pnas.1512255112.

Martinez-Perez E, Schvarzstein M, Barroso C, Lightfoot J, Dernburg AF, and Villeneuve AM. 2008. Crossovers trigger a remodeling of meiotic chromosome axis composition that is linked to two-step loss of sister chromatid cohesion. *Genes and Development* **22**:2886-2901. 10.1101/gad.1694108.

Melters DP, Paliulis LV, Korf IF, and Chan SW. 2012. Holocentric chromosomes: convergent evolution, meiotic adaptations, and genomic analysis. *Chromosome Research* **20**:579-593. 10.1007/s10577-012-9292-1.

Merai Z, Chumak N, Garcia-Aguilar M, Hsieh TF, Nishimura T, Schoft VK, Bindics J, Slusarz L, Arnoux S, Opravil S, Mechtler K, Zilberman D, Fischer RL, and Tamaru H. 2014. The AAA-ATPase molecular chaperone Cdc48/p97 disassembles sumoylated centromeres, decondenses heterochromatin, and activates ribosomal RNA genes. *Proc Natl Acad Sci U S A* **111**:16166-16171. 10.1073/pnas.1418564111.

Minh BQ, Nguyen MA, and von Haeseler A. 2013. Ultrafast approximation for phylogenetic bootstrap. *Mol Biol Evol* **30**:1188-1195. 10.1093/molbev/mst024.

Monen J, Maddox PS, Hyndman F, Oegema K, and Desai A. 2005. Differential role of CENP-A in the segregation of holocentric *C. elegans* chromosomes during meiosis and mitosis. *Nat Cell Biol* **7**:1248-1255. 10.1038/ncb1331.

Nguyen LT, Schmidt HA, von Haeseler A, and Minh BQ. 2015. IQ-TREE: a fast and effective stochastic algorithm for estimating maximum-likelihood phylogenies. *Mol Biol Evol* **32**:268-274. 10.1093/molbev/msu300.

Ohkura H. 2015. Meiosis: An overview of key differences from mitosis. *Cold Spring Harb Perspect Biol* **7**. 10.1101/cshperspect.a015859.

Pan J, Sasaki M, Kniewel R, Murakami H, Blitzblau HG, Tischfield SE, Zhu X, Neale MJ, Jasin M, Socci ND, Hochwagen A, and Keeney S. 2011. A hierarchical combination of factors shapes the genome-wide topography of yeast meiotic recombination initiation. *Cell* **144**:719-731. 10.1016/j.cell.2011.02.009.

Papeschi AG, Mola LM, Bressa MJ, Greizerstein EJ, Lia V, and Poggio L. 2003. Behaviour of ring bivalents in holokinetic systems: alternative sites of spindle attachment in *Pachylis argentinus* and *Nezara viridula* (Heteroptera). *Chromosome Research* **11**:725-733.

Perez R, Rufas JS, Suja JA, Page J, and Panzera F. 2000. Meiosis in holocentric chromosomes: orientation and segregation of an autosome and sex chromosomes in *Triatoma infestans* (Heteroptera). *Chromosome Research* **8**:17-25.

Pimpinelli S, and Goday C. 1989. Unusual kinetochores and chromatin diminution in *Parascaris*. *Trends in Genetics* **5**:310-315.

Powers J, Rose DJ, Saunders A, Dunkelbarger S, Strome S, and Saxton WM. 2004. Loss of KLP-19 polar ejection force causes misorientation and missegregation of holocentric chromosomes. *Journal of Cell Biology* **166**:991-1001. DOI 10.1083/jcb.200403036.

Ravi M, Shibata F, Ramahi JS, Nagaki K, Chen C, Murata M, and Chan SW. 2011. Meiosis-specific loading of the centromere-specific histone CENH3 in *Arabidopsis thaliana*. *PLoS Genet* **7**:e1002121. 10.1371/journal.pgen.1002121.

Rufas JS, and Gimenez-Martin G. 1986. Ultrastructure of the kinetochore in *Graphosoma italicum* (Hemiptera, Heteroptera). *Protoplasma* **132**:142-148. Doi 10.1007/Bf01276994.

San Martin JAB, Andrade CGTD, Mastroberti AA, Mariath JED, and Vanzela ALL. 2013. Asymmetric cytokinesis guide the development of pseudomonads in Rhynchospora pubera (Cyperaceae). *Cell Biology International* **37**:203-212. 10.1002/cbin.10028.

Schoft VK, Chumak N, Mosiolek M, Slusarz L, Komnenovic V, Brownfield L, Twell D, Kakutani T, and Tamaru H. 2009. Induction of RNA-directed DNA methylation upon decondensation of constitutive heterochromatin. *EMBO Rep* **10**:1015-1021. 10.1038/embor.2009.152.

Schubert V, Lermontova I, and Schubert I. 2014. Loading of the centromeric histone H3 variant during meiosis-how does it differ from mitosis? *Chromosoma* **123**:491-497. 10.1007/s00412-014-0466-9.

Schvarzstein M, Wignall SM, and Villeneuve AM. 2010. Coordinating cohesion, co-orientation, and congression during meiosis: lessons from holocentric chromosomes. *Genes and Development* **24**:219-228. 10.1101/gad.1863610.

Shakes DC, Wu JC, Sadler PL, Laprade K, Moore LL, Noritake A, and Chu DS. 2009. Spermatogenesis-specific features of the meiotic program in *Caenorhabditis elegans*. *PLoS Genet* **5**:e1000611. 10.1371/journal.pgen.1000611.

Sousa A, Barros e Silva AE, Cuadrado A, Loarce Y, Alves MV, and Guerra M. 2011. Distribution of 5S and 45S rDNA sites in plants with holokinetic chromosomes and the "chromosome field" hypothesis. *Micron* **42**:625-631. 10.1016/j.micron.2011.03.002.

Steiner FA, and Henikoff S. 2015. Diversity in the organization of centromeric chromatin. *Curr Opin Genet Dev* **31**:28-35. 10.1016/j.gde.2015.03.010.

Talbert PB, and Henikoff S. 2010. Centromeres convert but don't cross. *PLoS Biol* **8**. 10.1371/journal.pbio.1000326.

Viera A, Page J, and Rufas JS. 2009. Inverted meiosis: the true bugs as a model to study. *Genome Dyn* **5**:137-156. 10.1159/000166639.

Vincenten N, Kuhl LM, Lam I, Oke A, Kerr AR, Hochwagen A, Fung J, Keeney S, Vader G, and Marston AL. 2015. The kinetochore prevents centromere-proximal crossover recombination during meiosis. *Elife* **4**. 10.7554/eLife.10850.

Weisshart K, Fuchs J, and Schubert V. 2016. Structured Illumination Microscopy (SIM) and Photoactivated Localization Microscopy (PALM) to analyze the abundance and distribution of RNA Polymerase II molecules on flow-sorted *Arabidopsis* nuclei. *Bio-protocols, http://wwwbio-protocolorg*.

Wignall SM, and Villeneuve AM. 2009. Lateral microtubule bundles promote chromosome alignment during acentrosomal oocyte meiosis. *Nat Cell Biol* **11**:839-844. 10.1038/ncb1891.

Zamariola L, Tiang CL, De Storme N, Pawlowski W, and Geelen D. 2014. Chromosome segregation in plant meiosis. *Front Plant Sci* **5**:279. 10.3389/fpls.2014.00279.

Conclusões

A análise da estrutura e organização dos holocentrômeros funcionais de *R. pubera* permitiu a descoberta de sequências específicas das regiões centroméricas de uma espécie com cromossomos holocêntricos. A família de DNA satélite Tyba e retrolementos centroméricos (CRRh) são as principais sequências de DNA associadas com os centrômeros funcionais dessa espécie. Os arranjos de Tyba estão frequentemente intercalados com sequências gênicas ativas, indicando que não há uma compartimentalização de eu- e heterocromatina típica de espécies monocêntricas. Esses arranjos de Tyba também foram caracterizados por apresentarem trechos curtos de *high order repeat structure* (HOR), também observados em satélites encontrados em monocêntricos. Esse trabalho pôde fornecer grande conhecimento sobre a organização e dinâmica das unidades centroméricas em cromossomos holocêntricos.

A análise detalhada e comparativa da meiose de *R. pubera* e *R. tenuis* revelou para ambas espécies uma meiose invertida, confirmando assim análises anteriores. Adicionalmente, foi verificado que embora ambas apresentem meiose invertida, particularidades foram encontradas em cada espécie, como por exemplo, a meiose quiasmática de *R. pubera* e aquiasmática de *R. tenuis*. As adaptações meióticas encontradas em ambas as espécies para lidar com a natureza holocêntrica durante a meiose incluem: (I) ligação anfitélica das cromátides-irmãs em metáfase I, (II) separação equacional das cromátides-irmãs em anáfase I e (III) reassociação de cromátides homólogas não-irmãs na prófase II, aparentemente mediado por fibras de cromatina, ocasionando uma disjunção frequentemente regular na meiose II. Além do mais, em *Rhynchospora* os cromossomos meióticos apresentam uma condensação diferente da observada em mitose e a estrutura holocêntrica típica observada em mitose é difícil de ser distinguida, diferentemente do observado em *Luzula*, em que holocentrômeros e mesmo o sulco centromérico são claramente observados com anti-CENH3.

A análise comparativa da organização centromérica durante a mitose e a meiose em *R. pubera* revelou pela primeira vez em uma espécie vegetal uma organização diferencial da unidades centroméricas entre esses dois tipos de divisão celular. Ao

contrário da mitose, em que as múltiplas unidades centroméricas se associam formando os holocentrômeros em um sulco centromérico nessa espécie, durante a meiose vários aglomerados de unidades centroméricas (*cluster centromeres*) nos cromossomos são formados. Essa conformação diferencial dos centrômeros na meiose está também associada com a ausência de sulco centromérico nos cromossomos meióticos. A organização diferencial dos cromossomos na meiose sugere que não se faz necessário a manutenção de uma organização holocêntrica para que a meiose invertida ocorra. Por fim, a visualização dos centrômeros durante a meiose permitiu verificar uma orientação diferencial dos cromossomos na meiose I e II. Enquanto durante a meiose I os cromossomos são associados lateralmente, durante a meiose II eles são aparentemente associados terminalmente.